



2019

Synthesis and Conformational Studies of Various Amides

Marcos Beltran-Sanchez
University of the Pacific

Follow this and additional works at: https://scholarlycommons.pacific.edu/uop_etds

 Part of the [Medicinal-Pharmaceutical Chemistry Commons](#), and the [Pharmacy and Pharmaceutical Sciences Commons](#)

Recommended Citation

Beltran-Sanchez, Marcos. (2019). *Synthesis and Conformational Studies of Various Amides*. University of the Pacific, Thesis. https://scholarlycommons.pacific.edu/uop_etds/3661

This Thesis is brought to you for free and open access by the Graduate School at Scholarly Commons. It has been accepted for inclusion in University of the Pacific Theses and Dissertations by an authorized administrator of Scholarly Commons. For more information, please contact mgibney@pacific.edu.

SYNTHESIS AND CONFORMATIONAL STUDIES OF VARIOUS AMIDES

By

Marcos Beltran-Sanchez

A Thesis Submitted to the

Graduate School

In Partial Fulfillment of the

Requirements for the Degree of

MASTER OF SCIENCE

Thomas J. Long School of Pharmacy and Health Sciences
Pharmaceutical and Chemical Sciences

University of the Pacific
Stockton, California

2019

SYNTHESIS AND CONFORMATIONAL STUDIES OF VARIOUS AMIDES

By

Marcos Beltran-Sanchez

APPROVED BY:

Thesis Advisor: Vyacheslav V. Samoshin, Ph.D.

Committee Member: Liang Xue, Ph.D.

Committee Member: Jianhua Ren, Ph.D.

Committee Member: Andreas Franz, Ph.D.

Department Co-Chair: Jianhua Ren, Ph.D.

Department Co-Chair: Jerry Tsai, Ph.D.

DEDICATION

This thesis is dedicated to my parents, Marcos and Maria Beltran and my sister Crystal. This would not have been possible without their hard work, inspiration, and support.

ACKNOWLEDGMENTS

I would like to express my gratitude to my research advisor Dr. Vyacheslav Samoshin for his wisdom, advice, and patience throughout these three years of graduate school. I am forever grateful to him for allowing me to be a member of his lab and for sharing his immense wealth of knowledge, creativity, and experience with me.

I would also like to thank Carim van Beek and Dr. Ronnie Ruyonga who have been more than just lab mates, they have been and continue to be great friends. I am especially grateful to Carim since this thesis would not have been possible without his guidance and advice throughout the course of my research. He has been an excellent mentor and has always been willing to assist me in any way that he can. Although not technically a lab mate, I'd like to express my thanks to Mandeep Singh as well for also being a great mentor and friend.

Thank you to all of my other friends who have encouraged and motivated me along the way including Jose Esparza, Antoine and Wilfred Garcia.

I am very thankful to Dr. Andreas Franz, Dr. Jianhua Ren, and Dr. Liang Xue for agreeing to be my committee members and sharing their advice and expertise with me. Special thanks to Dr. Roshanak Rahimian for the use of the QuantaMaster Fluorometer, Dr. Xin Guo for the use of the DLS instrument, Professor David Sparkman and the Mass Spectrometry facility for helping me to obtain mass spectra for all of my compounds, and Dr. Franz and Dr. Samoshin again for allowing me to use the NMR instrument.

Last but certainly not least, I would like to thank the late Dr. Nataliya Samoshina. The synthesis and purification of the liposomes would not have been possible without her guidance. Her kind, warm presence in the chemistry department will be sorely missed.

SYNTHESIS AND CONFORMATIONAL STUDIES OF VARIOUS AMIDES

Abstract

By Marcos Beltran-Sanchez

University of the Pacific
2019

In the past, aminocyclohexanol rings have been successfully utilized as pH-triggered molecular switches in various *trans*-2-aminocyclohexanol derivatives. By changing the groups on the amine nitrogen, these models provided a wide pH range in which a switch can occur. The pH-induced switch of conformation was monitored by $^1\text{H-NMR}$ spectroscopy. The models were also incorporated into the bilayer membrane of liposome structures and tested for their ability to disrupt their membrane upon their conformational flip induced by a decrease in pH.

In this work, the amide bond has been studied as a molecular switch and various amide derivatives have been tested for their potential as lipid-like compounds that also exhibit a pH-sensitive conformational flip. The conformational analysis of these compounds was achieved by various NMR techniques and NMR acid-base titration studies were utilized to estimate the pKa of a number of the compounds described.

TABLE OF CONTENTS

List of Tables	10
List of Figures	11
List of Schemes	14
List of Abbreviations	15
Chapter 1: Introduction	17
1.1 Targeted Drug Delivery	17
1.2 Conformational Molecular Switches	19
1.3 Flipids	19
1.4 Cyclohexanol-Based Flipid Model	21
1.5 Novel Amide-Based Flipid Model.....	22
1.6 Studying Aryl Amide Compounds.....	24
1.7 The Nuclear Overhauser Effect	25
Chapter 2: Research Goals.....	28
Chapter 3: Results and Discussion.....	29
3.1 Amide Flipid Model with Alkyl Chain Tails	29
3.1.1 Synthesis of N-(2-(hexyl(methyl)amino)ethyl)- N-methyldecanamide (I).....	29
3.1.2 Conformational Analysis of N-(2-(hexyl(methyl)amino) ethyl)-N-methyldecanamide (I)	31
3.2 Preparation of Liposomes	37
3.3 ANTS/DPX Liposome Leakage Assay.....	39
3.4 Factors That May Affect Liposomal Leakage	41
3.4.1 Basicity of the Tertiary Amine	42

3.4.2 Overall Steric Effect of the Conformational Flip	42
3.5 Amide Model with Aryl Rings	44
3.5.1 Synthesis of N-methyl-N-(pyridin-2-yl) benzamide (IV)	45
3.5.2 Conformational Analysis of N-methyl-N-(pyridin-2-yl) benzamide (IV)	45
3.6 NOE Studies.....	48
3.6.1 NOESY Results of N-methyl-N-(pyridin-2-yl) benzamide (IV)	49
3.6.2 Disadvantages of NOESY.....	51
3.7 Exploring the Rotational Barriers of Similar Diaryl Compounds	54
3.7.1 Reported Rotational Barrier Trends of Anilide Compounds	54
3.7.2 Synthesis of <i>p</i> -Substituted Anilide Compounds	56
3.7.3 Conformational Analysis of <i>p</i> -Substituted Anilide Compounds	59
3.8 Comparative Evaluation of the Alkyl Chains and Aryl Rings Models.....	60
3.9 Hybrid Amide Flipid Model	61
3.9.1 Synthesis of the Hybrid Models.....	63
3.9.2 Conformational Analysis of the Hybrid Models.....	65
3.9.3 Acid-Base Titration Studies.....	66
Chapter 4: Conclusions	74
Chapter 5: Experimental	77
5.1 Materials	77
5.2 Conformational Analysis by NMR Spectroscopy.....	77
5.3 NMR Titration Studies.....	78

	8
5.4 Synthesis of Fliposomes	78
5.5 ANTS/DPX Leakage Assay.....	79
5.6 Synthesis of Compounds.....	80
5.6.1 Synthesis of Hexyl 4-methylbenzenesulfonate (II)	80
5.6.2 Synthesis of N-Hexyl-N,N'-dimethylethane-1,2- diamine (III)	81
5.6.3 Synthesis of N-(2-(hexyl(methyl)amino)ethyl)- N-methyldecanamide (I)	82
5.6.4 Synthesis of N-methyl-N-(pyridin-2-yl)benzamide (IV).....	83
5.6.5 Synthesis of N-(4-methoxyphenyl)-N-methyl- 4-nitrobenzamide (V).....	84
5.6.6 Synthesis of N-(4-methoxyphenyl)-4- nitrobenzamide (VI).....	85
5.6.7 Synthesis of N-(4-(dimethylamino)phenyl)-N-methyl-4-nitrobenzamide (VII).....	86
5.6.8 Synthesis of N-(4-(dimethylamino)phenyl)-4- nitrobenzamide (VIII)	87
5.6.9 Synthesis of Decanoyl chloride (IX)	88
5.6.10 Synthesis of N-(2-hydroxyethyl)-N- methyldecanamide (X).....	88
5.6.11 Synthesis of N-(2-chloroethyl)-N- methyldecanamide (XI)	89
5.6.12 Synthesis of N-methyl-N-(2-morpholinoethyl) decanamide (XII).....	90
5.6.13 Synthesis of N-methyl-N- (2-(piperidin-1-yl)ethyl)decanamide (XIII)	91
5.6.14 Synthesis of N-methyl-N- (2-(4-methylpiperazin-1-yl)ethyl)decanamide (XIV).....	92
References.....	93

Appendices

A. Selected ^1H -NMR Spectra	98
B. Selected ^{13}C -NMR Spectra	110
C. Selected ^1H - ^1H COSY Spectra.....	119
D. Selected ^1H - ^{13}C HMQC Spectra	129
E. Selected ^1H -NMR Titration Data.....	138
F. Selected Mass Spectra.....	143

LIST OF TABLES

Table

1. Titration Data for Compound I	36, 138
2. Dynamic Light Scattering Data of the Different Liposome Formulations	38
3. Fluorimetry Results for the Four Different Fliposome Formulations.....	40
4. The Effect of pH on the Fluorimetry Results.....	41
5. Calculated Resonance Energies for Various Anilide Compounds (Adapated From Szostak)	56
6. Titration Data for Compound XII	139
7. Titration Data for Compound XIII	140
8. Titration Data for Compound XIV	141

LIST OF FIGURES

Figure

1. Formation of liposomes and how they can encapsulate drugs of interest.....	18
2. Conformational flip of a lipid molecule.....	20
3. Liposomal drug delivery facilitated by a molecular switch.....	20
4. Shift in conformational equilibrium produced by protonation of a TACH flipid.....	21
5. Resonance stabilization of the C—N amide bond.....	23
6. General structure for the <i>syn</i> and <i>anti</i> isomers of an amide-based flipid molecule.....	23
7. General structures for the <i>syn</i> and <i>anti</i> isomers of anilide compounds.....	24
8. Molecular structures of the isomers of 3-ethylidenel-azabicyclo[2.2.2]octane.....	26
9. NOE signals produced by the two conformational isomers of N-phenyl-N-6- (azulenyl)acetamide.....	27
10. Shift in conformational equilibrium produced by protonation of compound I	29
11. Equilibrium between the two conformers of compound I	31
12. Observable separation of methyl group peaks of compound I (CH ₃ NC=O methyl group proton signals circled in red, CH ₃ N methyl group proton signals circled in blue).....	32
13. Section of a ¹ H-NMR spectrum illustrating the separation of the CH ₃ NC=O methyl group signals.....	33
14. Equilibrium between the two conformers of compound I depicted with dipoles.....	34
15. Effect of titrating compound I with <i>d</i> -TFA in a <i>d</i> -MeOH solution (ppm scales have been shifted to better show the different signals).....	35
16. Graph depicting the percentage of the <i>anti</i> conformation of compound I present as a function of pH.....	36

17. Conformational switch of compound I with decreased steric effect	43
18. Conformational switch of compound IV (hydrogen bond shown in blue).....	44
19. ¹ H-NMR spectrum in d-MeOH illustrating the lack of signal separation for the individual conformations of compound IV	46
20. Effect of adding <i>d</i> -TFA to compound IV in <i>d</i> -TFA: IV molar ratios of 0.0:1.0 (1), 0.5:1.0 (2), 1.0:1.0 (3), and 50.0:1.0 (4).....	47
21. Labeled chemical structures of compound IV in the <i>anti</i> and <i>syn</i> conformations	49
22. NOE produced upon irradiation of the N-methyl (CH ₃) signal.....	50
23. NOE produced upon irradiation of the H ^o signal	51
24. Molecular isomeric structures of N-methylbenzamide.....	52
25. Molecular structure of N,N-dimethylacetamide	53
26. Molecular structure of N-methyl, 2-pyrrolidone	54
27. Anilide general structure with N-aryl ring (blue) and C-aryl ring (red).....	55
28. <i>syn</i> -Favored conformation of anilides upon N-methylation of amide nitrogen	57
29. Set of <i>p</i> -substituted anilide compounds synthesized for conformational analysis.....	58
30. Expected NOE response from proton C (in <i>syn</i> conformation).....	59
31. NOE results depicting the appearance of a response from proton C exclusively in the N-methylated anilide compounds.....	60
32. General structure and conformational switch for the hybrid model compounds	62
33. Molecular structures for compounds XII – XIV	65
34. Portion of ¹ H-NMR spectrum for compound XII depicting the N-methyl group protons in the two conformations before addition of acid.....	67
35. Percentage of the <i>anti</i> conformation of compound XII plotted as a function of pD.....	68

36. Comparison of the pK_a values for morpholinium and N-ethylmorpholinium	69
37. Reported pK_a values for piperidinium and morpholinium	69
38. Percentage of the <i>anti</i> conformation of compound XIII as a function of pD	70
39. Graph depicting the percentage of the <i>anti</i> conformation of compound XIV present as a function of pD	71
40. Summary of the pK_a trends of compounds XII-XIV and their free amine moieties	72

LIST OF SCHEMES

Scheme

1. Synthesis of compound **I** (82% overall yield)30
2. Synthetic scheme for Compound **IV**.....45
3. General synthetic scheme for compounds **V-VIII**.....59
4. General synthetic scheme for compounds **IX-XIV**64

LIST OF ABBREVIATIONS

AcOH	Acetic acid
AcONa	Sodium acetate
ANTS	8-aminonaphthalene-1,3,6-trisulfonic acid disodium salt
C16 PEG2000 Ceramide	N-palmitoyl-sphingosine-1-(succinyl[methoxy (polyethylene glycol)2000])
COSNAR	Carbonyl Substitution Nitrogen Atom Replacement
COSY	Correlated Spectroscopy
DART	Direct Analysis in Real Time
d-CHCl ₃ /CDCl ₃	deuterated Chloroform
DCM	Dichloromethane
DFT	Density Functional Theory
DLS	Dynamic Light Scattering
d-MeOH/MeOD	deuterated Methanol
DPX	<i>p</i> -xylene-bis-pyridinium bromide
d-TFA	deuterated Trifluoroacetic acid
EDG	Electron Donating Group
Et ₃ N	Triethylamine
EtOAc	Ethyl acetate
EWG	Electron Withdrawing Group
HEPES	2-[4-(2-hydroxyethyl)piperazin-1-yl]-ethanesulfonic acid
HMQC	Heteronuclear Multiple Quantum Coherence
HRMS	High-Resolution Mass Spectrometry

NMR	Nuclear Magnetic Resonance
NOE	Nuclear Overhauser Effect
NOESY	Nuclear Overhauser Effect Spectroscopy
PdI	Polydispersity Index
PEG	Polyethylene glycol
pK_a	Acid Dissociation Constant
pK_{aH}	Conjugate Acid Dissociation Constant
POPC	1-palmitoyl-2-oleoyl- <i>sn</i> -glycero-3-phosphocholine
TACH	<i>trans</i> -2-aminocyclohexanol
TLC	Thin-Layer Chromatography
TOF	Time-of-Flight

CHAPTER 1: INTRODUCTION

1.1 Targeted Drug Delivery

Drug delivery can be described as the method of delivering therapeutic drugs and other pharmaceuticals to their site of action within an organism. In the case of drug delivery through the use of nanocarriers, therapeutic drugs are encapsulated by small vesicles and protected against degradation, thus greatly increasing their bioavailability.¹ They can also potentially make their way to the target tissues with more ease since the transport across certain membranes may be streamlined through the use of such carriers.¹

Targeted drug delivery describes an aim to deliver the drugs to the specific site of action whilst also minimalizing nonspecific side effects.² In the past, a number of targeted drug delivery systems have been developed and tested for the treatment of a variety of inflammatory diseases. A number of the drug delivery systems that have been described in the past revolve around the idea of using a liposome-like structure as an efficient drug carrier that can travel throughout the body while suppressing the detrimental effects of macrophages and protecting sensitive tissues from the potentially toxic drugs being transported.

Liposomes are spherical vesicles that are comprised of one or more bilayer membranes, which are typically formed by natural non-toxic lipid molecules. The structure of these molecules consists of a hydrophilic head region and a hydrophobic tail region, and the bilayer membrane is formed by hydrophobic effects which force the tail regions of various molecules to come together. This forms a spherical structure that has the hydrophilic heads facing towards the exterior of the liposome, allowing it to survive in an aqueous environment, and towards the interior of the liposome, allowing it to encapsulate aqueous solutions of the desired drugs³ (Figure 1).

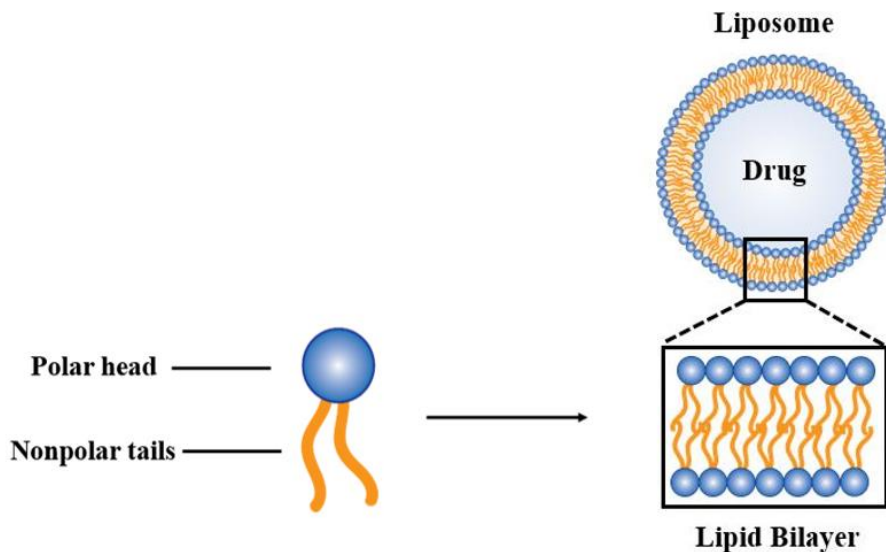


Figure 1. Formation of liposomes and how they can encapsulate drugs of interest

In 2001, Richards *et al.* studied how small liposomes could act as carriers for the delivery of clodronate to tissues affected by rheumatoid arthritis in rats.⁴ The use of polyethylene glycol-based (PEG) liposomes to effectively deliver drugs for the treatment of multiple sclerosis has also been examined in the past.⁵⁻⁷ In addition, such liposomal nanocarriers have been tested as drug delivery systems to treat against uveitis,^{8,9} which is a form of eye inflammation, and colitis,¹⁰ which is the inflammation of the colon.

Undoubtedly, the most attractive aspect of such drug delivery systems is their potential use in specifically targeting cancerous tissues. One of the major challenges in successfully treating diseases such as cancer is the ability to eradicate it while avoiding side effects that cause damage to normal tissues. In other words, the issue is not a lack of drugs or treatment options, but instead the lack of accurate and reliable targeted drug delivery methods.

1.2 Conformational Molecular Switches

Conformational switches are molecular devices designed to induce a conformational change in response to external stimuli such as certain ions, wavelengths of light, or pH values.^{11–13} These devices are of great chemical importance because the functionality of a molecule is usually highly dependent on its structure, therefore induced changes in conformation can have significant effects. A few examples of how molecular switches can be used are: to alter the chirality of molecules, to activate and/or deactivate fluorescence, and to control supramolecular organization and assembly.¹⁴ In recent years, these switches have been used in a variety of applications including information storage and transmission, fluorescence studies, and drug release.^{15–18}

The incorporation of molecular devices can be very advantageous in the design of targeted drug delivery vesicles since certain diseases have been found to alter local physiological conditions, such as pH levels, which can act as external triggers for a drug discharge. In the case of cancer, researchers have discovered that the pH of the extracellular fluid surrounding tumor cells is lower than that surrounding normal cells.¹⁹ Additionally, inflammation caused by conditions such as ischemia, rheumatoid arthritis, and even asthma has also been reported to lower the pH of affected tissues.²⁰ With the proper molecular switch mechanism, these relatively acidic conditions may be utilized for the specific targeting of such tissues as described further.

1.3 Flipids

In the past, molecular switches have been incorporated into drug delivery vesicles such as modified liposomes.^{21–24} Liposomes are structures comprised of lipids, which are molecules comprised of a polar, hydrophilic head region connected to nonpolar, hydrophobic tails.²⁵ The inclusion of a molecular switch to the head group of a lipid-like structure makes it possible to

induce a conformational change that can flip the tails from a “closed” position, where the tails are on the same side of the polar head, to an “open” position where the tails are apart (Figure 2).

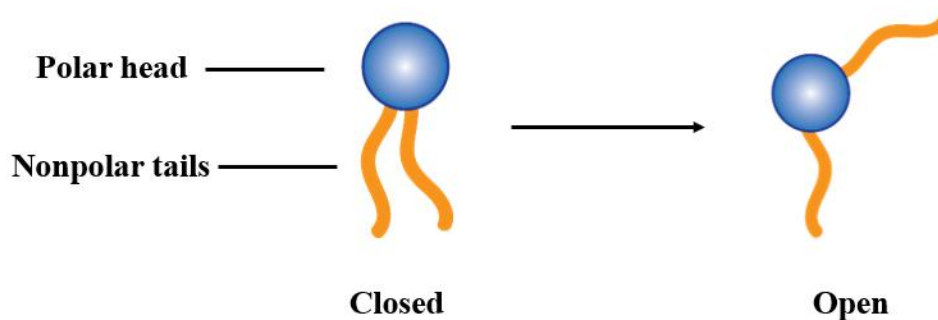


Figure 2. Conformational flip of a lipid molecule

If these flippable lipid molecules or “flipids”^{23,24} are incorporated into the lipid bilayer membrane of a liposomal structure, they can induce the rupture of the membrane due to the drastic conformational switch. Additionally, if these spherical structures are pre-loaded with a therapeutic drug, an efficient drug delivery system can be designed that will allow more control over the release of the drug upon being triggered by the external stimulus (Figure 3).

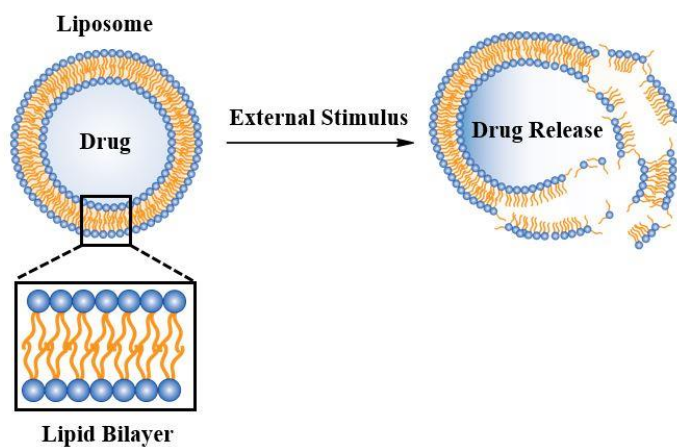


Figure 3. Liposomal drug delivery facilitated by a molecular switch

1.4 Cyclohexanol-Based Lipid Model

In previous years, the synthesis and characterization of conformationally-flipping liposome structures, or “fliposomes”, has been successfully achieved in the Samoshin lab using *trans*-2-aminocyclohexanol-based lipids.^{23,24} Those *trans*-2-aminocyclohexanol (TACH) lipid molecules (Figure 4) consisted of long alkyl chains functioning as nonpolar tails linked to the cyclohexanol ring by ester linkages. On the other end of the ring, which acts as the polar head, are the hydroxyl group and an amino group vicinal to each other and both predominantly in the axial position. In this conformation **A**, the alkyl chains are equatorially oriented and parallel to each other. Upon protonation of the tertiary amine, however, a hydrogen bond forms between the protonated nitrogen and the oxygen atom from the vicinal hydroxyl group. This favorable interaction draws the two groups closer together, forcing them into equatorial positions, which in turn produces an allosteric effect causing the entire ring to flip and forces the tails into the axial positions, disrupting their parallel orientation and giving conformation **B** (Figure 4).

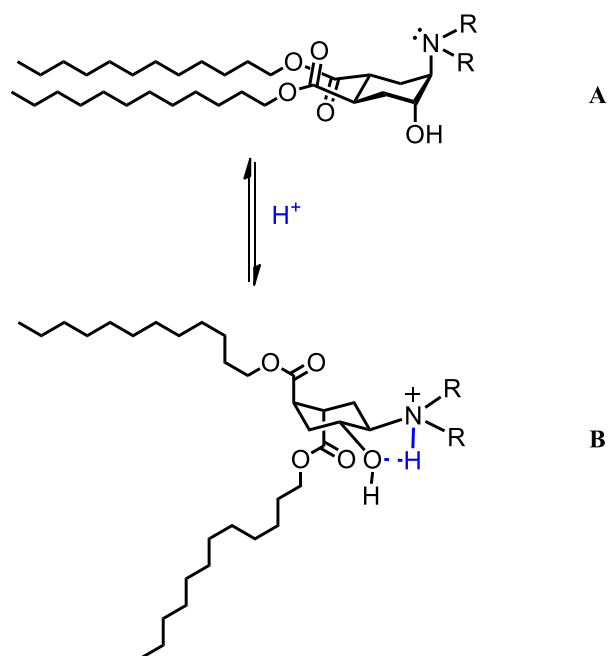


Figure 4. Shift in conformational equilibrium produced by protonation of a TACH lipid

In this case, the substituted *trans*-2-aminocyclohexanol ring is a molecular switch that induces a conformational change in the presence of acid. It works well because it has two stable chair conformations but is initially biased towards conformation **A** by the sterically demanding ester groups preferring to be equatorial. These flipids were synthesized and incorporated into the membrane of a liposome structure which was successfully ruptured by the induced conformational switch under acidic conditions, allowing the release of liposomal contents.

1.5 Novel Amide-Based Flipid Model

The aim of this project was to synthesize and characterize a series of compounds that utilized a simpler flipid design which potentially may allow for more variability of the structure whilst avoiding complex and potentially expensive synthetic processes. Any lipid model by definition includes a polar head group and nonpolar tails. However, in an effort to incorporate the switching mechanism utilized in the cyclohexanol-based flipid model, a tertiary amine is included in the structure to trigger the conformational switch in the presence of acid as a hydrogen bond donor. Additionally, the polar head region must: (1) include a hydrogen bond acceptor, (2) form a bridge to connect the two tails.

The typical amide functional group consists of a nitrogen atom covalently bound to a carbonyl group. Although nitrogen atoms can typically be protonated and make good hydrogen bond donors in amines, the resonance delocalization of the lone pair makes it much less basic (Figure 5). Instead, the carbonyl oxygen can function as a hydrogen bond acceptor.

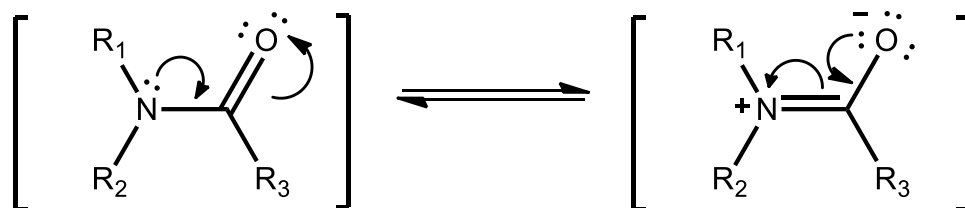


Figure 5. Resonance stabilization of the C—N amide bond

Moreover, if one nonpolar tail is connected to the carbon atom on one side of the C—N bond and the second tail is connected to the nitrogen atom on the other side, the amide group will effectively be a relatively polar group that connects both tails together, and also includes a hydrogen bond acceptor. Therefore, a molecule with these structural components should resemble a lipid structure that can interconvert between a *syn* form (closed lipid) where the two tails are on the same side of the amide bond and an *anti* form (open lipid) where the tails are on opposite sides of the bond (Figure 6).

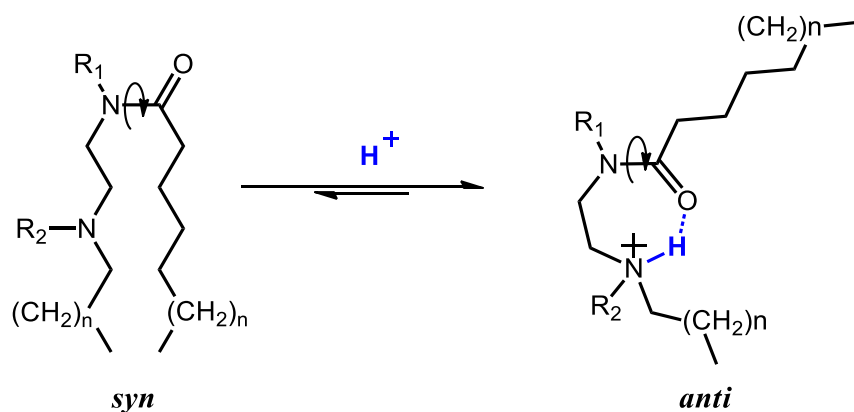


Figure 6. General structure for the *syn* and *anti* isomers of an amide-based lipid molecule

Amides are quite unique in that the C—N bond has a partial double-bond character, as depicted previously in Figure 5, that restricts rotation around it. To give an idea of the relative

amount of energy required, the rotational barrier around the C—C bond of ethane is about 3 kcal/mol,²⁶ the barrier around the C—N bond of dimethylacetamide is about 15 kcal/mol,²⁷ and the barrier around the C=C bond of 2-butene is about 39 kcal/mol.²⁸ Therefore, there is no free rotation around the amide bond as is typical in single bonds, but the rotation is also not completely restricted as is the case with double bonds. It is hypothesized that the rotation is restricted enough to allow for the molecule to be locked into an initial conformation that is stabilized by lipophilic interactions in the lipid bilayer of the membrane, but not so restrictive that it is impossible to overcome the rotational barrier and induce a conformational change as a function of a second favorable interaction, e.g. the formation of a hydrogen bond.

1.6 Studying Aryl Amide Compounds

One of the general model structures that are of interest consists of aromatic rings attached to either side of the amide bond since several studies of such structures have been reported in recent years.^{29–31} For example, in 2017 Szostak *et al.* reported the resonance energies for a range of anilides³¹ (Figure 7).

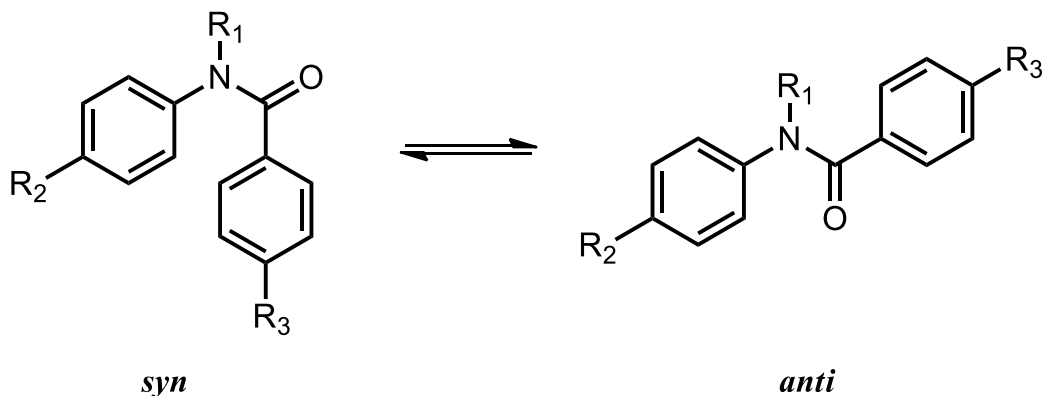


Figure 7. General structures for the *syn* and *anti* isomers of anilides

According to the report, the resonance energies were calculated using the Carbonyl Substitution Nitrogen Atom Replacement (COSNAR) computational method and further optimized using DFT and *ab initio* methods. The calculated values suggest that these anilide molecules “feature a significantly decreased barrier to rotation around the amide N—C bond.”³¹

These results posed new questions about these aromatic ring structures and inspired one of the projects discussed later in this thesis in which a series of anilide compounds were synthesized and their conformations were analyzed using various ¹H-NMR techniques including Nuclear Overhauser Effect Spectroscopy (NOESY).

1.7 The Nuclear Overhauser Effect

Nuclear Overhauser Effect Spectroscopy (NOESY) is an NMR technique that revolves around the observation and measurement of signals produced by the Nuclear Overhauser Effect, which is also known as the Nuclear Overhauser Enhancement because it enhances the integrated intensity of NMR signals. This can be best explained by considering an example involving two nuclei, X and Y, which local magnetic fields are influenced by each other's through an intramolecular dipole-dipole interaction. The intensity of the signal for X can be enhanced by saturating the Y nuclei, which can be achieved by irradiating at the resonance frequency of Y. The technique involves nuclear cross-relaxation processes, and since “the relaxation is very strongly dependent on the distance between a pair of nuclei,”³² it is possible to observe responses from nuclei that are in the same three-dimensional space but not necessarily spin-spin coupled. In other words, it measures the signals of nuclei, such as protons, that are in close spatial proximity of each other on time average, even if they are not directly connected through chemical bonds. It is an extremely useful technique that was predicted to be “of considerable stereochemical and

conformational interest in organic chemistry” back in 1965 by the researchers who reported the first proton intramolecular NOE, Anet and Bourn.³²

One example of how this technique has been used to distinguish between two isomers was reported by Nouis, van Binst, and Martin in 1967.³³ They reported the confirmation of the geometrical assignment for the two isomers of 3-ethylidene-azabicyclo[2.2.2]octane (Figure 8).

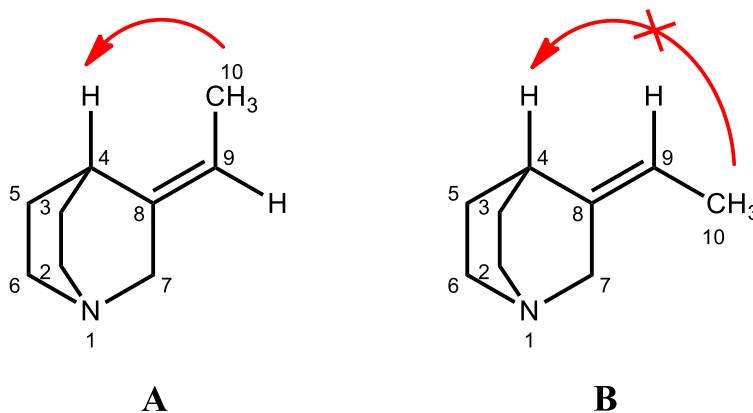


Figure 8. Molecular structures of the isomers of 3-ethylidene-azabicyclo[2.2.2]octane

The two isomers are very similar to each other, the only difference being that in one isomer the methyl group attached to the double bond is *cis* with respect to the C₄—H bond, and *trans* in the other. A mixture of the two in solution was analyzed by NMR and the proton on carbon-4 actually produced two distinct signals in the spectrum which corresponded to the two isomers. The protons on carbon-10 also gave distinct signals. However, it was unclear which set of signals corresponded to which isomers. NOE studies allowed for the correct determination of the signals since isomer **A** exhibited a clear NOE between the protons on carbon-10 and the proton on carbon-4 (shown as a red arrow), while isomer **B** showed no such effect due to the larger distance between the two sets of protons.³³

More recently, the conformation of N-aryl-N-6-(azulenyl)acetamides was determined through NOE studies conducted by Okamoto et al.³⁴ An example of one of the structures analyzed by the Okamoto group is shown in Figure 9. They were able to determine the conformation of the molecule by irradiating at the resonance frequency of the protons on the methyl group attached directly to the carbonyl group of the amide bond.

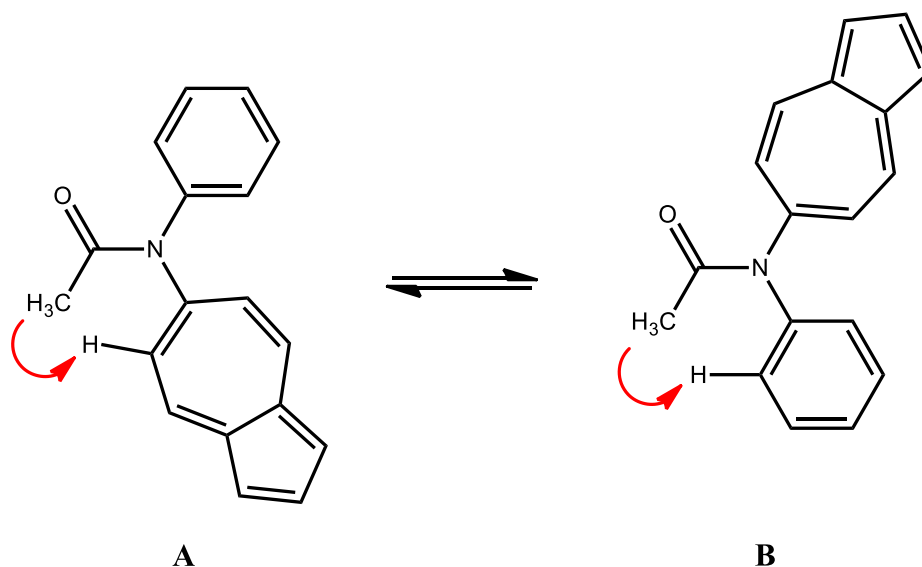


Figure 9. NOE signals produced by the two conformational isomers of N-phenyl-N-6-(azulenyl)acetamide

By being able to observe whether an NOE signal was produced by either the protons from the N-phenyl ring or the N-6-azulenyl ring, the researchers were able to reliably determine whether the molecule was in the **A** or **B** conformation.

CHAPTER 2: RESEARCH GOALS

The goal of this project was the development and examination of the pH-sensitive amide-based lipids and their potential for liposomal drug delivery. The research aims were:

- 1) Design and synthesis of a series of novel amide-based lipid molecules;
- 2) Study of conformational equilibrium of amide-based lipid molecules based on various ^1H -NMR techniques;
- 3) Study of pH-sensitivity of amide-based lipids and how it is affected by varying the amine moieties in the hydrophobic tails;
- 4) Evaluation of the amide-based lipids for their potential use in liposomal targeted drug delivery systems.

CHAPTER 3: RESULTS AND DISCUSSION

3.1 Amide Lipid Model with Alkyl Chain Tails

The initial design for a new lipid model includes: an amide bond that acts as a molecular switch, the two alkyl chain nonpolar tails, and a nitrogen atom embedded into one of the tails that is exactly five atoms away from the carbonyl oxygen in order to be able to form a stable hydrogen bond upon protonation (Figure 10). This amide lipid model with alkyl chain tails, N-(2-(hexyl(methyl)amino)ethyl)-N-methyldecanamide, will henceforth be referred to as compound **I**.

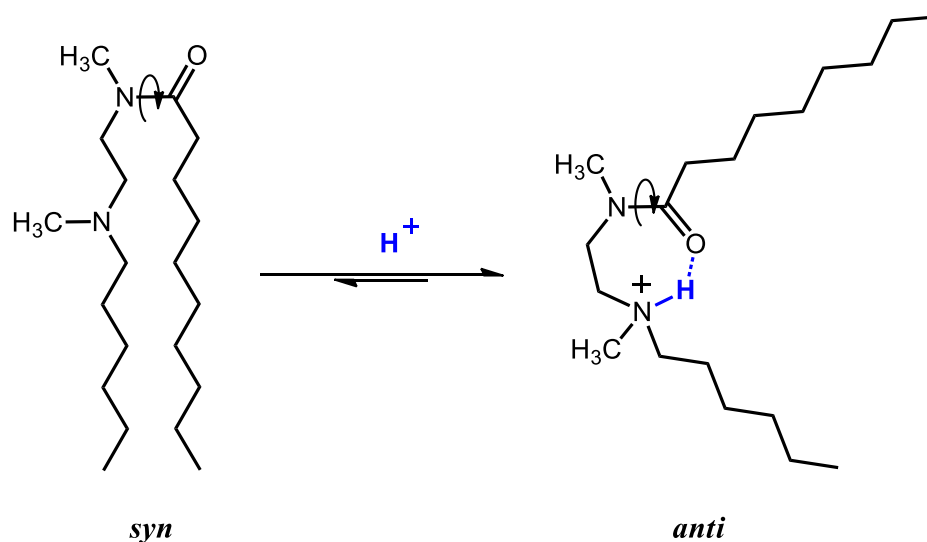


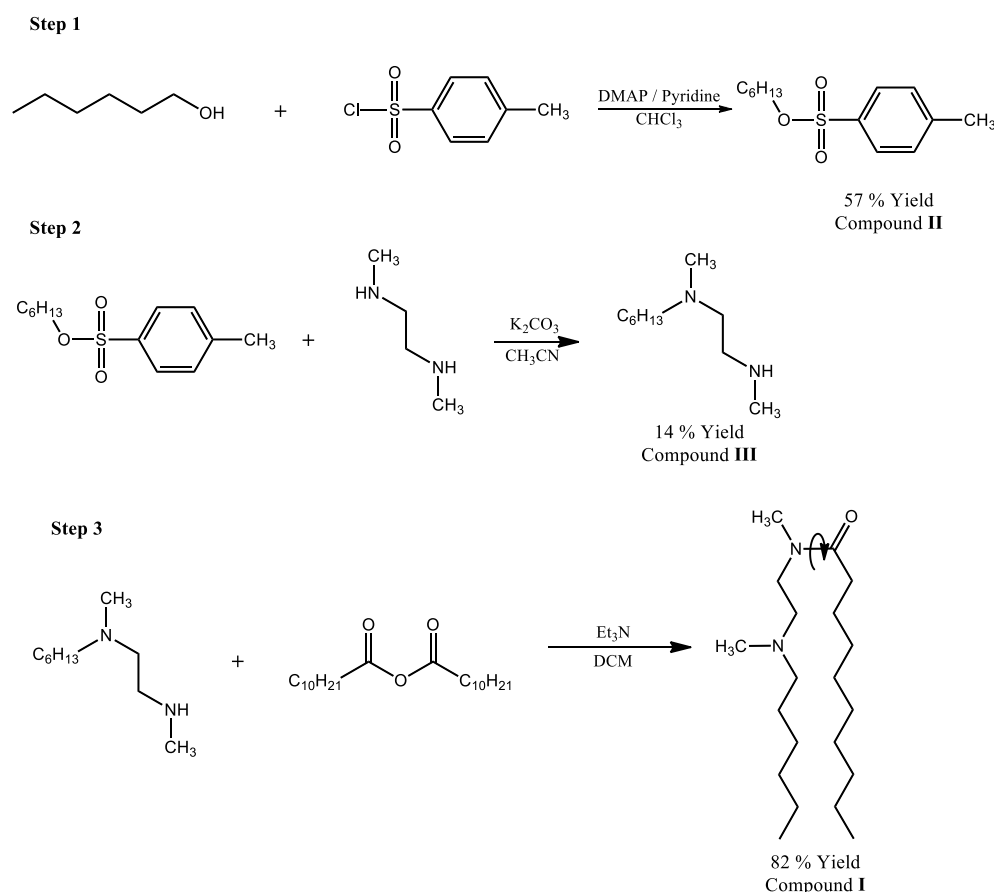
Figure 10. Shift in conformational equilibrium produced by protonation of compound **I**

3.1.1 Synthesis of N-(2-(hexyl(methyl)amino)ethyl)-N-methyldecanamide (**I**)

An amide lipid model with alkyl chains as hydrophobic tails was successfully synthesized (Scheme 1) by first sulfonating the hydroxyl group of 1-hexanol with p-toluenesulfonyl chloride in order to convert the alcohol moiety into a good leaving group. N,N'-Dimethyl-1,2-ethanediamine was then used to nucleophilically attack the obtained hexyl 4-

methylbenzenesulfonate (**II**) in the presence of a base to afford N-hexyl-N,N'-dimethylethane-1,2-diamine (**III**) (Scheme 1).

Finally, the target compound (**I**) was formed by reacting the diamine (**III**) produced from the previous reaction with decanoic anhydride in the presence of the base triethylamine. The amine attacked one of the carbonyl carbon atoms of the anhydride, releasing decanoic acid which was neutralized by triethylamine, and ultimately produced N-(2-(hexyl(methyl)amino)ethyl)-N-methyldecanamide (**I**) (Scheme 1). The product was successfully purified by column chromatography and its structure was confirmed by a combination of Nuclear Magnetic Resonance (NMR) spectroscopy and high-resolution mass spectrometry (HRMS).



Scheme 1. Synthesis of compound **I**

3.1.2 Conformational Analysis of N-(2-(hexyl(methyl)amino)ethyl)-N-methyldecanamide (I)

Due to the restricted rotation around the C—N amide bond, the interconversion between the two conformational isomers of compound **I** (Figure 11) was expected to occur slowly enough so that they appear as separate sets of signals on an NMR spectrum. This was confirmed when the $^1\text{H-NMR}$ spectrum revealed double sets of peaks which, through the use of NMR techniques such as 2D-COSY and 2D-HMQC, were shown to correspond to the same group of protons. For example, although one singlet peak is expected to be produced by each of the two methyl groups in compound **I**, two singlets were observed for the ($\text{CH}_3\text{NC}=\text{O}$) methyl group protons and a doublet was observed for the (CH_3N) methyl group protons (Figure 12). The appearance of these peaks indicates that one pair of signals must correspond to the methyl groups in the *syn* conformation of the compound, while the other corresponds to those of the *anti* conformation.

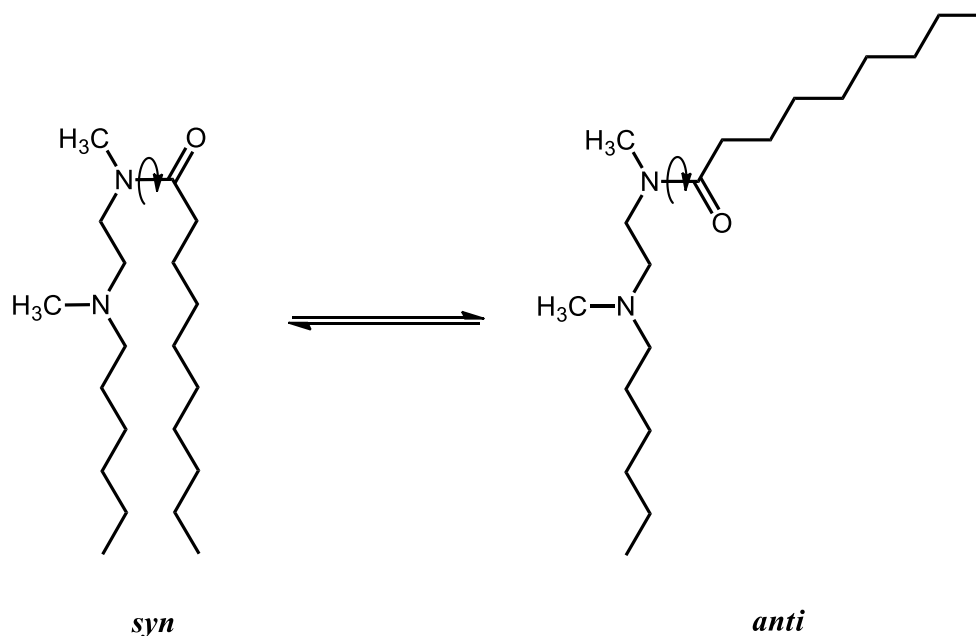


Figure 11. Equilibrium between the two conformers of compound **I**

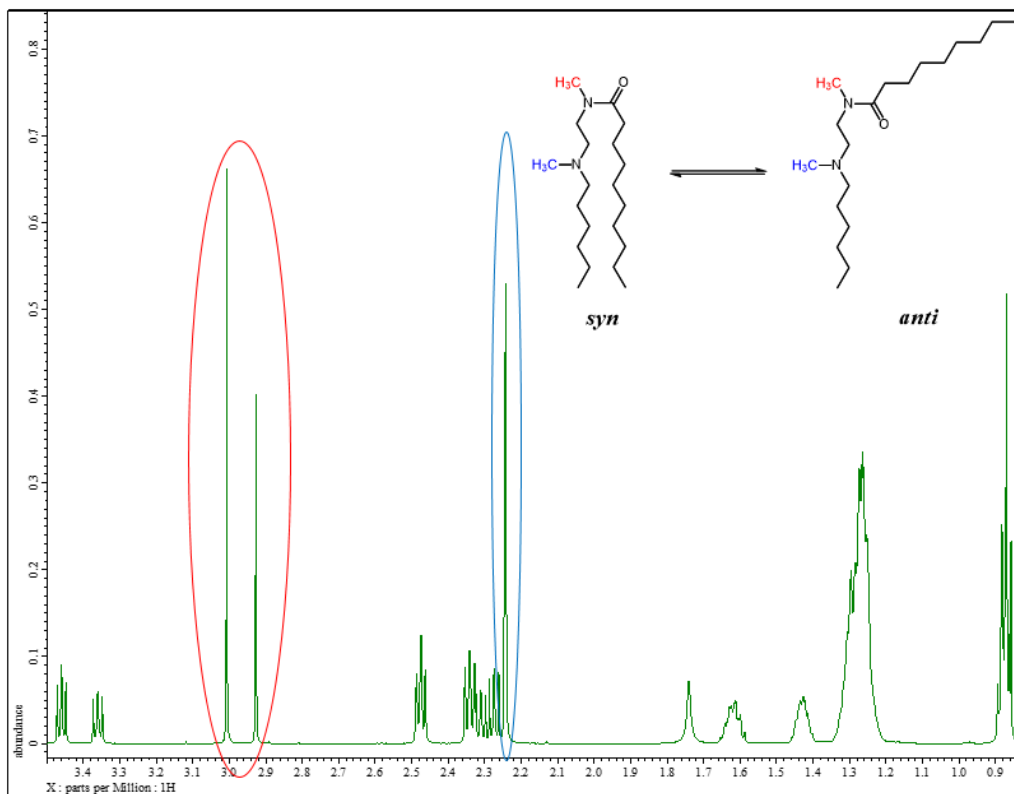


Figure 12. Observable separation of methyl group peaks of compound **I** ($\text{CH}_3\text{NC}=\text{O}$ methyl group proton signals circled in red, CH_3N methyl group proton signals circled in blue)

In addition, one pair of signals appeared more intense than the other in about a two-to-one integration ratio. This is most clearly demonstrated by the peaks produced by the protons on the methyl group directly attached to the amide nitrogen atom (Figure 13). Due to the reasons outlined in the following paragraphs, the more intense signal was expected to belong to the methyl group when it is in the *anti* conformation, and the smaller signal was expected to belong to that in the *syn* conformation. This determination was later supported by various NMR studies which are described in more detail below.

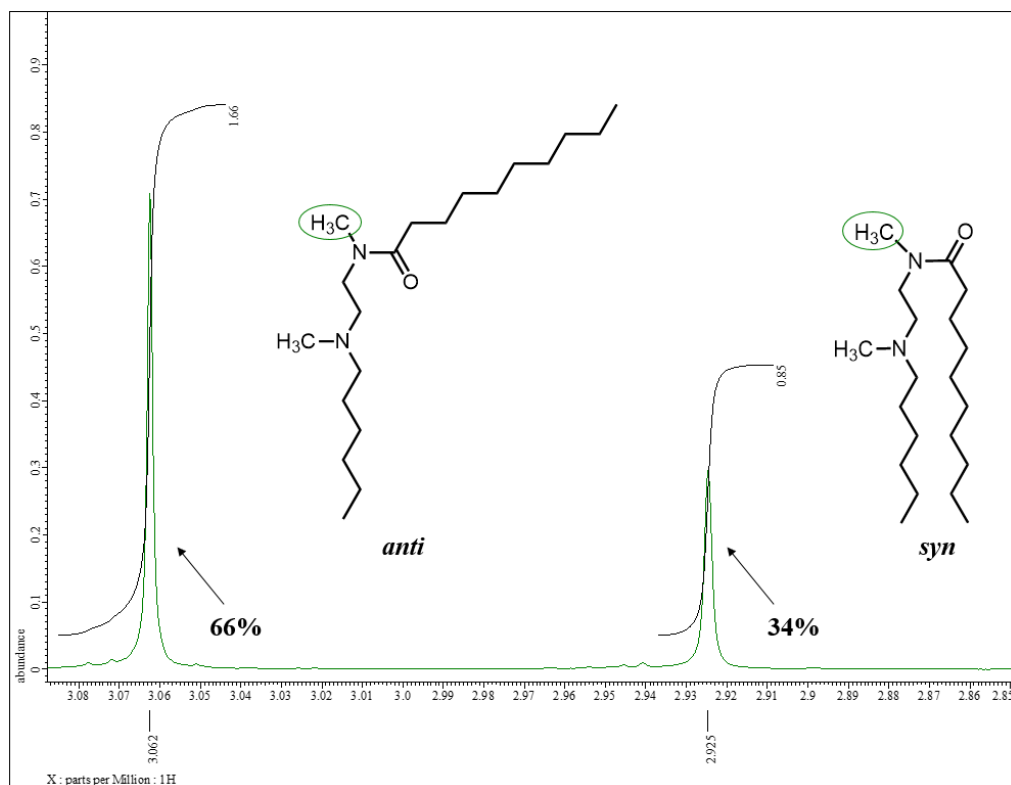


Figure 13. Section of a $^1\text{H-NMR}$ spectrum illustrating the separation of the $\text{CH}_3\text{NC}=\text{O}$ methyl group signals

The *anti* conformation was expected to produce the more intense signal in Figure 13 for a couple of reasons. First, the proximity between the two tails in the *syn* conformation causes them to repel each other and promote a shift in equilibrium to the *anti* isomer. In other words, the increased electrostatic and steric interactions in the crowded *syn* conformation cause the molecule to prefer to be in the *anti* conformation for longer periods of time. Second, the dipole moment across the amide bond³⁵ (Figure 14) depicts a partial positive charge on one side of the bond and a partially negative charge on the opposite side. The partially negative region has higher electron density at any given time, which produces a shielding effect on the surrounding protons.³⁶ In the *anti* conformation, the amide N-methyl group is directly on the positive end of the dipole, therefore the signal is expected to be less shielded and appear more downfield in the NMR spectrum. In the

syn conformation, the same N-methyl group is further from the positive end, so the signal is expected to be more upfield. Similar N-methyl group $^1\text{H-NMR}$ assignments have been made in the past for N-monosubstituted amides.³⁷

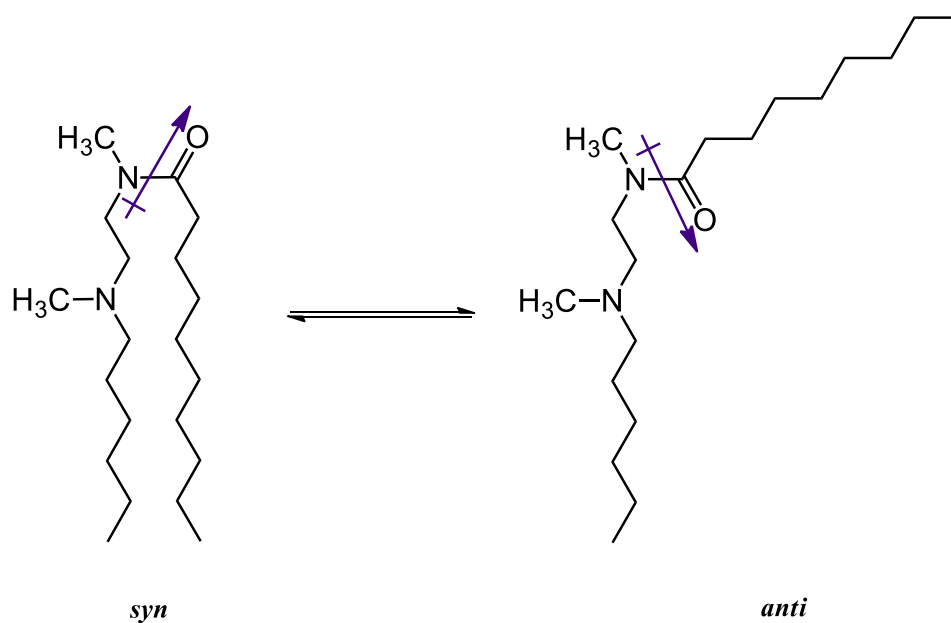


Figure 14. Equilibrium between the two conformers of compound I depicted with dipoles

In order to test this hypothesis, the NMR sample solution was titrated with small portions of a deuterated trifluoroacetic acid (*d*-TFA) solution in deuterated methanol (*d*-MeOH) and continuously monitored by $^1\text{H-NMR}$ spectroscopy. As expected, the integration values of one set of signals became higher as a function of increased acid concentration while the other set of signals became accordingly smaller (Figure 15). This data suggests that one of the conformations of the flipid becomes more prevalent in solution as the pH lowers, as should be expected of the *anti* conformation.

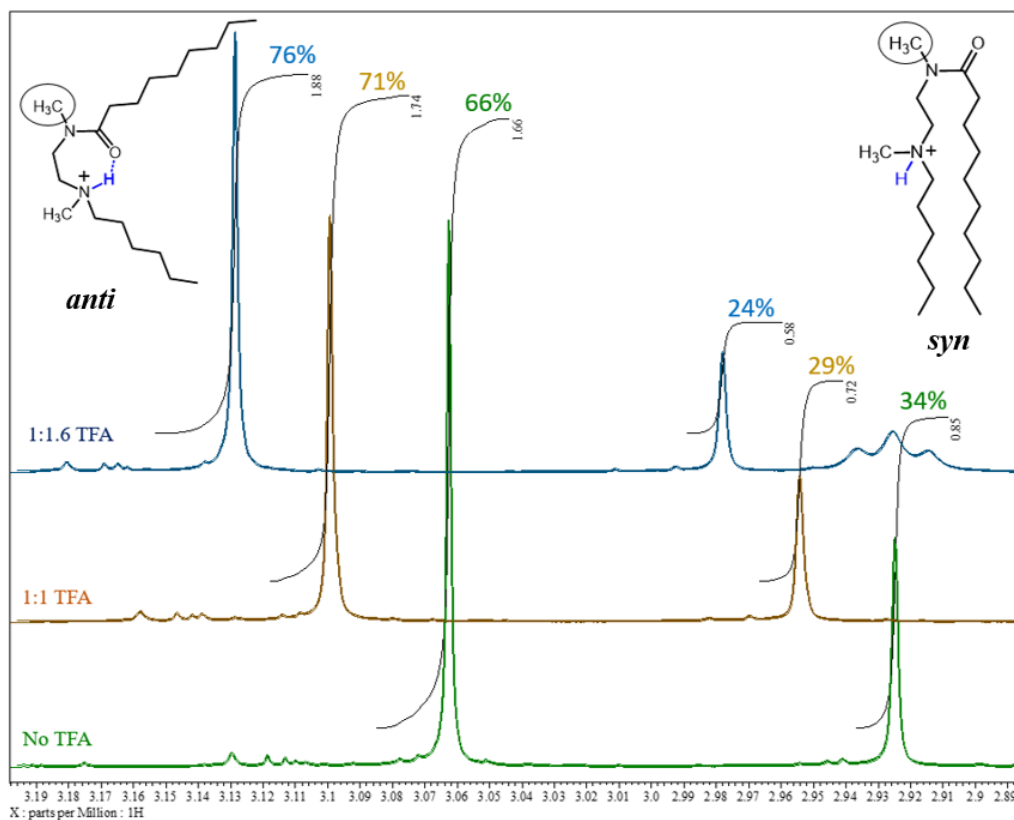


Figure 15. Effect of titrating compound **I** with *d*-TFA in a *d*-MeOH solution (ppm scales have been shifted to better show the different signals)

The integration values of the *anti* N-methyl peak (labelled **T** in Figure 13) and *syn* N-methyl peak (labelled **C** in Figure 13) were measured at each point of the titration to calculate the percentages of the two conformations present in solution. In order to best illustrate the effect of the addition of *d*-TFA, the percentage of the *anti* conformation present was plotted as a function of pH in Figure 16. The rest of the data from the titration of compound **I** can also be found below in Table 1 (also available in the Appendix).

The samples were titrated by adding small volumes of a 1.0 mM solution of deuterated trifluoroacetic acid (*d*-TFA) in *d*-MeOH using micropipettes, and the pH (in this case pD) was

measured once before running the sample in the NMR instrument and again after removing it from the instrument in order to calculate an average value. These values coincided within 0.1 units.

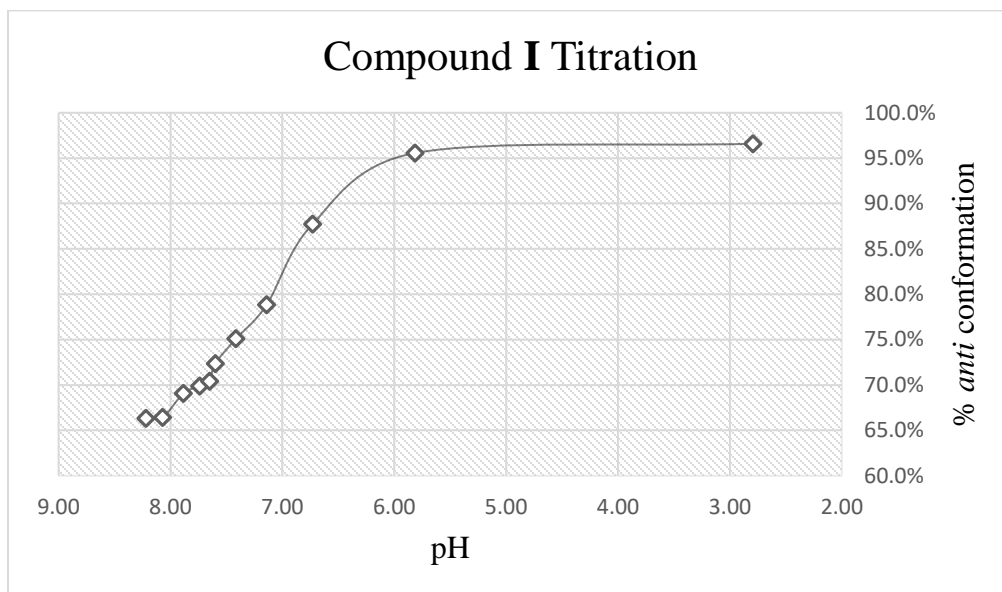


Figure 16. Graph depicting the percentage of the *anti* conformation of compound **I** present as a function of pH

Table 1

Titration Data for Compound **I**

TFA* Added (μL)	Total TFA* (μL)	TFA:Flipid Molar Ratio	Average pH	T (3.062ppm)	C (2.925ppm)	% <i>anti</i>
0.00	0.00	0.0 : 1.0	8.22	1.95	0.99	66.3%
7.00	7.00	0.2 : 1.0	8.07	1.92	0.97	66.4%
10.00	17.00	0.5 : 1.0	7.89	2.01	0.90	69.1%
7.00	24.00	0.7 : 1.0	7.74	2.04	0.88	69.9%
7.00	31.00	0.9 : 1.0	7.65	2.07	0.87	70.4%
10.00	41.00	1.2 : 1.0	7.60	2.12	0.81	72.4%
14.00	55.00	1.6 : 1.0	7.42	2.20	0.73	75.1%
14.00	69.00	2.0 : 1.0	7.14	2.31	0.62	78.8%
14.00	83.00	2.5 : 1.0	6.73	2.57	0.36	87.7%
14.00	97.00	2.9 : 1.0	5.82	2.80	0.13	95.6%
14.00	111.00	3.3 : 1.0	2.80	2.83	0.10	96.6%

*TFA refers to a 1.0 mM solution of deuterated TFA in *d*-MeOH

These findings suggest that an interconversion is occurring between the *syn* and *anti* isomers of the molecule in solution, and that this is happening slowly enough for the two conformations to be captured as separate signals in the proton NMR spectrum. If the interconversion were occurring too quickly for the NMR timescale to capture, then only one average set of peaks would be observed.³⁶ The fact that it occurs slowly is a result of the relatively high rotational barrier that restricts the rotation around the C—N amide bond.

However, the ¹H-NMR spectrum shown in Figure 13 which was produced before the addition of acid also shows a slight predominance of the *anti* conformation. This result is undesirable since an ideal flipid should have a predominance of the *syn* isomer in solution before the addition of acid in order to be able to make a large and significant conformational shift to the *anti* isomer. A significant shift from the amount of *syn* isomer to *anti* isomer is expected to have a large impact on the bilayer membrane of a fliposome structure and would thus be more likely to cause the membrane to rupture and allow the fliposome to release its contents. Therefore, the fact that the molecule already prefers the *anti* conformation is problematic.

3.2 Preparation of Liposomes

After synthesizing the pH-sensitive flipid model, it was incorporated into the bilayer membrane of a liposome and tested to see whether the induced conformational change would be enough to rupture the membrane and release the contents within the acidic environment/surroundings. Liposome preparation was commenced by mixing together the model compound **I** along with 1-palmitoyl-2-oleoyl-*sn*-glycero-3-phosphocholine (POPC), which is a phospholipid known to be able to form a liposome structure. N-palmitoyl-sphingosine-1-(succinyl[methoxy(polyethylene glycol)2000]) (C16 PEG2000 Ceramide) was also added to the mixture to form a coating around the membrane for steric stabilization of the liposome which

results in an extended half-life in blood circulation.³⁸ Four sets of liposomes were prepared by mixing POPC, compound **I**, and PEG Ceramide in molar ratios of 70:25:5, 45:50:5, 20:75:5, and 0:95:5 with agitation in a pH 8.5 aqueous solution of 50mM ANTS/DPX, 5 mM HEPES buffer, and 145 mM sodium chloride. The suspensions produced were frozen in -80 °C EtOAc/liquid nitrogen bath and then allowed to thaw and reach room temperature. This freeze/thaw cycle was repeated nine times in order to allow the components to come together into proper liposome structures through hydrophobic interactions. These liposome suspensions were subsequently extruded ten times through polycarbonate membranes with 200 nm diameter pores to yield a homogeneous liposome formulation, and then run on a Sephadex column using a 5mM HEPES buffer (pH 8.5) to obtain a suspension of the liposomes free of any ANTS/DPX. At this point, any ANTS/DPX present should be fully encapsulated by the liposome structures. The average sizes and size distributions of the liposomes were then determined by Dynamic Light Scattering (DLS) studies (See Table 2). A narrow size distribution is most desirable and is indicated by a low Polydispersity Index (PdI) value.

Table 2
Dynamic Light Scattering Data of the Different Liposome Formulations

POPC : Compound I : PEG* Molar Ratio	Temperature (°C)	Average Size (nm)	Polydispersity Index (PdI)	ζ potential (mV)
70 : 25 : 5 after extrusion	25.0	120.4	0.134	-0.634
45 : 50 : 5 after extrusion	25.0	125.2	0.206	0.450
20 : 75 : 5 after extrusion	25.0	84.15	0.369	-1.01
0 : 95 : 5 after extrusion	25.0	156.3	0.579	10.1

*PEG refers to C16 PEG2000 Ceramide

As is evident in Table 2, the amount of compound **I** introduced into the liposome structure results in the PdI values becoming larger, meaning that the size distribution of the liposomes

becomes larger. This can be an indication that incorporating too much of a foreign compound into the bilayer membrane can alter the stability of its formation. General trends can also be observed for the average fliposome size and ζ potential. The average size of the fliposomes seems to increase as the amount of POPC decreases which is likely due to POPC being able to form stable and more tightly-packed structures than the compound **I** molecules. The ζ potential also seems to increase as the amount of POPC decreases since POPC contributes to a negative charge on the surface of the fliposome membrane. As the amount of POPC in the membrane decreases, the charge becomes more positive. The only outlier that does not fit either of these trends is the 20 : 75 : 5 formulation. It is unclear why this set of data does not match the rest.

3.3 ANTS/DPX Liposome Leakage Assay

ANTS/DPX is a fluorophore/quencher pair and is one of the most frequently used marker pairs in testing membrane leakage and/or membrane fusion of vesicles.³⁹ In this case, it is used for evaluating the ability of the model lipid to successfully perturb the liposome membrane in response to changes in pH.

Once the liposomes are loaded with the solution, the restricted space inside the structures forces the fluorophore (ANTS) and quencher (DPX) to interact with each other and quench any fluorescence. Once this is achieved and the liposomes have been effectively extruded and purified on the Sephadex column, 100 μ L of each of the liposome preparations were transferred to a glass vial and dissolved in 2.9 mL of pH 8.5 HEPES buffer (5 mM HEPES + 145 mM NaCl). A set of samples were prepared for the four liposome formulations and were tested for fluorescence separately in cuvettes containing 50 μ L aliquots of the samples dissolved in 2 mL of pH 8.5 HEPES buffer, an assay that has been previously described by Guo *et al.*⁴⁰ and successfully employed recently for studies of fliposomes.^{22,23,41,42} The liposomes are expected to not exhibit any

fluorescence until the membrane has ruptured, which allows the release of ANTS and DPX. Once these molecules are released into the surrounding solution and allowed to diffuse freely into the solution, the fluorophore will no longer be quenched and fluorescence can be observed and accurately measured. In order to measure what the 100% leakage would yield in terms of fluorescence, 20 μ L of the detergent octaethylene glycol mono-n-dodecyl ether, which is known to fully disrupt any liposomal bilayer, were added to the samples at the end of each measurement. When this assay was attempted for the synthesized liposomes, however, fluorescence was already observed from the start before the addition of detergent. There was only a small increase in fluorescence after the suspensions were treated with the detergent, which suggests that most of the liposomes were likely already disrupted at the starting pH (Table 3).

Table 3
Fluorimetry Results for the Four Different Fliposome Formulations

POPC : Compound I : PEG* Molar Ratio	pH	% Leakage before addition of detergent
70 : 25 : 5	8.5	40
45 : 50 : 5	8.5	70
20 : 75 : 5	8.5	100
0 : 95 : 5	8.5	100

*PEG refers to C16 PEG2000 Ceramide

Since the 70:25:5 and 45:50:5 fliposome formulations presented the most promising results, new solutions of these formulations were prepared at different pH to study how this affected the leakage. Two sets of three solutions were prepared by dissolving 100 μ L of the liposome preparations in 2.9 mL of pH 4.5 acetic acid buffer (50 mM AcOH/AcONa + 145 mM NaCl), pH 8.5 HEPES buffer (5 mM HEPES + 145 mM NaCl), and pH 10.6 HEPES buffer (5 mM HEPES + 145 mM NaCl). The fluorimetry results are presented below in Table 4.

Table 4
The Effect of pH on the Fluorimetry Results

POPC : Compound I : PEG* Molar Ratio	pH	% Leakage before addition of detergent
70 : 25 : 5	10.6	33
70 : 25 : 5	8.5	41
70 : 25 : 5	4.5	52
45 : 50 : 5	10.6	74
45 : 50 : 5	8.5	76
45 : 50 : 5	4.5	81

*PEG refers to C16 PEG2000 Ceramide

As expected, the amount of leakage measured by the fluorimetry assay increases as the pH is lowered for both formulations. This supports our hypothesis that the lowering of pH can promote the protonation of compound I, thus forcing it to shift into the *anti* conformation and ultimately disrupting the bilayer membrane to induce the leakage of ANTS/DPX. However, all of the samples produced significant leakage before the addition of detergent even at pH 10.6 and were not able to achieve 100% leakage at a pH as low as 4.5. This suggests that the liposomes are already unstable at high pH and yet the lipid molecules are incapable of producing a disruption in the bilayer membrane that is significant enough to completely rupture the structure.

3.4 Factors Affecting Liposomal Leakage

There are a few major factors that affect liposomal leakage and may be directly or partially responsible for the results of the ANTS/DPX assay. These include the possibility of the tertiary amine being too strong of a base because the pK_a for the N,N'-Dimethylethylenediamine itself is reported to be 10.16.⁴³ This high basicity may prematurely promote the formation of a hydrogen bond and force the switch to the *anti* conformation, as well as the possibility of the conformational change being ineffective in drastically perturbing the membrane as previously predicted.

3.4.1 Basicity of the Tertiary Amine

One factor that may affect liposomal leakage may be the basicity of the tertiary amine embedded in one of the alkyl chain tails being too high. The previous $^1\text{H-NMR}$ analysis of compound **I** describes a situation in which the two conformers can be observed separately and the amount of the *anti* conformation relative to the *syn* conformation becomes higher as more acid is added. However, as shown previously in Figure 13 about 66% of compound **I** is estimated to be *anti* before the addition of acid while the other 34% is *syn*. An increased basicity may be a contributing factor for the abundance of the *anti* isomer.

The tertiary amine is responsible for the formation of the hydrogen bond that induces the conformational change. Therefore, if too basic, it may be prematurely protonated in certain solvents and result in the abundance of the *anti* conformation. Ideally, an initial high abundance of the *syn* conformation is desirable in order to have a more drastic steric effect when acid is added.

3.4.2 Overall Steric Effect of the Conformational Flip

The two main components of compound **I** are the relatively polar head amide group and the two alkyl chain tails. One major characteristic of saturated alkyl chains such as these is their very high flexibility. The single bonds that connect the carbon atoms to each other are almost freely rotating and when unhindered can result in a variety of shapes and types of movement for the tails.

Lipids are generally tightly packed in the bilayer membrane by hydrophobic interactions that cause the nonpolar tails to come together and shield themselves from the surrounding aqueous environment. Because compound **I** previously demonstrated the ability to convert to the *anti* conformation upon the addition of acid, it is speculated that the switch may be successfully occurring within the membrane of the liposomes as well, but the steric effect is just not drastic

enough to significantly disrupt and break the membrane apart. The decreased steric effect is thought to be a consequence of the flexibility of the lipid tails that, even though a switch may occur, are still able to keep the lipid bilayer together. This lack of rigidity is speculated to be able to cause a decreased steric effect by allowing the tails to still be relatively proximal to each other even after a successful conformational switch (Figure 17).

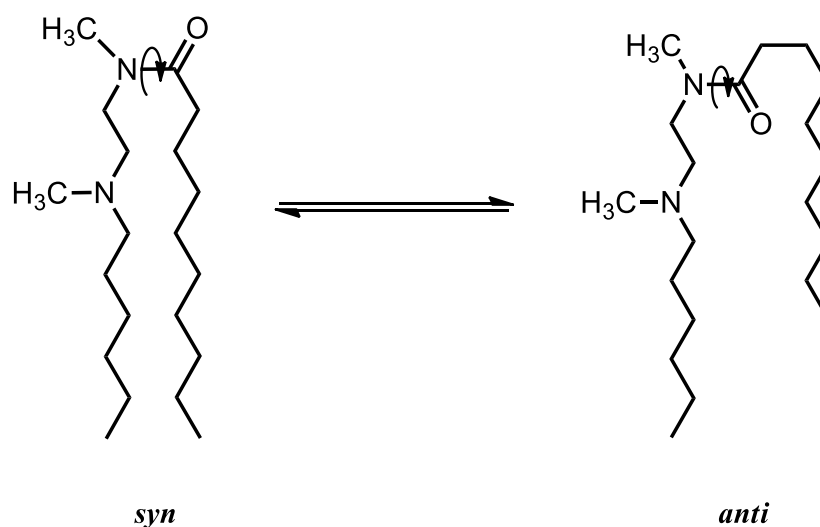


Figure 17. Conformational switch of compound I with decreased steric effect

Thus, the tails may have mostly remained embedded in the nonpolar region of the bilayer membrane and the conformational change may have failed to cause a drastic enough effect to disrupt the (now slightly less) efficient packing of the liposomal bilayer. Making the switch drastic enough to force the nonpolar tails of the individual lipid molecules far apart and thus alter the efficient packing of lipids in the bilayer membrane is not a trivial task.

3.5 Amide Model with Aryl Rings

In order to test if the rigidity of a flipid structure has a significant steric effect on the conformational flip, we synthesized a flipid model, N-methyl-N-(pyridin-2-yl)benzamide, that had been described previously by Okamoto *et al.*³⁰ and analyzed it by NMR. This model compound, henceforth referred to as compound **IV**, also includes an amide bond as the molecular switch, but instead of having long nonpolar alkyl chain tails, aromatic rings are directly attached to either side of the C—N amide bond. One of these rings is simply a phenyl ring, which is attached to the carbonyl carbon, while the other is a pyridine ring and is attached to the nitrogen atom of the amide bond at the *ortho* position. This position is important because it allows the pyridine nitrogen atom to be four bonds away from the carbonyl oxygen atom and form a six-membered ring structure upon protonation and the formation of a hydrogen bond. (Figure 18).

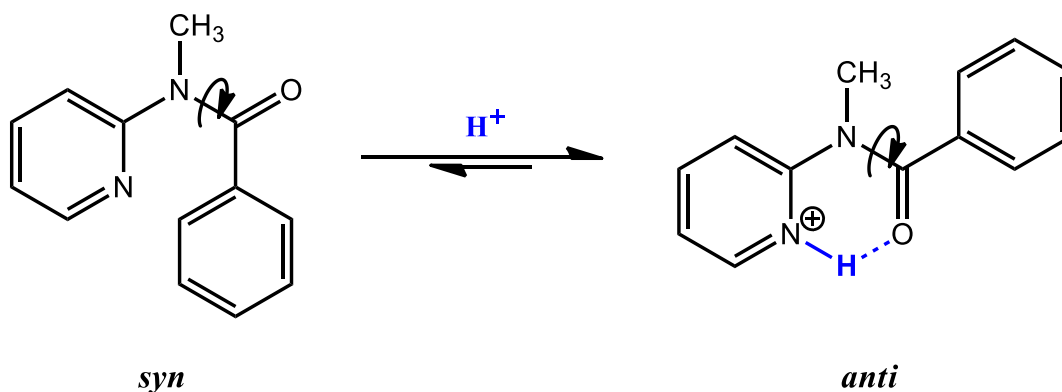


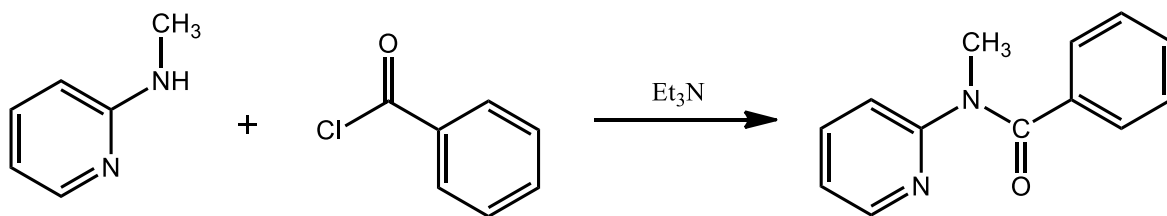
Figure 18. Conformational switch of compound **IV** (hydrogen bond shown in blue)

Okamoto *et al.* reported that this compound exhibited different ¹H-NMR peaks for the N-methyl group protons in the *syn* and *anti* conformations, and that the shift from *syn* to *anti* upon the addition of acid was monitorable by ¹H-NMR.³⁰ Therefore, we hypothesized that it may be

possible to synthesize a series of similar aryl ring amide compounds by adding tails to the *para* or *meta* positions of the aryl rings via ether linkages.

3.5.1 Synthesis of N-methyl-N-(pyridin-2-yl)benzamide (IV)

Compound **IV** was synthesized in a slightly different fashion from the previous alkyl chain model (**I**). The reaction involved the nucleophilic substitution of benzoyl chloride with 2-methylamino pyridine in the presence of a base. This resulted in the elimination of a chloride ion, which abstracted a proton to form hydrochloric acid. This was neutralized by the base and subsequently removed in the work-up steps. The product was successfully synthesized with a 33% yield (Scheme 2) and its identity/structure confirmed by NMR spectroscopy and mass spectrometry.



Scheme 2. Synthetic scheme for compound **IV**

3.5.2 Conformational Analysis of N-methyl-N-(pyridin-2-yl)benzamide (IV)

In accordance with compound **I**, we studied the conformation of compound **IV** by NMR spectroscopy. However, the ^1H -NMR revealed only one set of proton signals in standard conditions. This is most clearly elucidated by the single peak corresponding to the methyl group in the structure (Figure 19).

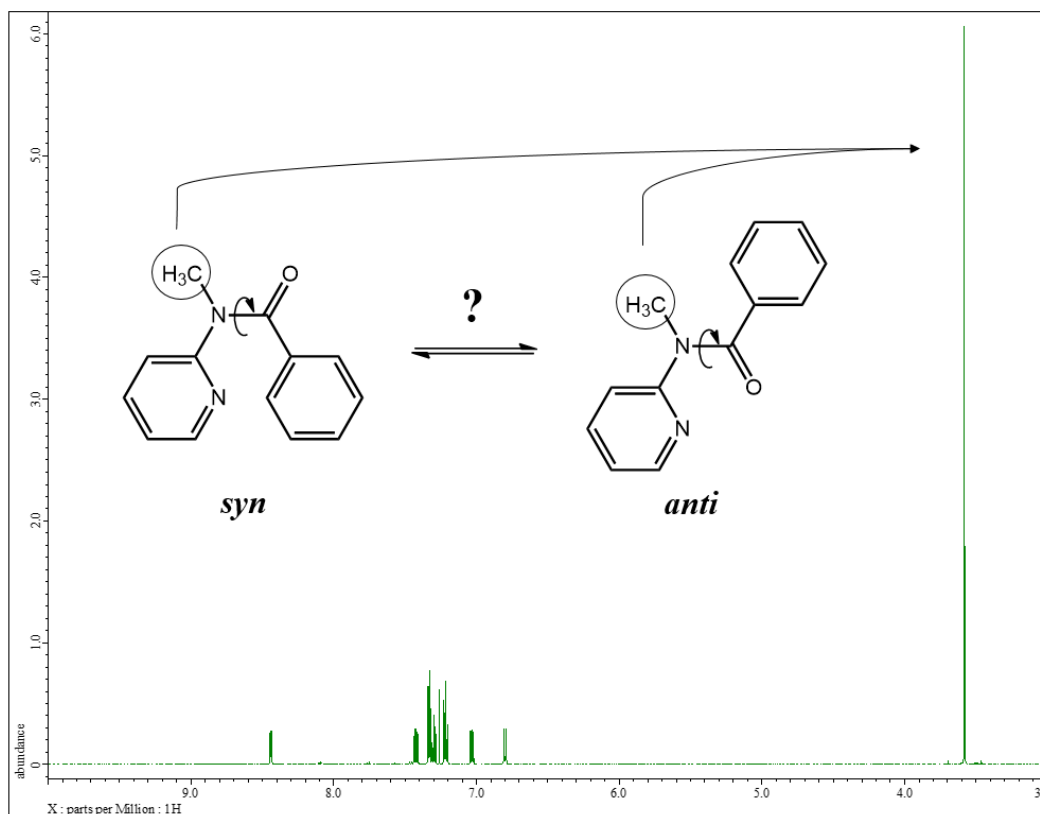


Figure 19. ^1H -NMR spectrum in $d\text{-MeOH}$ illustrating the lack of signal separation for the individual conformations of compound **IV**

This lack of signal separation indicates that the switch or interconversion occurring between the *syn* and *anti* conformations cannot be monitored by integration of signals in the NMR spectrum in standard conditions. In an attempt to replicate the Okamoto results,³⁰ varying amounts of *d*-TFA were added to the NMR sample solution to see if a distinction between the two conformations. However, contrary to what was previously reported,³⁰ the only effect produced was a shift in resonance frequency for the peak. Figure 20 clearly shows this phenomenon occurring with the N-methyl group of compound **IV**.

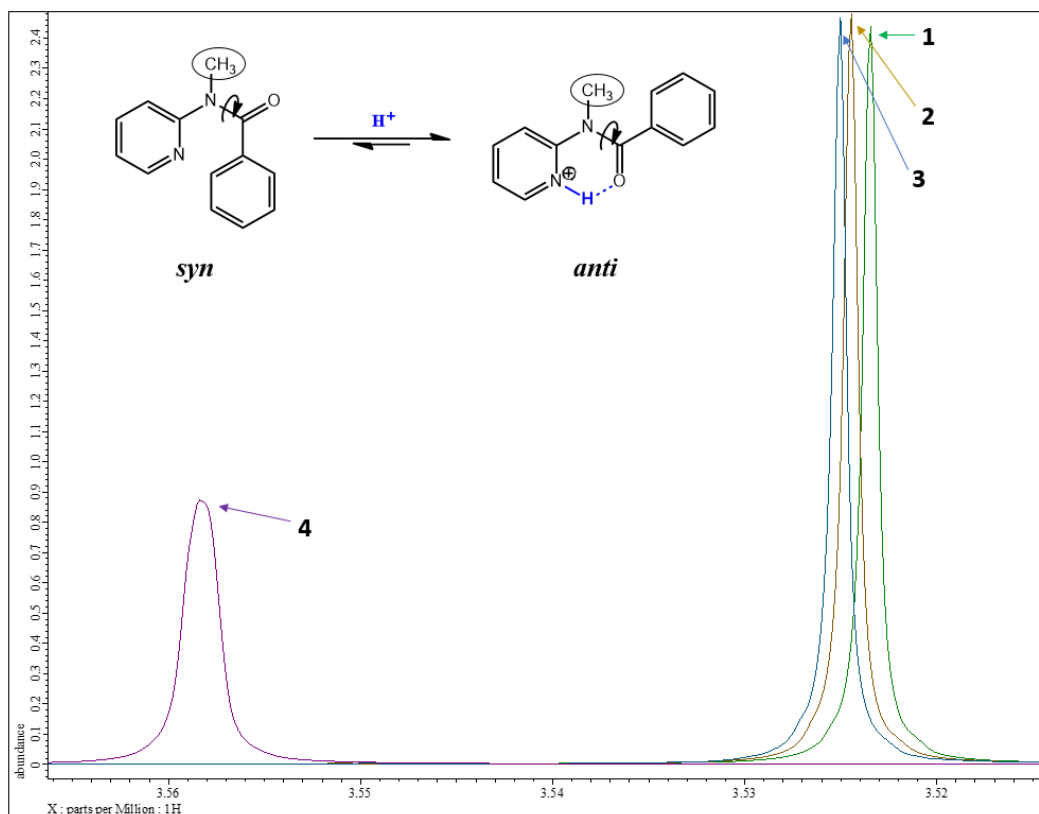


Figure 20. Effect of adding *d*-TFA to compound **IV** in *d*-TFA:**IV** molar ratios of 0.0:1.0 (**1**), 0.5:1.0 (**2**), 1.0:1.0 (**3**), and 50.0:1.0 (**4**)

One situation that may explain the lack of signal separation would be that the switch between conformations is not occurring at all. The addition of aromatic rings to the structure may have introduced some steric hindrance or more resonance-stabilization of the amide bond, both of which could result in an increase in the energetic barrier for the rotation around the bond. This unexpectedly high rotational barrier would prevent the conformational switching and would instead cause the compound to remain frozen in either the *syn* or *anti* conformation.

However, because the reaction likely yields a mixture of isomers, then one would expect the lack of interconversion to result in two distinguishable sets of signals in the ^1H -NMR spectrum,

especially for the methyl group protons because they are in quite different environments in the different conformations. This explanation can therefore be disregarded.

Alternatively, a rapid interconversion between the two conformations could explain the lack of separate signals. In this case, it may be that only one average set of signals would be observed in the spectrum, analogous to the rapidly interconverting chair conformations of cyclohexane.⁴⁴ This is also supported by some data presented in the same Okamoto paper that described the previous ¹H-NMR analysis of compound **IV**. In the paper, the researchers present the ¹H-NMR spectrum of a compound similar to compound **IV** except both rings are pyridine rings and the nitrogen atom on the amide bond is non-methylated. This compound also displayed a lack of signal separation between the two conformations at standard conditions, but the Okamoto group reported the successful separation of the conformations by performing variable temperature NMR studies and lowering the temperature in the NMR instrument. As the temperature decreased the signals became better separated and the distinction between conformations became increasingly clear.³⁰ This indicates that there was a rapid interconversion between conformations occurring for that particular compound, which leads us to believe that this may also be the case for compound **IV**.

3.6 NOE Studies

As mentioned in the introduction, NOESY is an NMR technique that can measure the interaction between nuclear spins that are in the same three-dimensional space even in cases when they are not directly connected through chemical bonds. It is very useful in the determination of three-dimensional structures and we were able to utilize it to determine whether both *syn* and *anti* conformations of the compound **IV** were present and rapidly interconverting in the solution.

3.6.1 NOESY Results of N-methyl-N-(pyridin-2-yl)benzamide (IV)

As shown below in Figure 21, the H^{O} protons are very close to the methyl group protons when the molecule is in the *anti* conformation but are a great distance apart in the *syn* conformation. Alternatively, the H^{O} protons are very close to the H^{3} proton of the pyridine ring in the *syn* conformation, but not in the *anti*. Therefore, a large NOE is expected to be observed for the H^{O} protons when irradiating the resonance frequency of the methyl group protons if the structure is in the *anti* conformation, and *vice versa*. Conversely, a large NOE is expected to be observed for the H^{3} protons by irradiating the resonance frequency of the H^{O} proton peak if in the *syn* conformation.

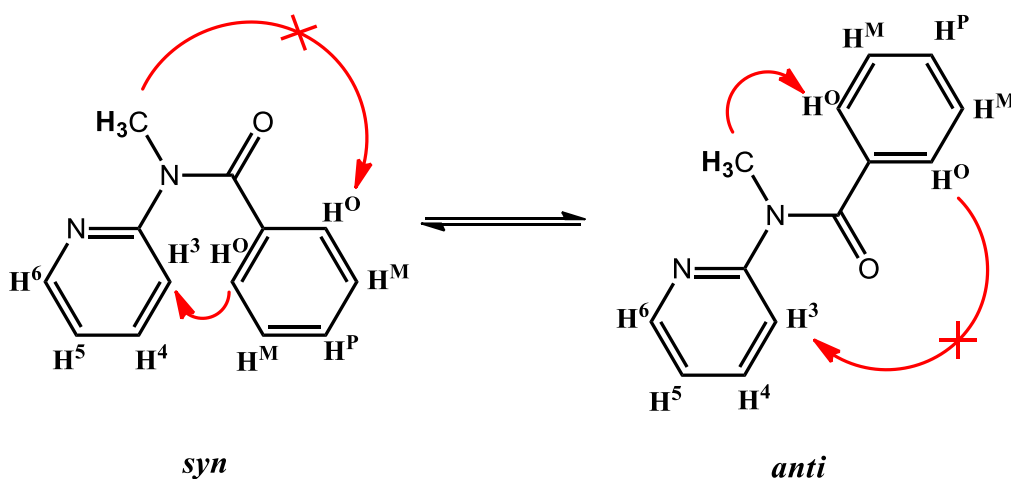


Figure 21. Labeled chemical structures of compound IV in the *anti* and *syn* conformations

The first experiment was conducted by irradiating the N-methyl group signal. As expected of the *anti* conformer, an NOE was observed for the H^{O} proton signal (Figure 22).

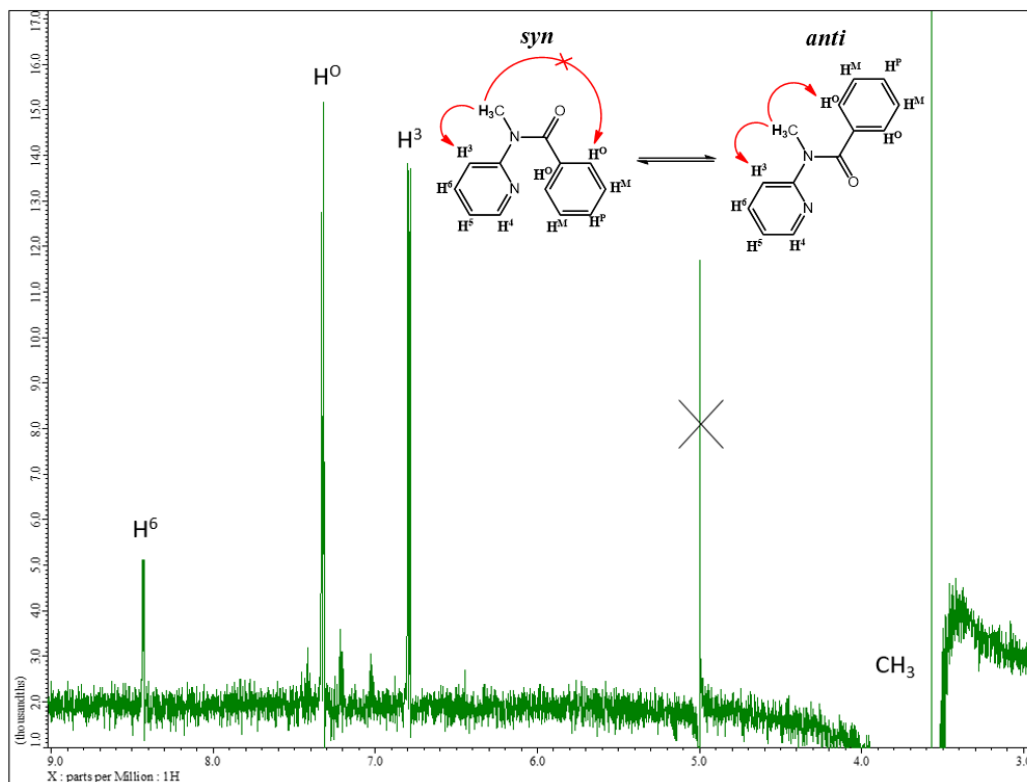


Figure 22. NOE produced upon irradiation of the N-methyl (**CH₃**) signal

This result may mean that the molecule is locked into the *anti* conformation. However, there may be a rapid interconversion occurring in solution because the presence of an NOE signal does not negate the possibility of the *syn* conformer also being present. In order to test whether or not the latter is occurring, the second experiment was conducted by irradiating the **H⁰** proton signal. This resulted in the appearance of an NOE for the **H³** proton and suggests that there is indeed a rapid interconversion occurring between the two conformations (Figure 23).

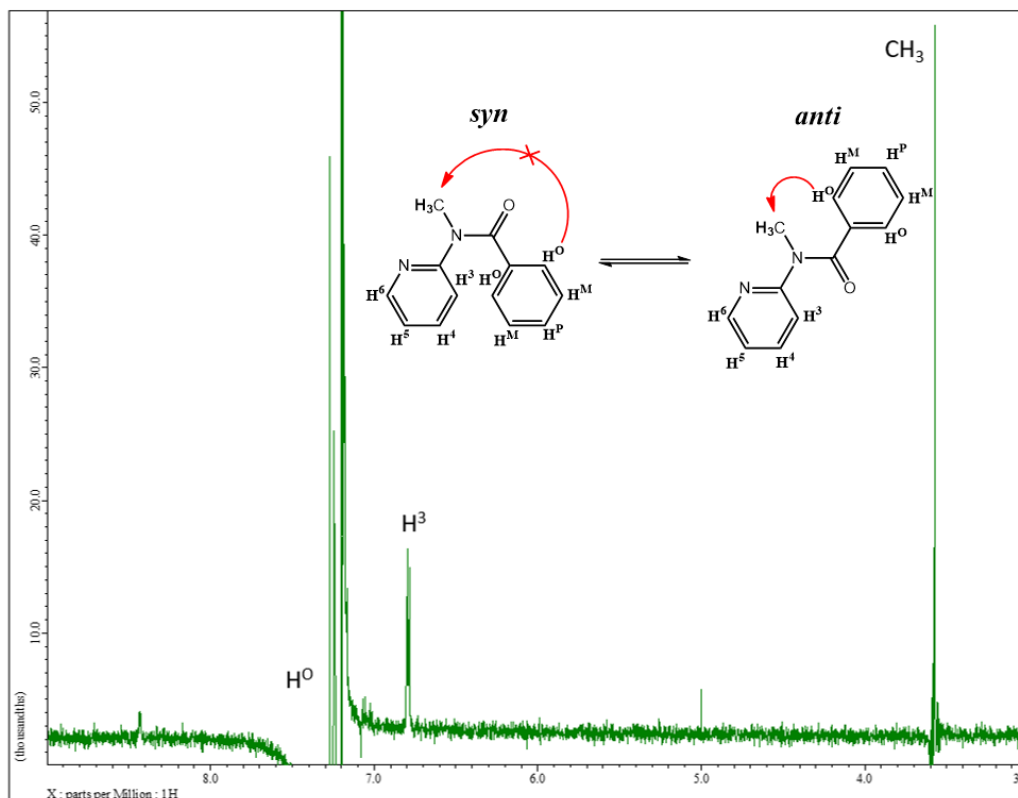


Figure 23. NOE produced upon irradiation of the $\mathbf{H}^{\mathbf{O}}$ signal

It is important to note that irradiation of the $\mathbf{H}^{\mathbf{O}}$ signal also produced an NOE for the methyl group protons (\mathbf{CH}_3), again suggesting the presence of the *anti* conformation, but the signal produced was much more intense than the NOE produced for the $\mathbf{H}^{\mathbf{3}}$ proton. Although NOESY does not provide any reliable quantitative information, it is reasonable that this clear difference in NOE signal intensity suggests that although there seems to be a rapid interconversion occurring between the two conformers, the amount of the *anti* conformer is still more prevalent in solution.

3.6.2 Disadvantages of NOESY

As mentioned previously, the major disadvantage of the NOESY technique is, arguably, the inability to quantify the data presented in the spectra. The intensities of the signals in the spectra do not accurately reflect the distance between nuclei. Therefore, not only is it impossible

to establish a *syn:anti* ratio for compound **IV**, the assumptions made regarding the prevalence of one conformer over the other must be taken with a grain of salt. In order to get a better idea of just how reliable and informative this technique is for this model, a series of additional NOESY experiments were conducted with compounds of similar structure.

The first compound studied was the commercially available N-methylbenzamide (Figure 24). If the assumptions made for compound **IV** are correct, then one would expect that irradiation of the signal for the protons on the *ortho* position of the phenyl ring (H^O) would result in an NOE from either the proton directly on the amide nitrogen atom (**N-H**) or the protons on the methyl group (**N-CH₃**). Both of these were observed, but also exhibited similar intensities. One would expect a preference for the conformation in which the methyl group and phenyl ring are facing away from each other (Figure 24), especially because it was reported that the N-methylation of the amide nitrogen atom promoted stabilization of the *syn* conformation of similar aryl ring compounds.⁴⁵ The NOESY results obtained for compound **IV** contradict that idea.

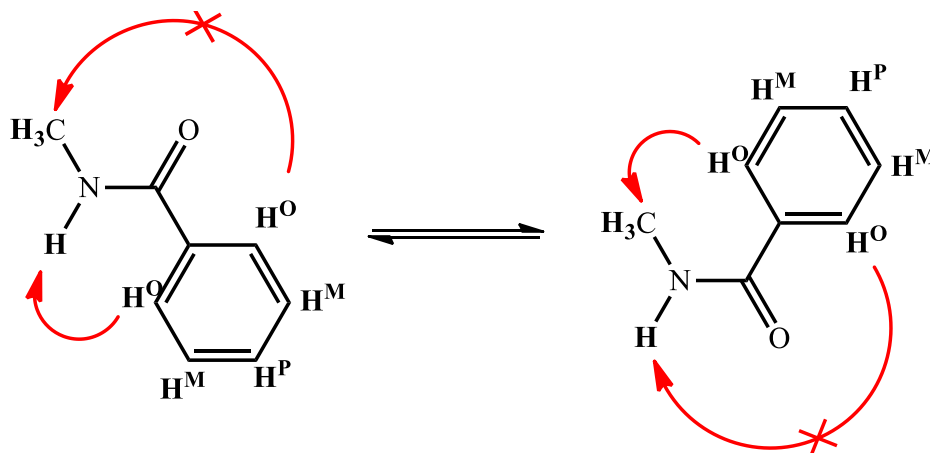


Figure 24. Molecular isomeric structures of N-methylbenzamide

The commercially available N,N-Dimethylacetamide was also analyzed by NOESY (Figure 25). This compound has been studied extensively in the past and it has been established that there is a restricted rotation around the C—N bond.^{46,47} However, upon irradiation of **C**, we observed NOE for both **A** and **B** at similar intensities. These observations indicate that at relatively short distances both NOE and the through-bond interactions may produce similar results, thus preventing the assignment of conformations.

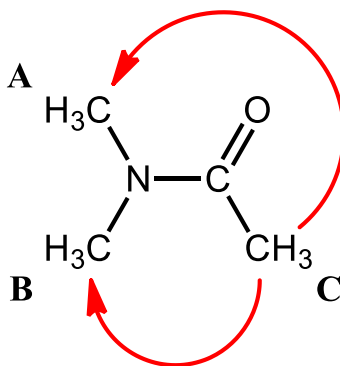


Figure 25. Molecular structure of N,N-dimethylacetamide

Finally, the commercially available N-methyl-2-pyrrolidone (Figure 26) was also analyzed in order to get a better idea of the NOE responses to be expected in the case of a conformationally-locked structure. For example, in this fixed ring structure, one would expect that the distance between the N-methyl protons and the protons on the α -carbon would be too great to produce any NOE between the two. However, irradiation of the α -carbon protons (shown in red) did produce a signal from the N-methyl protons and *vice versa* thus practically reproducing the results for N,N-dimethylacetamide (see above).

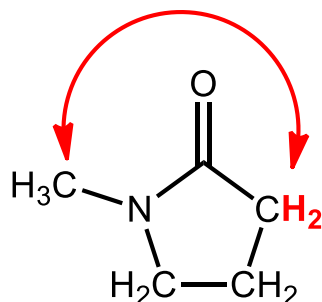


Figure 26. Molecular structure of N-methyl, 2-pyrrolidone

Therefore, the NOESY results obtained for Compound **IV** seem to be less reliable than previously thought. It still seems likely that there is a rapid interconversion occurring between the conformers, but it is unclear if there is a preference for one conformer over the other. The most convenient and reliable method of accurately measuring the ratio between two conformers is to compare the intensities of the signals from the separate isomers on a $^1\text{H-NMR}$ spectrum, as was done with compound **I**. In order to be able to do this, however, we sought a methodology to reduce the speed of interconversion down to a level where the two conformers would provide distinguishable signals in the $^1\text{H-NMR}$ spectrum.

3.7 Exploring the Rotational Barriers of Similar Diaryl Compounds

3.7.1 Reported Rotational Barrier Trends of Anilide Compounds

The recently published computational study of a range of anilide compounds included *para*-substituted derivatives similar to our models with various “electron-rich (NMe₂, OMe, Me), neutral (H), electron-withdrawing (NO₂, CN, COMe, CF₃), and halide (Br, Cl, F) substituents.³¹ In this study, the amidic resonance energies of these compounds were calculated and compared to each other. Resonance energy is defined as the difference in potential energy between a molecule of interest and the contributing resonance structure of the lowest potential energy.⁴⁸ Therefore,

molecules with higher resonance energies exhibit a decrease in the rate of rotation around the amide bond. The Szostak results show a very interesting trend in which a significant decrease in the resonance energy was calculated when the C-aryl ring was *para*-substituted with an electron-donating group (EDG) while the N-aryl ring was *para*-substituted with an electron withdrawing group (EWG) (Figure 27). The opposite also holds true in that a significant increase in resonance energy was calculated when electron withdrawing substituents were attached to the C-aryl ring and electron-donating substituents to the N-aryl ring.

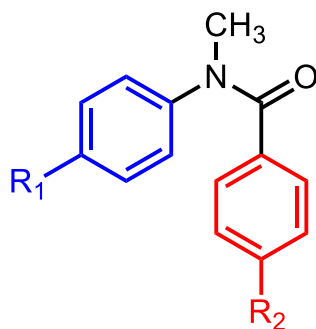
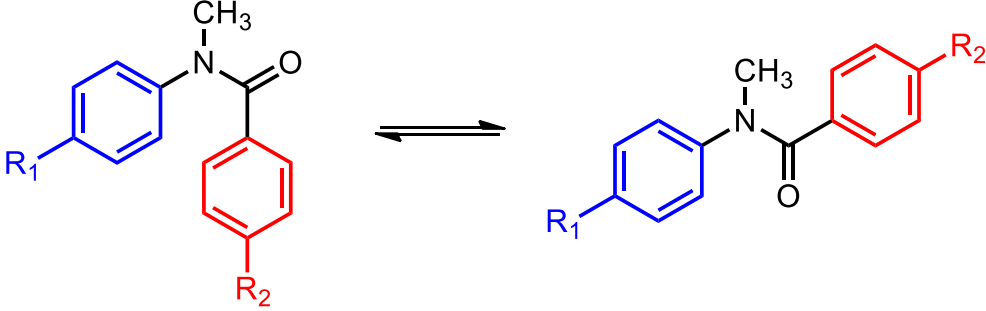


Figure 27. Anilide general structure with N-aryl ring (blue) and C-aryl ring (red)

Table 5 summarizes the calculated results of how much the resonance energy can be affected by varying the electronic effects of the substituents on two aromatic rings. According to the calculations, there should be about a 10 kcal/mol difference in the resonance energy between the two extremes.

Table 5

Calculated Resonance Energies for Various Anilide Compounds (Adapted From Szostak)³¹



R₁	R₂	Calc. Resonance Energies
4-NO ₂	4-NMe ₂	8.8 kcal/mol
4-CN	4-MeO	10.7 kcal/mol
4-MeO	4-CN	17.5 kcal/mol
4-NMe ₂	4-NO ₂	18.3 kcal/mol

Importantly, the idea that a rapid interconversion is occurring in solution for compound **IV** is corroborated by these resonance energy calculations.

3.7.2 Synthesis of p-Substituted Anilide Compounds

One of the questions that arose from studying the anilide compounds was “Can these increased rotational barriers restrict the rotation around the C—N bond enough to significantly reduce the speed of the interconversion and produce two sets of signals on the ¹H-NMR spectrum as was observed with compound **I**?” The computational results³¹ (see above) predict this possibility. In order to answer this question, we synthesized a series of four anilide compounds and analyzed them by ¹H-NMR spectroscopy. Two of the four compounds were inspired by some of the compounds studied in the Szostak study and consisted of structures that had EWG’s on the C-aryl rings and EDG’s on the N-aryl rings.

The rapid interconversion was only one of the issues that had to be addressed in order to successfully synthesize a potential lipid molecule, however. Besides being able to observe separate peaks on a ¹H-NMR spectrum for more complete and quantifiable data, it is also

imperative that the structure be initially locked in the *syn* conformation to accurately resemble a lipid-like structure. The Szostak study reported that such structures actually preferred the *anti* conformation due to the repulsion of the two large aromatic rings.³¹ On the other hand, as previously mentioned, the N-methylation of the amide nitrogen atom has been reported to promote stabilization of the *syn* conformation of similar compounds⁴⁵ (Figure 28).

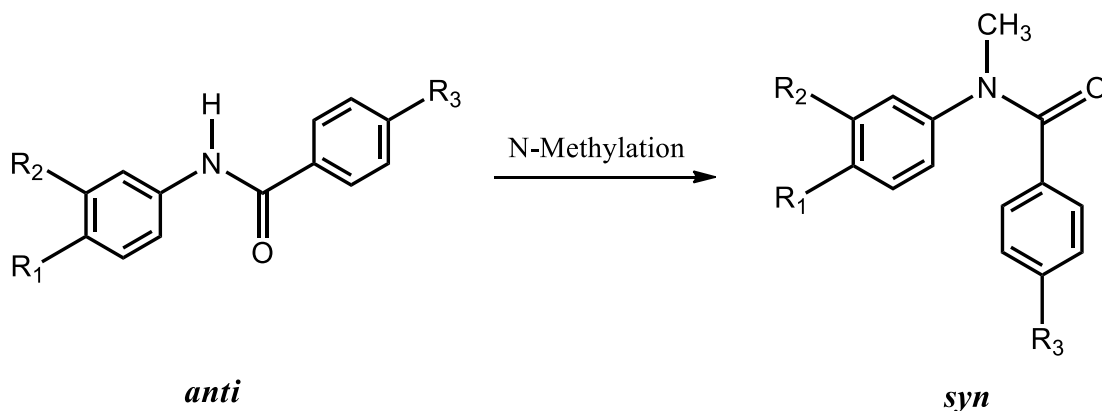


Figure 28. *syn*-Favored conformation of anilides upon N-methylation of amide nitrogen

Therefore, the next set of compounds was designed to test if: (1) the rapid interconversion could be hindered by varying the electronic effects imposed by the aromatic rings on the amide bond, and (2) if the inclusion or removal of the amide methyl group had any effect on either the speed of interconversion or the initial conformational preference. The structure of the new set of compounds is shown in Figure 29.

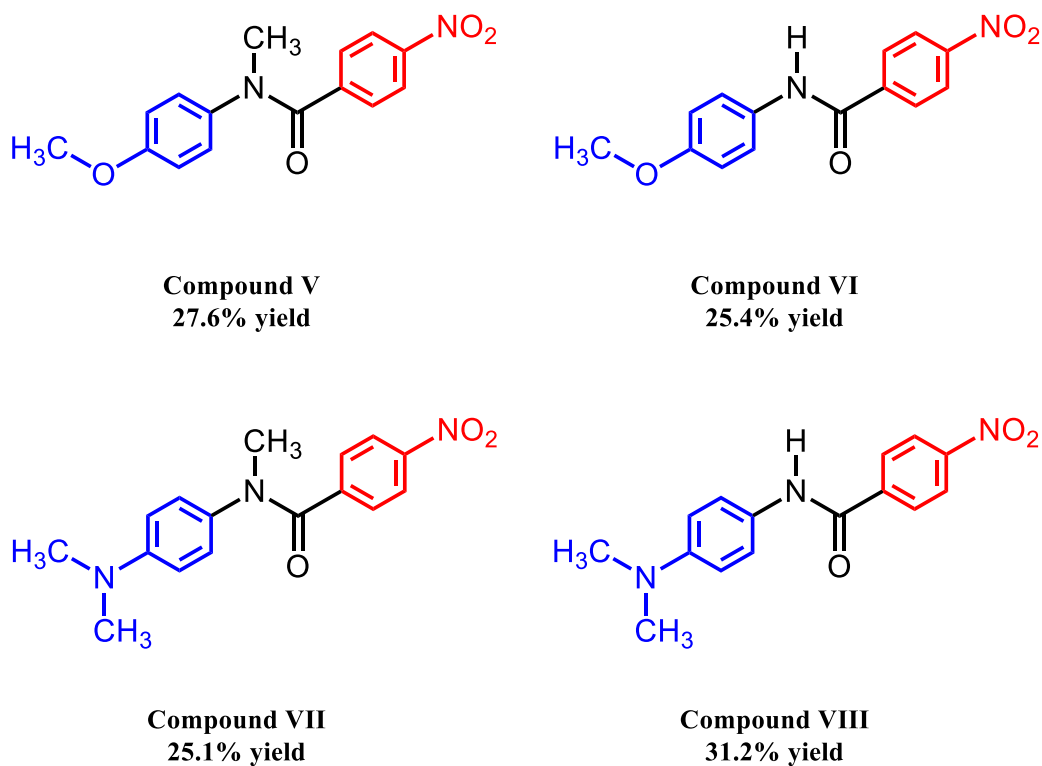
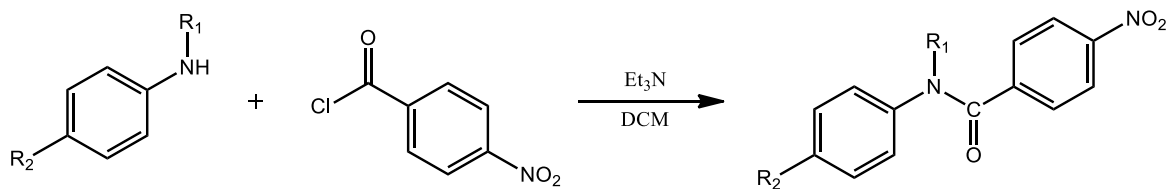


Figure 29. Set of *p*-substituted anilide compounds synthesized for conformational analysis

These compounds were synthesized in a very similar manner to compound **IV** by acylation of the amine nitrogen atom of *p*-anisidine, *N,N*-dimethyl-*p*-phenylenediamine, *p*-methoxy-*N*-methylaniline, or *N,N,N'*-trimethylbenzene-1,4-diamine by *p*-nitrobenzoyl chloride in the presence of excess base. The role of the base was to neutralize the hydrochloric acid that was formed as a byproduct of the reaction. The products were successfully synthesized and confirmed by NMR spectroscopy and mass spectrometry (Scheme 3).



Scheme 3. General synthetic scheme for compounds **V-VIII**

3.7.3 Conformational Analysis of *p*-Substituted Anilide Compounds

All four of these compounds were first analyzed by $^1\text{H-NMR}$ spectroscopy but, unfortunately, none of them produced separate proton signals for the *syn* and *anti* isomers. Even the structures calculated to have the highest increase in rotational barrier in the Sztosak study³¹ were unable to significantly decrease the speed of the interconversion between conformers to allow for a separation of the NMR signals.

NOE studies were performed on these compounds and seemed to show that N-methylation of the amide nitrogen atom may result in a noticeable amount of the *syn* conformation present in solution.

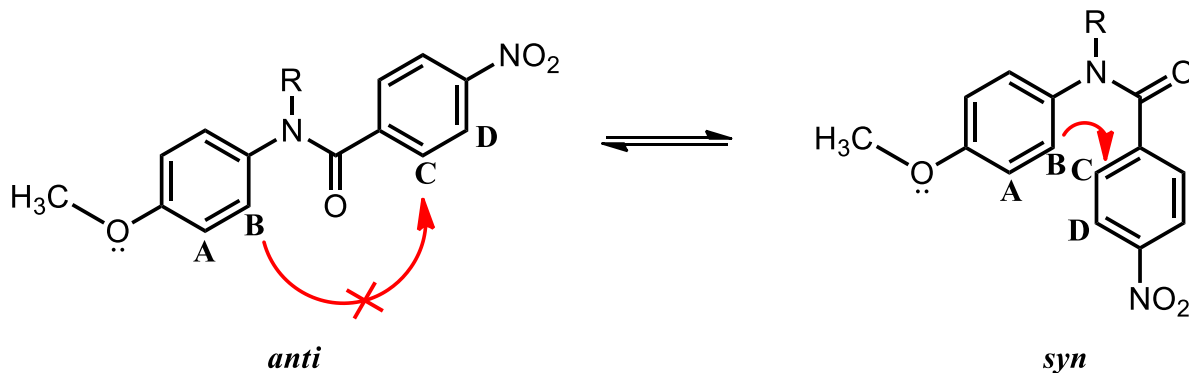


Figure 30. Expected NOE response from proton **C** (in *syn* conformation)

No NOE at all was observed from proton **C** after irradiation of the proton **B** signal (Figure 30) in the compounds **VI** and **VIII** that are non-N-methylated, which would suggest that the molecules are entirely in the *anti* conformation. This supports what has been previously reported by Okamoto *et al.*³⁰ that the *anti* isomer is naturally more abundant and stable for such structures.

When the N-methylated compounds **V** and **VII** were analyzed by NOESY in the same fashion, a small NOE was observed for proton **C** (Figure 31). Again, this result does not provide any quantitative information but, qualitatively, it attests for a noticeable contribution of the *syn* form to the equilibrium.

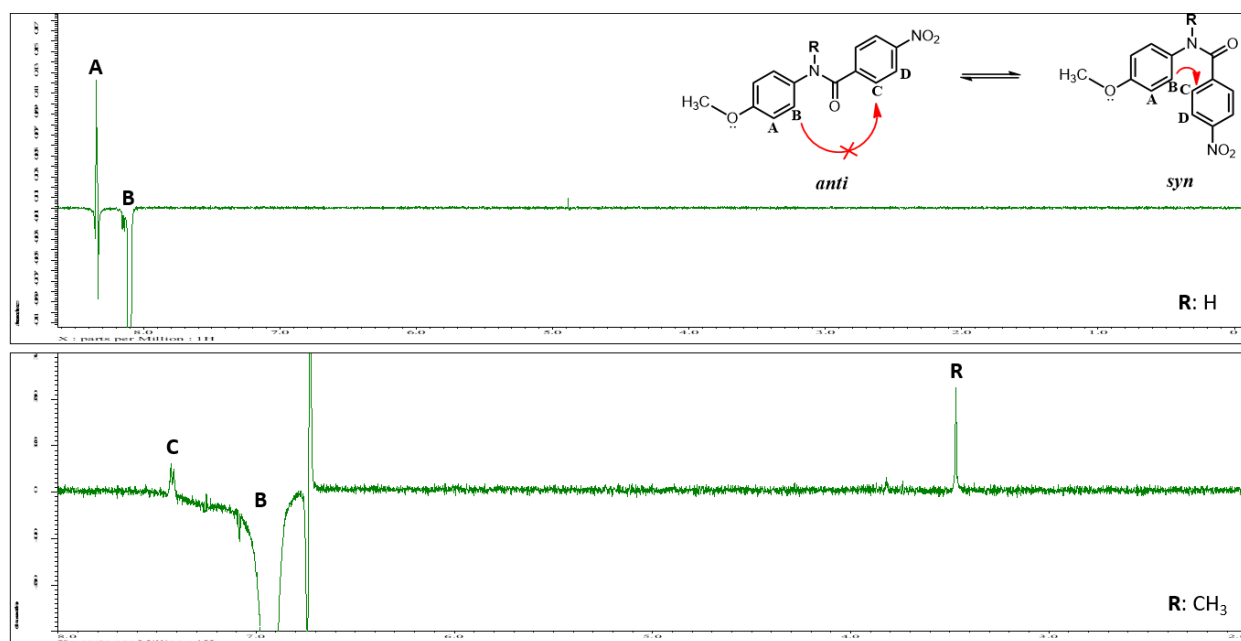


Figure 31. NOE results depicting the appearance of a response from proton **C** exclusively in the N-methylated anilide compounds

3.8 Comparative Evaluation of the Alkyl Chains and Aryl Rings Models

Upon comparison between the alkyl chain and aryl ring amide switch model compounds, it becomes evident that they behave quite differently but each have their advantages and

disadvantages as a scaffold for potential flipid models. The alkyl chain model, compound **I**, is an attractive candidate because it was shown to switch between the *syn* and *anti* conformations in solution. More importantly, it allows for the direct observation of the separate conformers using $^1\text{H-NMR}$ spectroscopy. On the other hand, the prevalence of the *anti* conformation before any addition of acid poses a problem and hinders the ability of the flipids to undergo a drastic enough conformational change to significantly disrupt the membrane of a liposome to the point where it releases the liposomal contents.

The aryl ring model, compound **IV**, displays an increased rigidity in the molecular structure of a potential flipid, which should produce a much more pronounced steric effect upon switching conformation. Unfortunately, the inability to observe the two conformers using $^1\text{H-NMR}$ in standard conditions severely minimizes the amount of available information and quantitative data that is necessary to study the behavior of these molecules. In addition to this, there is still a problem regarding the prevalence of the *anti* conformation before the addition of acid, likely caused by the repulsion of the two large aryl rings being in such close proximity to each other in the *syn* conformation.

Therefore, an intermediate model that can include both the ability to increase the rotational barrier enough to distinguish separate isomers using $^1\text{H-NMR}$, and a relative increase in rigidity from compound **I** is desirable. It is also necessary to reintroduce an amine of suitable pK_a in the structure in order to be able to produce flipid molecules that can actually induce a shift in equilibrium to the *anti* conformation by forming a hydrogen bond lock upon addition of acid.

3.9 Hybrid Amide Flipid Model

Taking these desirable qualities into account, as well as the previous drawbacks, a new set of amide-switch flipid molecules were synthesized and characterized. In order to regain the ability

to monitor the equilibrium between conformations via $^1\text{H-NMR}$, and to eliminate the steric strain produced by having two aryl rings intramolecularly repelling each other, one of the rings from compound **IV** was replaced with a simple alkyl chain tail. Conversely, the other aromatic ring was replaced with a heterocyclic nonaromatic amine that contains a nitrogen atom five bonds away from the carbonyl oxygen atom of the amide moiety in order to be able to form a stable seven-member ring structure upon protonation and formation of a hydrogen bond. The heterocyclic ring was also not directly attached to the amide bond as was the case with compound **IV** but was instead connected to the amide bond through a dimethylene bridge in order to produce a slightly more elongated tail structure (Figure 32).

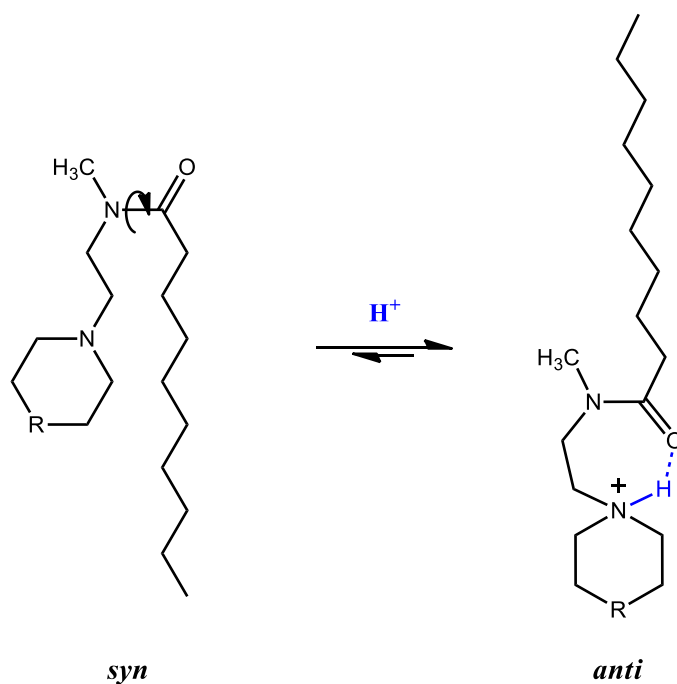
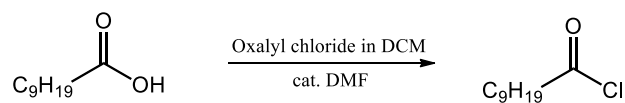


Figure 32. General structure and conformational switch for the hybrid model compounds

3.9.1 Synthesis of the Hybrid Models

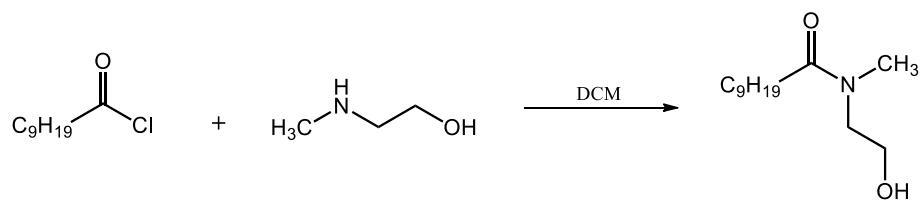
These alkyl chain/ring hybrid models were synthesized by reacting a carboxylic acid with an amine to produce the amide bond. Decanoic acid was utilized as the carboxylic acid in order to be able to have a relatively long nine-carbon chain tail, and the amine used was (N-methyl)-aminoethanol in order to introduce the dimethylene bridge with the ethanol component. The carboxylic acid is first activated via a halogenation reaction with oxalyl chloride to facilitate the nucleophilic attack by the amine. Then, a nitrogen-containing heterocycle was attached to the dimethylene bridge by first converting the hydroxy group of the ethanol moiety into a good leaving group by tosylation and then allowing the heterocyclic ring to displace the tosyloxy group via nucleophilic substitution (Scheme 4). The heterocyclic rings morpholine, piperidine, and N-methylpiperazine were used to produce three different models, compounds **XII**, **XIII**, and **XIV** respectively (Figure 33).

Step 1



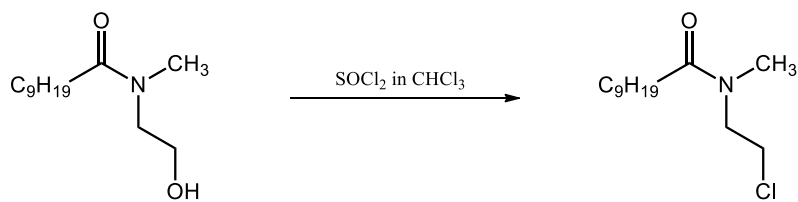
(IX)

Step 2



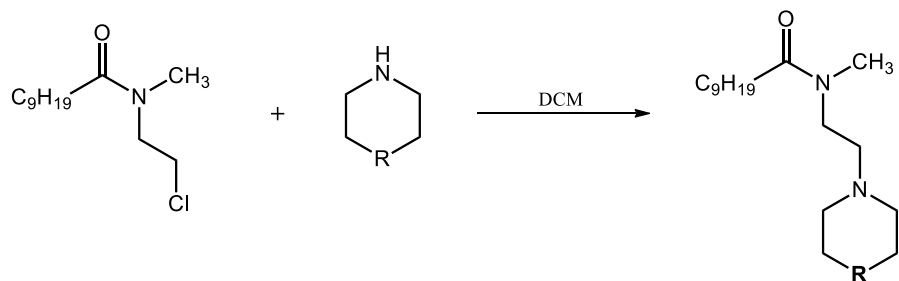
(X)

Step 3



(XI)

Step 4



R = O, CH_2 , N- CH_3
(XII, XIII, XIV)

Scheme 4. General synthetic scheme for compounds IX-XIV.

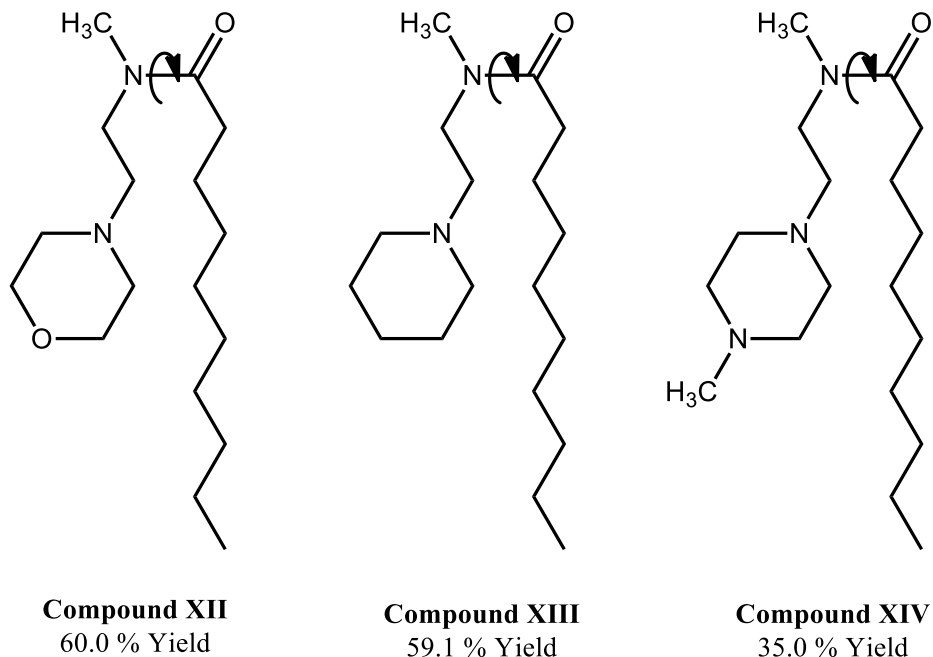


Figure 33. Molecular structures for compounds **XII** – **XIV**

3.9.2 Conformational Analysis of the Hybrid Models

The three model compounds were successfully synthesized and analyzed by $^1\text{H-NMR}$ spectroscopy. Fortunately, it became immediately clear that one of the goals for these compounds was achieved in that the $^1\text{H-NMR}$ spectra for all three compounds showed two distinct sets of signals, in particular the signals for the N-methyl protons on the separate conformers. In other words, it was possible to directly observe and measure the ratio between the two conformations.

In addition, small consecutive additions of *d*-TFA to the NMR samples revealed that lowering the pH of the solution effectively induced a shift in equilibrium to the *anti* conformation (Figure 32). This strongly supports the idea that an equilibrium between conformations was occurring in solution and that the heterocyclic rings were being protonated and inducing the conformational switch.

Unfortunately, the spectra also still revealed a preference for the *anti* conformation of the three molecules even before the addition of acid. The removal of one of the ring structures from the molecules, in combination with ensuring that the amide nitrogen atom was methylated and reducing the steric strain around the amide bond by distancing the heterocyclic ring with a dimethylene bridge, was evidently not enough to promote a complete shift in equilibrium to the *syn* conformation as desirable. The *syn:anti* ratios for the piperidine, morpholine, and N-methylpiperazine models were all about 1 : 2. It may be possible that this continued preference for the *anti* isomer was a result of some steric hindrance or repulsion between the two tails.

Despite this, the three model compounds were also tested for their pH-sensitivity by subjecting them to acid-base titration studies. As was the case with the compound **I** titration results, the signals for the *anti* conformation were expected to become more intense as more *d*-TFA is added while the *syn* signals become less intense.

3.9.3 Acid-Base Titration Studies

The first compound that was titrated was compound **XII**. In consistency with the titration of compound **I**, compound **XII** was dissolved in *d*-MeOH and treated with several small amounts of a 1.0 mM solution of *d*-TFA in *d*-MeOH with intermittent analysis by ¹H-NMR spectroscopy. The separation of peaks for the two conformers is best illustrated by the proton signals for the N-methyl group (See Figure 34).

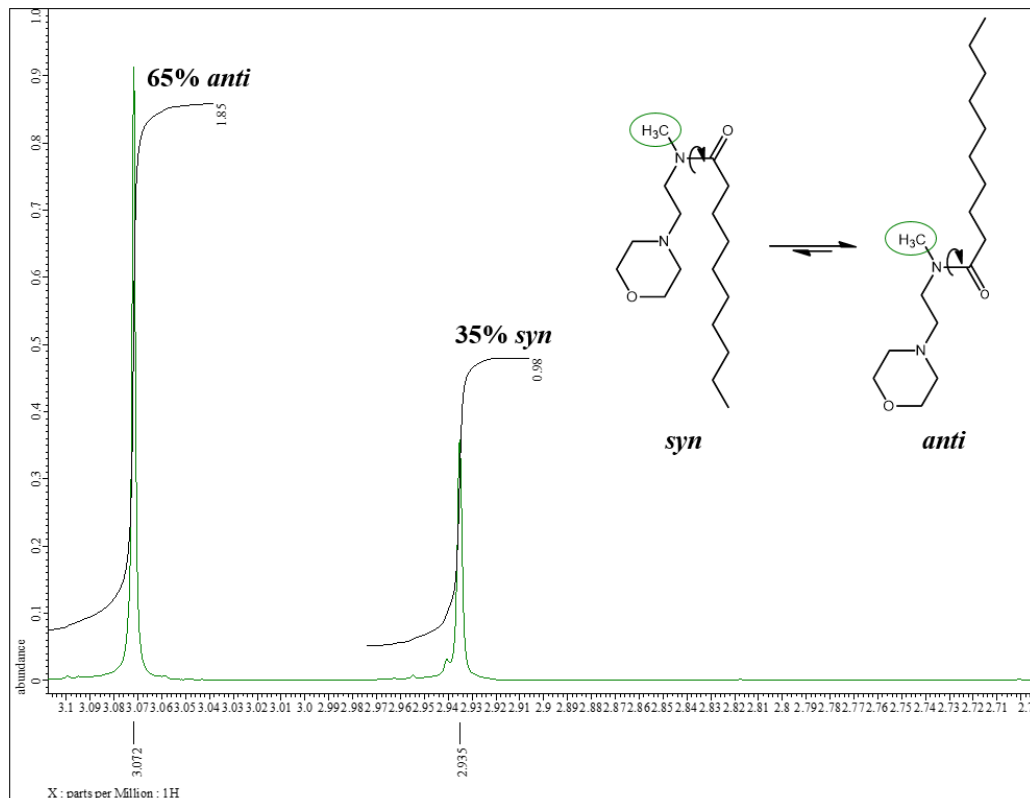


Figure 34. Portion of $^1\text{H-NMR}$ spectrum for compound **XII** depicting the N-methyl group protons in the two conformations before addition of acid

The results from the titration with *d*-TFA can be found below in Figure 35 where the measured percentage of the *anti* conformation present in solution is plotted against the pD. The percentage of the *anti* conformation (% *anti*) was estimated from the integration values of the $\text{CH}_3\text{N}(\text{C}=\text{O})$ group peaks in the $^1\text{H-NMR}$ spectrum (Figure 34). The numerical data can be found in Table 6 (See Appendix). As was observed with compound **I**, there is also an abundance of the *anti* isomer of compound **XII** before the addition of acid. The addition of acid does promote a further shift in equilibrium and seems to reach a maximum at around 93% *anti* conformation. This illustrates that the switch is pD-sensitive.

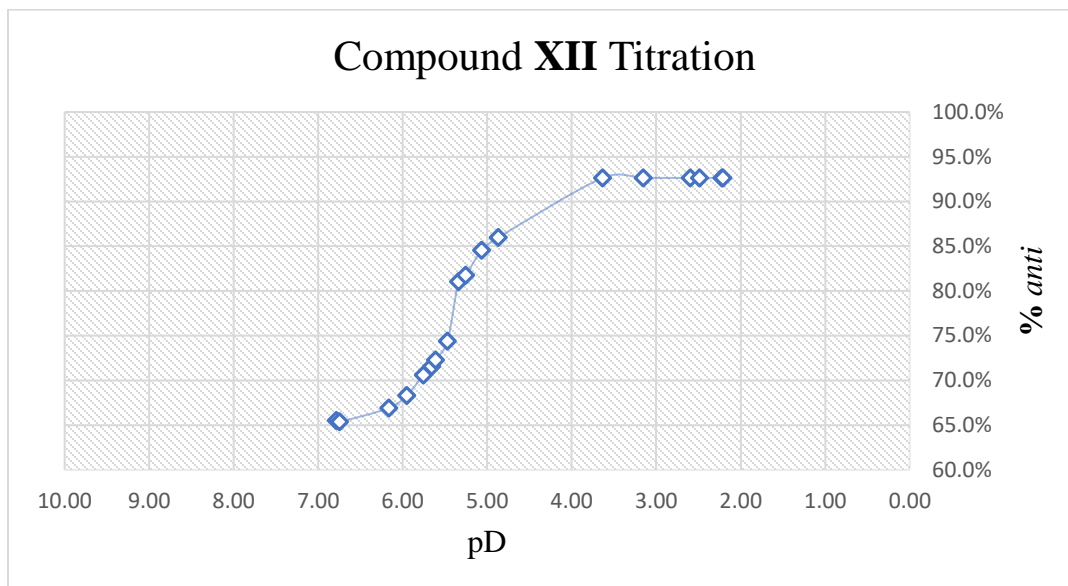


Figure 35. Percentage of the *anti* conformation of compound **XII** plotted as a function of pD

According to the Henderson-Hasselbalch equation, the concentration of the conjugate acid and the base is equal when the pH is equal to the pK_a .⁴⁹ In other words, at this specific pH, or pD in this case, half of the lipid molecules are protonated while the other half are not. Since the protonated forms of the molecules are fully expected to be in the *anti* conformation and the titration curve from Figure 35 represents a shift from the *syn* conformation to the *anti* conformation with decrease of pD, the curve can also serve as a means to monitor the shift from non-protonated to protonated molecules. Therefore, the midpoint of the curve serves as a good estimation for the pK_a ⁵⁰ of the conjugate acid of compound **XII**, which can also be referred to as the pK_{aH} of compound **XII**. The pK_{aH} is thus estimated to be about 5.5.

The pK_{aH} of morpholine has been reported to be 8.36,⁵¹ which indicates that the conjugate acid of compound **XII** is about three orders of magnitude more acidic than the conjugate acid of morpholine, also known as morpholinium. This increased acidity is expected since the pK_{aH} of a

secondary amine, morpholine, is being compared to the pK_{aH} of a tertiary amine, compound **XII**. This is also exemplified in Figure 36 when comparing morpholinium to N-ethylmorpholinium.

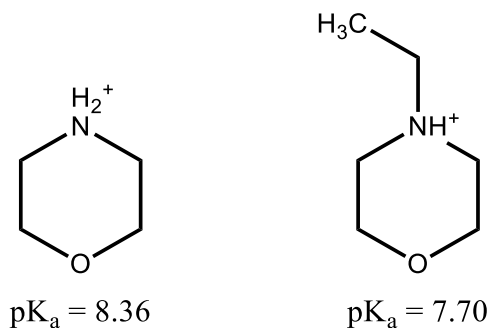


Figure 36. Comparison of the pK_a values for morpholinium and N-ethylmorpholinium

Another factor that may contribute to this increased acidity may be the electron-withdrawing effect caused by the amide bond which is only two bonds away from the basic nitrogen atom of the morpholine moiety in compound **XII**. A similar effect is seen between the conjugate acid of piperidine, known as piperidinium, and morpholinium (Figure 37). Morpholinium is much more acidic than piperidinium and the increased acidity of morpholinium is largely due to the electron withdrawing effect of the oxygen atom located two bonds away from the basic nitrogen atom.⁵²

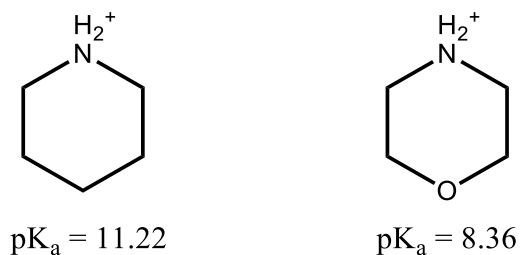


Figure 37. Reported pK_a values for piperidinium and morpholinium⁵¹

The next compound studied was compound **XIII** which contains a piperidine ring as the heterocycle. The titration results for this compound can be seen in Figure 38 and Table 7 (See Appendix).

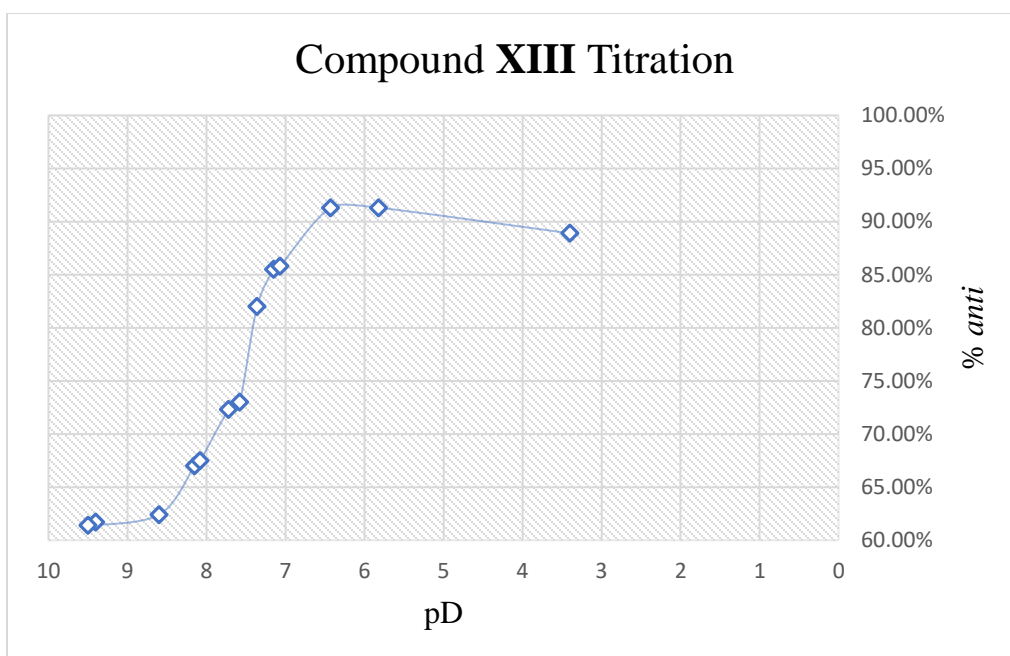


Figure 38. Percentage of the *anti* conformation of compound **XIII** as a function of pD

Evidently, compound **XIII** is considerably more acid-sensitive than compound **XII**. This is to be expected since, as mentioned above, piperidine is much more basic than morpholine. According to the titration curve shown in Figure 38, the pK_{aH} for this compound is about 7.5. This estimated pK_{aH} value is higher than that estimated for compound **XII**, but it is also about three to four orders of magnitude smaller than that of piperidine. This again indicates that the structure of these compounds, namely the close proximity of the amide bond, significantly decreases the basicity of the heterocyclic amine moieties.

Finally, the N-methylpiperazine compound, compound **XIV**, was also titrated and the results can be found below in Figure 39 and Table 8 (See Appendix). Interestingly, this compound showed a curve similar to that of diprotic systems which suggests that the nitrogen atom of the N-methyl group of the piperazine ring can also be protonated and also contributes to a shift in equilibrium to the *anti* conformation.

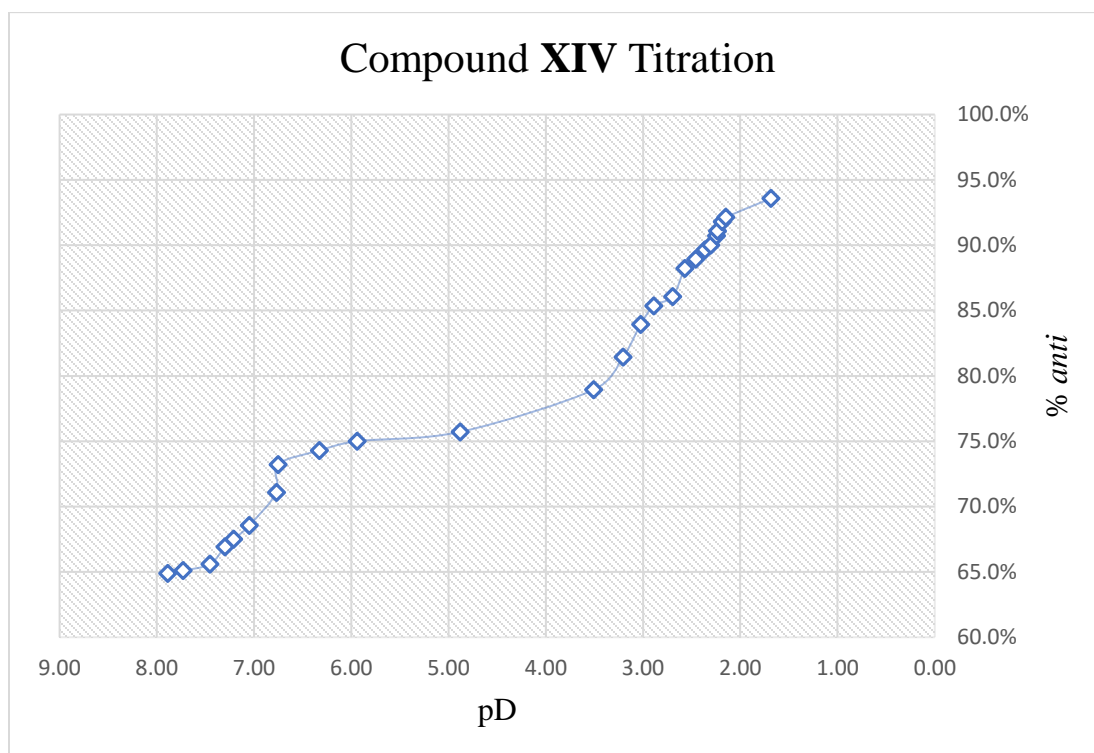


Figure 39. Graph depicting the percentage of the *anti* conformation of compound **XIV** present as a function of pD

The pK_{aH1} for compound **XIV** is estimated to be about 7.0 according to the titration curve shown in Figure 39 and the pK_{aH2} is estimated to be about 2.6. The reported pK_{aH1} and pK_{aH2} for N-methylpiperazine are 9.1 and 4.6 respectively.⁵³ Again, a decrease in the basicity of the heterocyclic amine moiety is observed. It is also important to note, however, that the trend of the

estimated pK_{aH} values of compounds **XII-XIV** match the trend of the reported pK_{aH} values of the three heterocyclic amines (Figure 40).

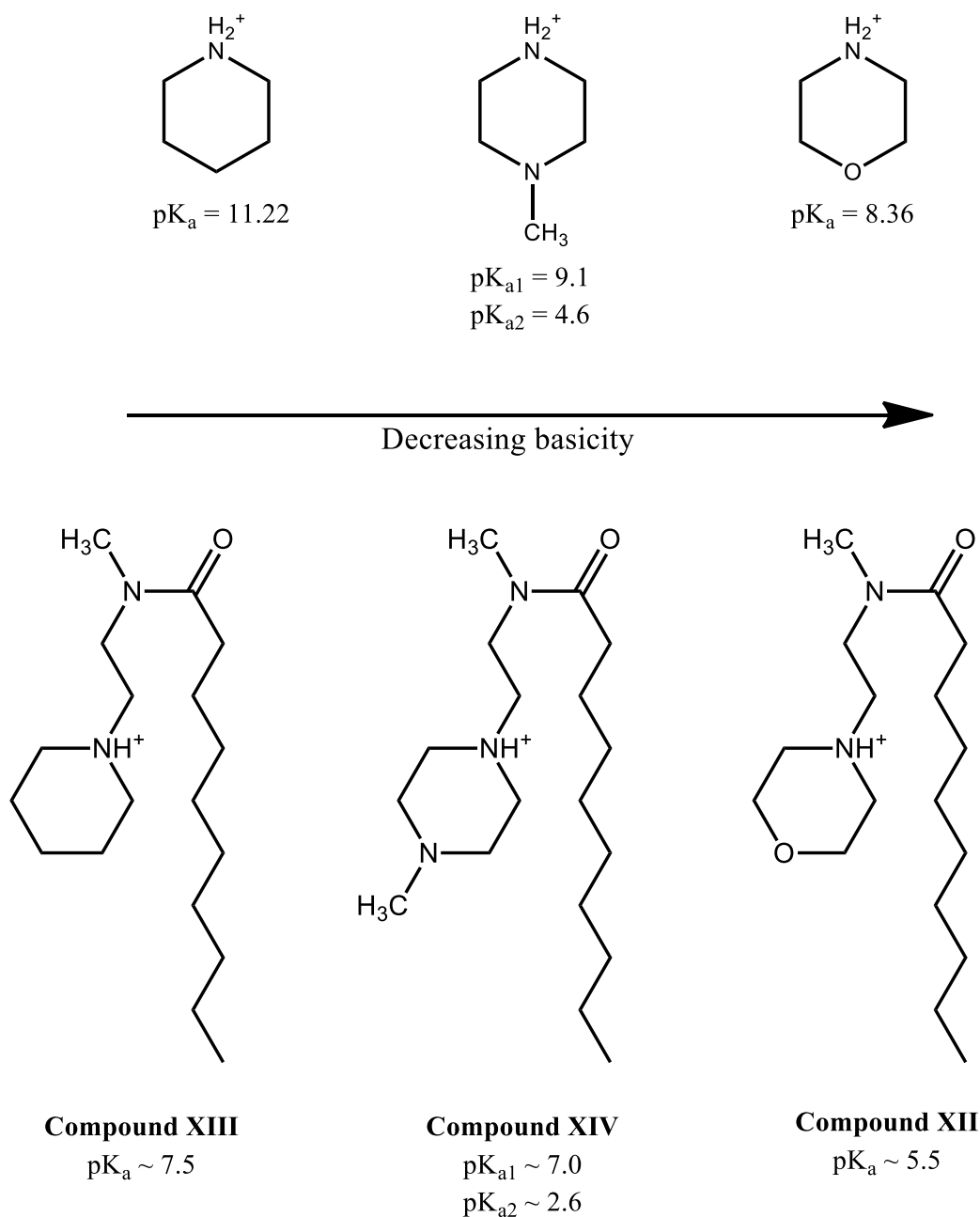


Figure 40. Summary of the pK_a trends of compounds **XII-XIV** and their free amine moieties

To summarize, the three hybrid conformational switches show similar behavior in that they all start out with a predominance of the *anti* conformation (60~66%) and all seem to reach a maximum of 89~94% *anti* upon protonation. They also all behave similarly to compound **I** which started at 66% and reached a maximum at 97 % *anti*. This leads us to believe that, if these structures were to be incorporated into liposome structures, the liposomes would result in the early leakage of contents and would thus not be able to serve as a viable pH-triggered liposomal drug delivery system. In addition, we are able to show that the pK_{aH} of these compounds can be significantly altered by using different amine moieties.

CHAPTER 4: CONCLUSIONS

Several amide-based flipid model compounds have been designed and synthesized. The compounds studied include a flipid model consisting of long alkyl chain tails (**I**), structures that include aromatic rings in the place of flipid tails (**IV-VIII**), and hybrid models that include one alkyl chain tail and one heterocycle tail (**XII-XIV**). The products were confirmed by various ^1H -NMR techniques, and Direct Analysis in Real Time (DART) mass spectrometry.

The conformational equilibria of the amide compounds have also been studied by various ^1H -NMR techniques, including NOESY. For some of the models, (**I & XII-XIV**) the amide bond had a relatively high rotational barrier which allowed for a rotation around the bond and an interconversion between the *syn* and *anti* conformations that were slow enough to be captured as separate structures by ^1H -NMR. By identifying the peaks from the separate conformational isomers and integrating their signals, we were able to compare the signal intensities and successfully estimate a ratio between the two conformers. Unfortunately, all of these compounds exhibited a predominance of the *anti* conformation, which would make the structures of this type unsuitable for preparation of the conformationally switchable lipid-like components (flipids) for liposomes.

The aryl rings compounds (**IV-VIII**) did not produce separate NMR peaks for the different conformers and instead produced one average peak due to the fast interconversion of conformers that occurs too rapidly for the NMR timescale. This is supported by data found in literature for the calculated rotational barriers of similar aryl amide compounds and by our own NOESY studies. These studies not only support the hypothesis that a rapid interconversion is occurring in solution, but also suggest that there is still a predominance of the *anti* conformation. Due to the qualitative

nature of the NOESY technique, however, we are currently unable of establishing an accurate ratio between the conformations as was done with the previous compounds.

The pH-sensitivity of the various amide compounds has been tested by $^1\text{H-NMR}$ titration studies. The addition of *d*-TFA successfully produced a shift in the equilibria further to the *anti* conformation, which was observable and quantifiable by comparing the intensity of the $^1\text{H-NMR}$ peaks of the separate conformers. This allowed us to measure and plot the increase in the percentage of the *anti* conformation present in solution as a function of pH. By varying the tertiary amine moieties present in the tails of the model structures, we were able to determine how the basicity and steric nature of the moieties affects the pH-sensitivity of the molecules. Interestingly, although they have different tertiary amine groups, compounds **I** and **XII-XIV** seemed to behave very similarly by starting out with a predominance of the *anti* isomer (60~66% *anti*) and all reaching a maximum *anti* content of about 89~94%.

pK_{aH} values were also estimated for compounds XII-XIV (pK_{aH} 5.5, pK_{aH} 7.5, pK_{aH1} 7.0 and pK_{aH2} 2.6 respectively) and the trend showed that the pH-sensitivity of these compounds can be significantly altered by using different amine moieties. Even after the addition of the strong acid *d*-TFA, there was no observable separation for the two conformers in *bis*-aryl compounds **IV-VIII**. Therefore, it was not possible to establish accurate *syn:anti* ratios or conduct $^1\text{H-NMR}$ titration studies for these compounds.

The potential for compound **I** as a part of a pH-sensitive drug delivery system was tested by incorporating it into the membrane of a liposome structure which encapsulated the fluorophore/quencher pair ANTS/DPX. The liposomes were successfully formed, and their diameter and surface charge were determined using a Dynamic Light Scattering (DLS) instrument. A fluorimeter was then used to study the liposomal leakage of ANTS/DPX. However, the

liposomes exhibited significant liposomal leakage before the addition of acid (pH ~8.5) and showed only a slight increase in fluorescence after acid was added and even after the liposomes were all effectively destroyed by the addition of a detergent. This suggests that the liposome structures may already be unstable or the lipid/flipid molecules are not being tightly and uniformly packed into the bilayer membranes. Although the hybrid models (**XII-XIV**) (containing both cyclic and non-cyclic substituents at the amide bond) have not been incorporated into liposome structures and tested for liposomal leakage, they behaved very similarly to compound **I** both in their predominance of the *anti* conformation before treatment with acid and their pH-sensitivity upon the addition of acid. Therefore, alkyl chain flipids like compound **I** need substantial structural re-design and optimization in order to become a viable option for targeted drug delivery.

CHAPTER 5: EXPERIMENTAL

5.1 Materials

The phospholipid 1-palmitoyl-2-oleoyl-*sn*-glycero-3-phosphocholine (POPC) and N-palmitoyl-sphingosine-1-(succinyl[methoxy(polyethylene glycol)2000]) (PEG) were purchased from Avanti Polar Lipids, Inc. (Alabaster, AL, USA). 8-aminonaphthalene-1,3,6-trisulfonic acid disodium salt (ANTS) and *p*-xylene-bis-pyridinium bromide (DPX) were purchased from Invitrogen-Molecular Probes (Eugene, OR, USA). 2-[4-(2-Hydroxyethyl)piperazin-1-yl]-ethanesulfonic acid (HEPES) and the sodium chloride were purchased from Sigma Aldrich (St. Louis, MO, USA). Octaethylene glycol monododecyl ether detergent was purchased from Santa Cruz Biotechnology (Santa Cruz, CA, USA). The deuterated solvents were purchased from Cambridge Isotope Laboratories (Tewksbury, MA, USA). All other solvents were purchased from Fisher Scientific and were distilled by fractional distillation before use. ¹H-NMR and ¹³C-NMR were acquired by using a JEOL ECA 600 MHz FT-NMR spectrometer (Peabody, MA, USA). High resolution mass spectra were acquired by using a JEOL Accu-TOF mass spectrometer (JEOL, Peabody, MA, USA) equipped with a DART ionization source (IonSense, Saugus, MA, USA).

5.2 Conformational Analysis by NMR Spectroscopy

Samples of compounds **I**, **IV-VIII**, and **XII-XIV** (about 10 mg each) were dissolved in 0.6 μ L of deuterated solvent (*d*-CHCl₃ or *d*-MeOH) and analyzed by ¹H-NMR, ¹³C-NMR, ¹H-¹H COSY, and ¹H-¹³C HMQC. The % *anti* values reported in Chapter 3 are calculated from the ¹H-NMR spectra obtained from dissolving the samples in *d*-MeOH in order to remain consistent with the titration studies which are conducted solely with *d*-MeOH. The % *anti* values were calculated

by integrating the peaks from the separate conformers that correspond to the amide N-methyl group protons and comparing the integration values to each other to establish a *syn:anti* ratio.

5.3 NMR Titration Studies

Compounds **I** and **XII-XIV** (about 10 mg each) were dissolved in 0.6 μL of deuterated methanol and analyzed by $^1\text{H-NMR}$. For each spectrum, all of the peaks were identified and integrated, and the *syn:anti* ratio was established and recorded as described in section 5.2. The NMR samples were transferred to a small glass vial and their pH, or in this case, pD values were determined through the use of a Fisher Scientific Orion Micro pH Electrode (Thermo Fisher Scientific, Waltham, MA). Then, small volumes of a 1.0 mM solution of deuterated trifluoroacetic acid (*d*-TFA) in *d*-MeOH were added to the samples using micropipettes. The vials were agitated on a vortex to fully dissolve the acid in the *d*-MeOH, the new pD values were determined, and the samples were transferred back into the same NMR tubes as before. Samples were analyzed by $^1\text{H-NMR}$ spectroscopy once again, the data was recorded, and the pD was measured a second time to calculate an average pD value. The data was subsequently organized into tables. The % *anti* values were calculated for each run using the calculated *syn:anti* ratios and plotted against the pD in order to visualize the shift in the conformational equilibria of the compounds as a function of acid concentration. *d*-TFA was added to the samples until the pD curve reached a plateau, signifying that all or almost all of the compound had been protonated.

5.4 Synthesis of Liposomes

Compound **I** was mixed with 1-palmitoyl-2-oleoyl-*sn*-glycero-3-phosphocholine (POPC). N-palmitoyl-sphingosine-1-(succinyl[methoxy(polyethyleneglycol)2000]) (C16 PEG2000 Ceramide) was also added to the mixture to form a coating around the membrane for steric stabilization of the liposome. Three sets of liposomes were prepared by mixing POPC, compound

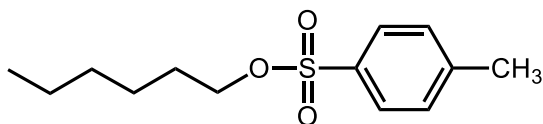
I, and PEG in molar ratios of 70:25:5, 45:50:5, 20:75:5, and 0:95:5 with agitation on a vortex in a pH 8.5 aqueous solution of 50 mM ANTS/DPX solution, 5 mM HEPES buffer, and 145 mM sodium chloride. The suspensions produced were frozen in -80 °C EtOAc/liquid N₂ bath and then allowed to thaw and reach room temperature. This freeze/thaw cycle was repeated nine times in order to allow the components to come together into proper liposome structures. These liposome suspensions were subsequently extruded ten times to yield a homogeneous liposome formulation. The extruded liposomes were purified with a Sephadex G-75 column (pH 8.5 buffer [5 mM HEPES, 145 mM NaCl]) and were subsequently analyzed with a Malvern Zeta 3000 dynamic light scattering instrument (Malvern Instruments Ltd., Worcestershire, UK).

5.5 ANTS/DPX Leakage Assay

100 μ L of the liposome suspensions obtained from the Sephadex column were dissolved in 2.9 mL of pH 8.5 HEPES buffer (5 mM HEPES + 145 mM NaCl). Samples were tested for fluorescence in cuvettes containing 50 μ L aliquots of the samples dissolved in 2 mL of pH 8.5 HEPES buffer (5 mM HEPES + 145 mM NaCl). The fluorescence ($\lambda_{\text{ex}} = 350$ nm, $\lambda_{\text{em}} = 550$ nm) from ANTS was monitored on a QuantaMaster fluorometer (Photon Technology International, Lawrenceville, NJ). Then, 20 μ L of the detergent, octaethylene glycol mono-n-dodecyl ether, were added to the samples at the end of each measurement.

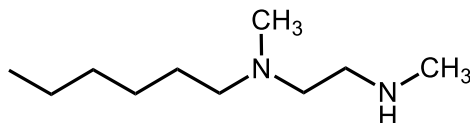
5.6 Synthesis of Compounds

5.6.1 Synthesis of Hexyl 4-methylbenzenesulfonate (II)



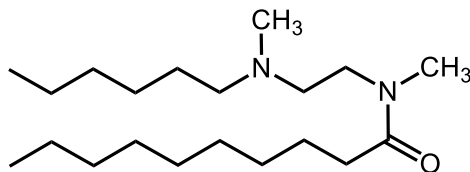
1-Hexanol (1.830 g, 14.68 mmol) was dissolved in chloroform (15.0 mL) and the resulting solution was cooled down to 0 °C by placing the reaction flask into an ice bath. Pyridine (2.360 mL, 29.30 mmol) was added to the mixture with stirring. Then, p-toluenesulfonyl chloride (4.200 g, 22.03 mmol) was added in small portions and the resulting mixture was stirred at 0 °C for 2.5 h. The solvent was subsequently removed by evaporation under reduced pressure and the residue was dissolved in dichloromethane. The resulting solution was washed with 4 x 20.0 mL 1.0 M HCl and 2 x 20.0 mL 2.0 M NaOH and was dried over anhydrous Na₂SO₄. The Na₂SO₄ salt was removed via vacuum filtration and was rinsed with dichloromethane, then the excess solvent was removed by rotary evaporation. The resulting residue was purified as a yellow-brown oil by column chromatography (silica gel; Hexane : EtOAc, 39 : 1). Yield: 2.153 g (57.2 % yield). ¹H-NMR (600 MHz, CDCl₃) δ 7.79 (dt, J = 8.4, 1.8 Hz, 2H, CH₂), 7.34 (d, J = 7.9 Hz, 2H, CH₂), 4.01 (t, J = 6.5 Hz, 2H, CH₂), 2.45 (s, 3H, CH₃), 1.62 (q, J = 6.6 Hz, 2H, CH₂), 1.35-1.15 (m, 6H, CH₂), 0.84 (t, J = 7.1 Hz, 3H, CH₃). ¹³C-NMR (150 MHz, CDCl₃) δ 144.71 (CH₂), 133.30 (CH₂), 129.89 (CH₂), 127.97 (CH₂), 70.80 (CH₂), 31.17 (CH₂), 28.85 (CH₂), 25.08 (CH₂), 22.50 (CH₂), 21.72 (CH₂), 14.00 (CH₃). HRMS: C₁₃H₂₀O₃S calcd. *m/z* [M+H]⁺ 257.1206, found 257.1216.

5.6.2 Synthesis of N-Hexyl-N,N'-dimethylethane-1,2-diamine (III)



N,N'-dimethylethylenediamine (0.970 mL, 9.01 mmol) was dissolved in acetonitrile (14.5 mL), followed by the addition of K_2CO_3 salt (1.879 g, 13.60 mmol). The resulting suspension was cooled to 0 °C using an ice bath under stirring. Hexyl 4-methylbenzenesulfonate (**II**) (1.152 g, 4.494 mmol) was added to the reaction and the resulting mixture was stirred at 0 °C for 24 h. The K_2CO_3 salt was removed via vacuum filtration and the solvent was removed by rotary evaporation. The residue was then dissolved in dichloromethane (10.0 mL) and the solution was washed with 2 x 5.0 mL H_2O and dried over anhydrous Na_2SO_4 . The Na_2SO_4 salt was removed via vacuum filtration and was rinsed with dichloromethane. The residue was purified as a clear, pale-yellow oil by column chromatography (silica gel; DCM : MeOH : Et_3N , 9 : 1 : 0.1). Yield 220 mg (14.2 %). 1H -NMR (600 MHz, $CDCl_3$) δ 2.63 (t, $J = 6.1$ Hz, 2H, CH_2N), 2.44 (t, $J = 6.1$ Hz, 2H, CH_2N), 2.42 (s, 3H, CH_3N), 2.30 (t, $J = 7.2$ Hz, 2H, CH_2N), 2.18 (s, 3H, CH_3N), 1.91 (bs, 1H, NH), 1.42 (quint, $J = 7.2$ Hz, 2H, CH_2), 1.32-1.21 (m, 6H, CH_2), 0.86 (t, $J = 7.0$ Hz, 3H, CH_3). HRMS: $C_{10}H_{24}N_2$ calcd. m/z $[M+H]^+$ 173.2012, found 173.2005.

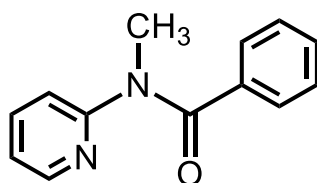
5.6.3 Synthesis of N-(2-(hexyl(methyl)amino)ethyl)-N-methyldecanamide (I)



N-Hexyl-N,N'-dimethylethane-1,2-diamine (**III**) (0.212 g, 1.23 mmol) was placed into a reaction flask under argon atmosphere and was dissolved in dichloromethane (4.4 mL). Then, triethylamine (0.266 mL, 1.91 mmol) was added to the solution with stirring. The flask was subsequently placed into an ice bath to lower the temperature to 0 °C. Decanoic anhydride (0.649 g, 1.99 mmol) was slowly added to the solution in small portions with stirring. The reaction mixture was allowed to slowly reach room temperature and was stirred for 20 h. The organic layer was then washed with 3 x 2.5 mL aq. sat. Na₂CO₃ and dried over anhydrous Na₂SO₄. The Na₂SO₄ salt was removed via vacuum filtration and was rinsed with dichloromethane. The solvent was then removed by rotary evaporation and the residue was purified as a clear, pale-yellow oil by column chromatography (silica gel; DCM : MeOH, 9:1). Yield 331 mg (82.4 %). Rf: 0.52 (DCM : MeOH, 9:1). ¹H-NMR (600 MHz, CDCl₃) δ 3.46 (t, J = 7.0 Hz, 2H, *t*-CH₂N), 3.36 (t, J = 7.4 Hz, 2H, *c*-CH₂N), 3.01 (s, 3H, *t*-CH₃NC=O), 2.93 (s, 3H, *c*-CH₃NC=O), 2.48 (t, J = 7.2 Hz, 2H, CH₂), 2.37-2.26 (m, 4H, CH₂), 2.25 (s, 3H, CH₃N), 2.24 (s, 3H, CH₃N), 1.62 (m, 2H, CH₂), 1.43 (m, 2H, CH₂), 1.35-1.20 (m, 18H, CH₂), 0.91-0.84 (4t, 6H, CH₃). ¹³C-NMR (150 MHz, CDCl₃) δ 173.30, 173.10 (C=O), 58.46 (*c*-CH₂), 58.18 (*t*-CH₂), 55.88-54.92 (CH₂), 48.51 (*c*-CH₂), 45.90 (*t*-CH₂), 42.77 (*t*-CH₃), 42.48 (*c*-CH₃), 36.20 (*t*-CH₃), 33.99 (*c*-CH₃), 33.70, 33.06 (CH₂), 31.96 (CH₂), 31.90 (CH₂), 31.89 (CH₂), 29.66 (CH₂), 29.58 (CH₂), 29.39 (CH₂), 27.45 (CH₂), 25.60 (CH₂),

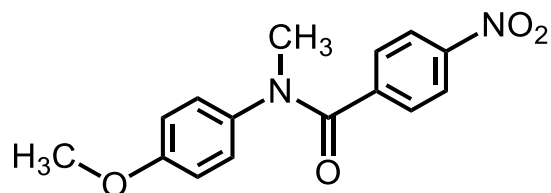
25.16 (CH₂), 22.75 (CH₂), 22.72 (CH₂), 14.19, 14.15 (CH₃). HRMS: C₂₀H₄₂N₂O calcd. *m/z* [M+H]⁺ 327.3370, found 327.3357.

5.6.4 Synthesis of N-methyl-N-(pyridin-2-yl)benzamide (IV)



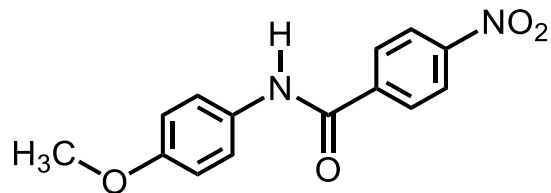
2-(methylamino) pyridine (1.020 mL, 9.923 mmol) was placed in a reaction flask under argon atmosphere and dissolved in triethylamine (20.6 mL). The flask was placed into a water bath at ambient temperature and benzoyl chloride (2.320 mL, 19.97 mmol) was added to the solution in a dropwise fashion. The mixture was subsequently stirred overnight. The organic layer was then washed with 3 x 5.0 mL 10 % aq. NH₄Cl solution, 2 x 5.0 mL H₂O, 1 x 5.0 mL 10 % aq. NaCl solution, and then dried over anhydrous Na₂SO₄. The Na₂SO₄ salt was removed via vacuum filtration and was rinsed with dichloromethane. Then, the product was purified as a yellow oil by column chromatography (silica gel; Hexane : EtOAc, 2:1). Yield 700 mg (16.5 %). ¹H-NMR (600 MHz, METHANOL-D₄) δ 8.38 (dd, J = 4.9, 1.4 Hz, 1H, CH), 7.64 (td, J = 7.8, 1.9 Hz, 1H, CH), 7.33 (tt, J = 7.8, 1.2 Hz, 1H, *p*-CH), 7.29 (d, J = 7.0 Hz, 2H, *o*-CH), 7.24 (t, J = 7.2 Hz, 2H, *m*-CH), 7.20 (dd, J = 7.4, 4.9 Hz, 1H, CH), 7.04 (d, J = 8.1 Hz, 1H, CH), 3.52 (s, 3H, CH₃). ¹³C-NMR (150 MHz, METHANOL-D₄) δ 171.80 (C=O), 156.54 (C), 148.44 (CH), 138.46 (CH), 135.86 (C), 130.08 (*p*-CH), 128.10 (*o*-CH), 127.86 (*m*-CH), 122.10 (CH), 121.90 (CH), 35.32 (CH₃). HRMS: C₁₃H₁₂N₂O calcd. *m/z* [M+H]⁺ 213.1022, found 213.1002.

5.6.5 Synthesis of N-(4-methoxyphenyl)-N-methyl-4-nitrobenzamide (V)



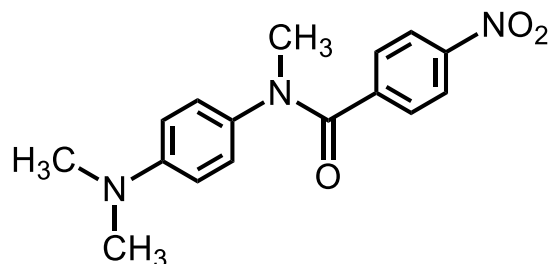
4-methoxy-N-methylaniline (33 mg, 0.24 mmol) was dissolved in dichloromethane (1.800 mL) in a reaction flask under argon atmosphere. The flask was placed in a water bath at ambient temperature, and triethylamine (0.210 mL, 1.51 mmol) was added to the reaction flask with stirring. *p*-Nitrobenzoyl chloride (92 mg, 0.50 mmol) was added to the solution dropwise and the mixture was stirred overnight. The organic layer was subsequently washed with 3 x 5.0 mL 10 % aq. NH₄Cl solution, 2 x 5.0 mL H₂O, 1 x 5.0 mL 10 % aq. NaCl solution, and then dried over anhydrous Na₂SO₄. The Na₂SO₄ salt was removed via vacuum filtration and was rinsed with dichloromethane. The residue was then isolated as yellow crystals, which were subsequently recrystallized using methanol. Yield: 19 mg (28 %). ¹H-NMR (600 MHz, METHANOL-D₄) δ 8.06 (d, J = 8.4 Hz, 2H, CH), 7.49 (d, J = 8.5 Hz, 2H, CH), 7.08 (d, J = 8.7 Hz, 2H, CH), 6.80 (d, J = 8.7 Hz, 2H, CH), 3.71 (s, 3H, CH₃N), 3.45 (s, 3H, CH₃O). ¹³C-NMR (150 MHz, METHANOL-D₄) δ 169.55 (C=O), 158.96 (C), 147.99 (C), 142.56 (C), 136.29 (C), 129.16 (2 x CH), 128.40 (2 x CH), 122.68 (2 x CH), 114.30 (2 x CH), 54.53 (CH₃), 37.27 (CH₃). HRMS: C₁₅H₁₄N₂O₄ calcd. *m/z* [M+H]⁺ 287.1026, found 287.1014.

5.6.6 Synthesis of N-(4-methoxyphenyl)-4-nitrobenzamide (VI)



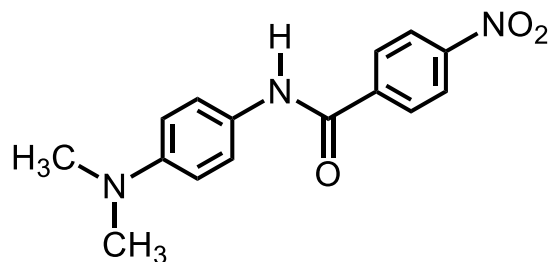
p-Anisidine (26 mg, 0.21 mmol) was dissolved in dichloromethane (1.620 mL) in a reaction flask under argon atmosphere. The flask was placed in a water bath at ambient temperature, and triethylamine (0.209 mL, 1.50 mmol) was added to the reaction flask followed by the addition of *p*-Nitrobenzoyl chloride (92.5mg, 0.498 mmol) to the solution in small portions. The resulting mixture was stirred overnight. The organic layer was then washed with 3 x 3.0 mL 10 % aq. NH₄Cl solution, 2 x 5.0 mL H₂O, 1 x 5.0 mL 10 % aq. NaCl solution, and then dried over anhydrous Na₂SO₄. The Na₂SO₄ salt was removed via vacuum filtration and was rinsed with dichloromethane. The residue was then isolated as fluffy yellow crystals, which were subsequently recrystallized using methanol. Yield: 15 mg (25 %). ¹H-NMR (600 MHz, CDCl₃) δ 8.33 (d, J = 8.7 Hz, 2H, CH), 8.03 (d, J = 8.7 Hz, 2H, CH), 7.85 (s, 1H, NH), 7.54 (d, J = 8.9 Hz, 2H, CH), 6.92 (d, J = 8.9 Hz, 2H, CH), 3.82 (s, 3H, CH₃O). ¹³C-NMR (150 MHz, CDCl₃) δ 163.62 (C=O), 157.22 (C), 149.75 (C), 140.67 (C), 130.28 (C), 128.31 (2 x CH), 124.09 (2 x CH), 122.40 (2 x CH), 114.45 (2 x CH), 55.61 (CH₃O). HRMS: C₁₄H₁₂N₂O₄ calcd. *m/z* [M+H]⁺ 273.0870, found 273.0879.

5.6.7 Synthesis of N-(4-(dimethylamino)phenyl)-N-methyl-4-nitrobenzamide (VII)



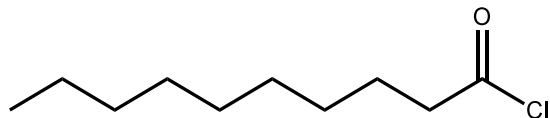
1-N,1-N,4-N-trimethylbenzene-1,4-diamine di-HCl salt (110 mg, 0.493 mmol) was dissolved in dichloromethane (5.9 mL) in a reaction flask under argon atmosphere. The flask was placed in a water bath at ambient temperature, and triethylamine (0.559 mL, 4.01 mmol) was added to the reaction flask. Nitrobenzoyl chloride (186 mg, 1.00 mmol) was slowly added to the solution in small portions and the mixture was stirred overnight. The organic layer was washed with 3 x 5.0 mL 1.0 M NaOH solution and then dried over anhydrous Na_2SO_4 . The Na_2SO_4 salt was removed via vacuum filtration and was rinsed with dichloromethane. The solvent was removed by rotary evaporation and the residue was purified as a dark orange oil by column chromatography (silica gel; Hexane : EtOAc, 1:1). Yield: 26 mg (17 %). $^1\text{H-NMR}$ (600 MHz, METHANOL- D_4) δ 8.05 (d, $J = 8.8$ Hz, 2H, CH), 7.49 (d, $J = 8.8$ Hz, 2H, CH), 6.96 (d, $J = 8.9$ Hz, 2H, CH), 6.58 (d, $J = 8.9$ Hz, 2H, CH), 3.43 (s, 3H, $\text{CH}_3\text{NC=O}$), 2.86 (s, 6H, CH_3N). $^{13}\text{C-NMR}$ (150 MHz, METHANOL- D_4) δ 170.96 (C=O), 151.14 (C), 149.19 (C), 144.24 (C), 133.50 (C), 130.46 (2 x CH), 129.06 (2 x CH), 123.93 (2 x CH), 113.65 (2 x CH), 40.53 (2 x CH_3N), 38.70 ($\text{CH}_3\text{NC=O}$). HRMS: $\text{C}_{16}\text{H}_{17}\text{N}_3\text{O}_3$ calcd. m/z $[\text{M}+\text{H}]^+$ 300.1343, found 300.1318.

5.6.8 Synthesis of N-(4-(dimethylamino)phenyl)-4-nitrobenzamide (VIII)



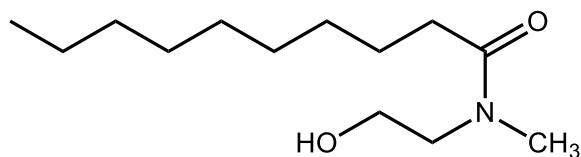
N,N-dimethyl-*p*-phenylenediamine (44 μ L, 0.35 mmol) was dissolved in dichloromethane (2.510 mL) in a reaction flask under argon atmosphere. The flask was placed in a water bath at ambient temperature, and triethylamine (0.293 mL, 2.10 mmol) was added to the reaction flask. *p*-Nitrobenzoyl chloride (130 mg, 0.701 mmol) was slowly added to the solution in small portions and the mixture was stirred overnight. The organic layer was washed with 3 x 6.0 mL 10 % aq. NH_4Cl solution, 1 x 10.0 mL H_2O , 1 x 5.0 mL 10 % aq. NaCl solution, and then dried over anhydrous Na_2SO_4 . The Na_2SO_4 salt was removed via vacuum filtration and was rinsed with dichloromethane. Then, the solvent was removed by rotary evaporation and the residue was isolated as dark red crystals, which were subsequently recrystallized using methanol. Yield: 31 mg (31 %). $^1\text{H-NMR}$ (600 MHz, METHANOL-D_4) δ 8.35 (d, $J = 9.0$ Hz, 2H, CH), 8.11 (d, $J = 9.0$ Hz, 2H, CH), 7.51 (d, $J = 9.3$ Hz, 2H, CH), 6.80 (d, $J = 9.3$ Hz, 2H, CH), 4.63 (s, 1H, NH), 2.93 (s, 6H, CH_3). HRMS: $\text{C}_{15}\text{H}_{15}\text{N}_3\text{O}_3$ calcd. m/z $[\text{M}+\text{H}]^+$ 286.1186, found 286.1190.

5.6.9 Synthesis of Decanoyl chloride (IX)



Decanoic acid (0.906 g, 5.26 mmol) was dissolved in dichloromethane (6.8 mL) in a reaction flask under argon atmosphere. Then, a 2.0 M solution of oxalyl chloride in dichloromethane (3.670 mL, 7.340 mmol) was added to the flask dropwise along with 2 drops of dimethylformamide. The resulting solution was stirred at ambient temperature until the decanoic acid had completely reacted, as monitored by Thin-Layer Chromatography (TLC), and the solvent was removed by rotary evaporation. The residue was then dissolved in chloroform and the excess oxalyl chloride was removed along with the chloroform through three consecutive simple distillations which yielded a yellow-brown oil. The acid chloride product was used in the next step without further purification or isolation.

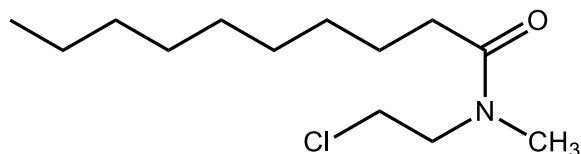
5.6.10 Synthesis of N-(2-hydroxyethyl)-N-methyldecanamide (X)



2-(methylamino) ethanol (1.550 mL, 19.34 mmol) was dissolved in dichloromethane (10.0 mL) in a reaction flask under argon atmosphere. The flask was cooled down to about -10 °C by submerging it into an acetone/ice bath. Then, decanoyl chloride (IX) (0.922 g, 4.81 mmol) was dissolved in 2.000 mL of dichloromethane and the resulting solution was added to the reaction mixture dropwise. The mixture was stirred for two hours. The organic layer was then washed

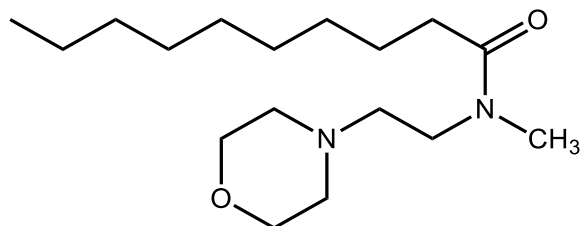
with 4 x 20.0 mL 10 % NH₄Cl aq. solution and 2 x 20.0 mL Na₂CO₃ sat. aq. solution, and then dried over anhydrous Na₂SO₄. The Na₂SO₄ salt was removed via vacuum filtration and was rinsed with dichloromethane. The solvent was then removed by rotary evaporation and the residue was purified as an orange oil by column chromatography (silica gel; EtOAc). Yield: 2.480 g (94.1%). Rf: 0.25 (EtOAc). ¹H-NMR (600 MHz, METHANOL-D₄) δ 3.65 (dt, J = 15.0, 5.4 Hz, 2H, CH₂NC=O), 3.46 (m, 2H, CH₂OH), 3.09 (s, 3H, *t*-CH₃NC=O), 2.92 (s, 3H, *c*-CH₃NC=O), 2.38 (dt, J = 32.9, 7.6 Hz, 2H, CH₂C=O), 1.58 (quint, J = 7.2 Hz, 2H, CH₂), 1.38-1.21 (m, 12H, CH₂), 0.87 (t, J = 7.2 Hz, 3H, CH₃). ¹³C-NMR (150 MHz, METHANOL-D₄) δ 175.03, 174.77 (C=O), 59.41, 58.92 (CH₂NC=O), 51.80, 50.23 (CH₂OH), 36.21 (*t*-CH₃NC=O), 33.09 (CH₂C=O), 32.76 (*c*-CH₃NC=O), 32.63 (CH₂C=O), 31.70 (CH₂), 29.36-29.02 (4 x CH₂), 25.28, 24.90 (CH₂), 22.38 (CH₂), 13.09 (CH₃). HRMS: C₁₃H₂₇NO₂ calcd. *m/z* [M+H]⁺ 230.2115, found 230.2069.

5.6.11 Synthesis of N-(2-chloroethyl)-N-methyldecanamide (XI)



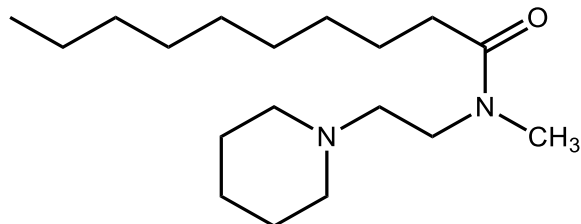
N-(2-hydroxyethyl)-N-methyldecanamide (**X**) (2.480 g, 10.81 mmol) was dissolved in chloroform (24.8 mL) in a reaction flask under argon atmosphere. Thionyl chloride (0.902 mL, 12.4 mmol) was added to the flask with stirring and the mixture was allowed to reflux for 30 minutes. The excess thionyl chloride was removed along with the chloroform by three consecutive simple distillation cycles and yielded a yellow oil. The product was then used in the following reactions without further purification.

5.6.12 Synthesis of N-methyl-N-(2-morpholinoethyl)decanamide (XII)



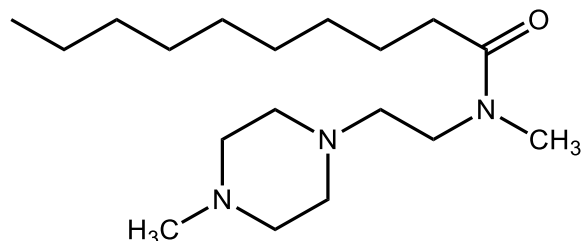
N-(2-chloroethyl)-N-methyldecanamide (**XI**) (0.199 g, 0.802 mmol) was dissolved in dichloromethane (2.000 mL) in a reaction flask under argon atmosphere. Then, pyridine (0.259 mL, 3.22 mmol) was added to the solution with stirring, followed by the addition of morpholine (0.173 mL, 2.00 mmol) dropwise. The resulting mixture was allowed to reflux overnight and the organic layer was washed with 3 x 3.0 mL NH₄Cl aq. solution and then dried over anhydrous Na₂SO₄. The Na₂SO₄ salt was removed via vacuum filtration and was rinsed with dichloromethane, which was then removed by rotary evaporation. The residue was purified as a brown oil by column chromatography (silica gel; EtOAc). Yield: 153 mg (60.0 %). R_f: 0.60 (DCM : MeOH, 9:1). ¹H-NMR (600 MHz, METHANOL-D₄) δ 3.68 (2d, 4H, CH₂N), 3.51 (t, 2H, CH₂NC=O), 3.07 (s, 3H, *t*-CH₃NC=O), 2.94 (s, 3H, *c*-CH₃NC=O), 2.57-2.48 (m, 6H, CH₂O + CH₂N), 2.39 (2t, J = 7.8 Hz, 2H, CH₂C=O), 1.60 (quint, J = 7.2 Hz, 2H, CH₂), 1.39-1.24 (m, 12H, CH₂), 0.90 (t, J = 7.2 Hz, 3H, CH₃). ¹³C-NMR (150 MHz, METHANOL-D₄) δ 174.53, 174.46 (C=O), 66.54 (CH₂N), 66.47 (CH₂N), 56.39, 55.34 (CH₂N), 53.76 (CH₂O), 53.51 (CH₂O), 47.05, 44.24 (CH₂NC=O), 35.13 (*t*-CH₃NC=O), 33.02 (*c*-CH₃NC=O), 32.46 (CH₂C=O), 29.30 (CH₂), 29.24 (CH₂), 29.19 (CH₂), 29.08 (CH₂), 25.30 (CH₂), 24.98 (CH₂), 22.39 (CH₂), 13.10 (CH₃). HRMS: C₁₇H₃₄N₂O₂ calcd. *m/z* [M+H]⁺ 299.2693, found 299.2646.

5.6.13 Synthesis of N-methyl-N-(2-(piperidin-1-yl)ethyl)decanamide (XIII)



N-(2-chloroethyl)-N-methyldecanamide (**XI**) (0.199 g, 0.802 mmol) was dissolved in dichloromethane (1.840 mL) in a reaction flask under argon atmosphere. Then, pyridine (0.286 mL, 3.55 mmol) was added to the solution with stirring, followed by the addition of piperidine (0.198 mL, 2.00 mmol) dropwise. The resulting mixture was allowed to reflux overnight and the organic layer was washed with 3 x 1.0 mL 0.01 M HCl aq. solution and then dried over anhydrous Na_2SO_4 . The Na_2SO_4 salt was removed via vacuum filtration and was rinsed with dichloromethane, which was then removed by rotary evaporation. The residue was isolated as bright yellow crystals. Yield: 147 mg (59.1 %). Rf: 0.47 (DCM : MeOH, 9:1). $^1\text{H-NMR}$ (600 MHz, METHANOL- D_4) δ 3.50 (m, J = 6.2 Hz, 4H, CH_2N), 3.11 (s, 3H, *t*- $\text{CH}_3\text{NC}=\text{O}$), 3.06 (s, 3H, *c*- $\text{CH}_3\text{NC}=\text{O}$), 2.41 (m, 12H, 3 x CH_2 + 2 x CH_2N + $\text{CH}_2\text{C}=\text{O}$), 1.61 (quint, J = 7.2 Hz, 2H, CH_2), 1.41-1.24 (m, 12H, CH_2), 0.90 (t, J = 7.0 Hz, 3H, CH_3). $^{13}\text{C-NMR}$ (150 MHz, METHANOL- D_4) δ 174.5, 174.41 ($\text{C}=\text{O}$), 56.48 ($\text{CH}_2\text{C}=\text{O}$), 54.59 ($\text{CH}_2\text{NC}=\text{O}$), 54.29 (CH_2N), 44.62 (2 x CH_2N), 36.20 (*t*- $\text{CH}_3\text{NC}=\text{O}$), 35.16 (*c*- $\text{CH}_3\text{NC}=\text{O}$), 33.09 (CH_2), 33.02 (CH_2), 32.97 (CH_2), 31.71 (CH_2), 29.29 (CH_2), 29.08 (CH_2), 25.25 (CH_2), 24.93 (CH_2), 23.79 (CH_2), 22.39 (CH_2), 13.09 (CH_3). HRMS: $\text{C}_{18}\text{H}_{36}\text{N}_2\text{O}$ calcd. m/z $[\text{M}+\text{H}]^+$ 297.2900, found 297.2851.

5.6.14 Synthesis of N-methyl-N-(2-(4-methylpiperazin-1-yl)ethyl)decanamide (XIV)



N-(2-chloroethyl)-N-methyldecanamide (**XI**) (0.199 g, 0.802 mmol) was dissolved in dichloromethane (1.840 mL) in a reaction flask under argon atmosphere. Then, pyridine (0.286 mL, 3.55 mmol) was added to the solution with stirring, followed by the addition of N-methylpiperazine (0.223 mL, 2.01 mmol) dropwise. The resulting mixture was allowed to reflux overnight and the organic layer was washed with 3 x 1.0 mL 10% NH₄Cl aq. solution and then dried over anhydrous Na₂SO₄. The Na₂SO₄ salt was removed via vacuum filtration and was rinsed with excess dichloromethane. The solvent was removed by rotary evaporation and the residue was purified as a thick yellow oil by column chromatography (silica gel; DCM : MeOH, 8:2). Yield: 88 mg (35.1%). Rf: 0.29 (DCM : MeOH, 8:2). ¹H-NMR (600 MHz, METHANOL-D₄) δ 3.51 (dt, J = 16.2, 7.2 Hz, 2H, CH₂NC=O), 3.06 (s, 3H, *t*-CH₃NC=O), 2.93 (s, 3H, *c*-CH₃NC=O), 2.85-2.45 (m, 10H, CH₂N), 2.43-2.34 (m, 5H, CH₂C=O + CH₃N), 1.59 (quint, J = 7.2 HZ, 2H, CH₂), 1.39-1.25 (m, 12H, CH₂), 0.90 (t, J = 7.2 Hz, 3H, CH₃). ¹³C-NMR (150 MHz, METHANOL-D₄) δ 174.50 (C=O), 55.66 (CH₂N), 54.57 (CH₂N), 54.39 (CH₂N), 54.22 (2 x CH₂N), 44.45 (*t*-CH₃N), 44.28 (CH₂NC=O), 44.06 (*c*-CH₃N), 35.10 (*t*-CH₃NC=O), 33.02 (*c*-CH₃NC=O), 32.46 (CH₂C=O), 31.71 (CH₂), 29.31 (CH₂), 29.25 (CH₂), 29.10 (CH₂), 25.31 (CH₂), 24.98 (CH₂), 22.39 (CH₂), 13.10 (CH₃). HRMS: C₁₈H₃₇N₃O calcd. *m/z* [M+H]⁺ 312.3009, found 312.2941.

REFERENCES

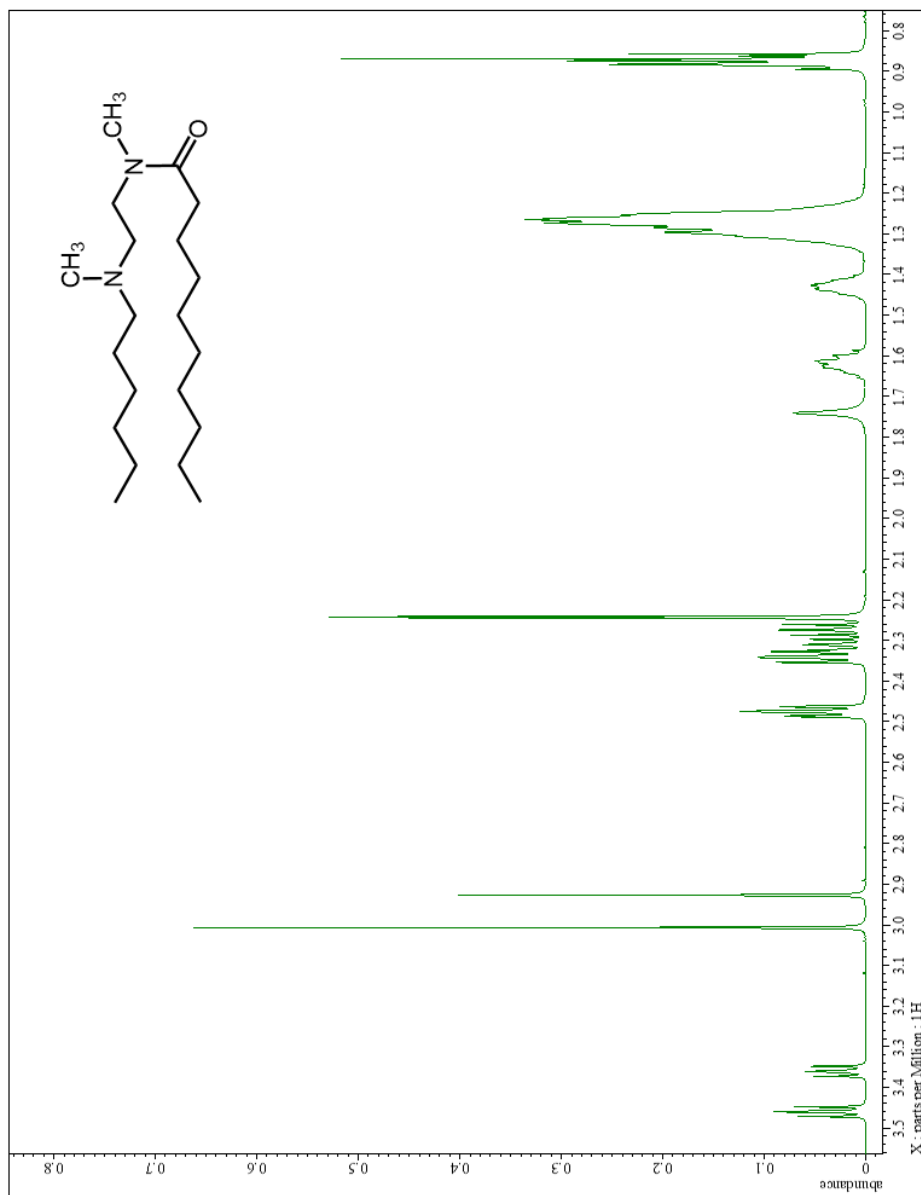
1. Ulbrich W, Lamprecht A. Targeted drug-delivery approaches by nanoparticulate carriers in the therapy of inflammatory diseases. *J R Soc Interface*. 2010; 7 (Suppl 1): S55-S66.
2. Pattni BS, Torchilin VP. *Targeted Drug Delivery : Concepts and Design. Advances in Delivery Science and Technology*. Springer, Cham; 2015.
3. Akbarzadeh A, Rezaei-Sadabady R, Davaran S, et al. Liposome: classification, preparation, and applications. *Nanoscale Res Lett*. 2013; 8 (1): 102-110.
4. Richards PJ, Williams BD, Williams AS. Suppression of chronic streptococcal cell wall-induced arthritis in Lewis rats by liposomal clodronate. *Rheumatology*. 2001; 40 (9): 978-987.
5. Schmidt J, Metselaar JM, Wauben MHM, Toyka KV, Storm G, Gold R. Drug targeting by long-circulating liposomal glucocorticosteroids increases therapeutic efficacy in a model of multiple sclerosis. *Brain*. 2003; 126 (8): 1895-1904.
6. Linker RA, Weller C, Lühder F, et al. Liposomal glucocorticosteroids in treatment of chronic autoimmune demyelination: Long-term protective effects and enhanced efficacy of methylprednisolone formulations. *Exp Neurol*. 2008; 211 (2): 397-406.
7. Yong VW, Wells J, Giuliani F, Casha S, Power C, Metz LM. The promise of minocycline in neurology. *Lancet Neurol*. 2004; 3 (12): 744-751.
8. Hashida N, Ohguro N, Yamazaki N, et al. High-efficacy site-directed drug delivery system using sialyl-Lewis X conjugated liposome. *Exp Eye Res*. 2008; 86 (1): 138-149.
9. Lajavardi L, Bochot A, Camelo S, et al. Downregulation of Endotoxin-Induced Uveitis by Intravitreal Injection of Vasoactive Intestinal Peptide Encapsulated in Liposomes. *Invest Ophthalmol Vis Sci*. 2007; 48 (7): 3230-3238.
10. Jubeh TT, Nadler-Milbauer M, Barenholz Y, Rubinstein A. Local treatment of experimental colitis in the rat by negatively charged liposomes of catalase, TMN and SOD. *J Drug Target*. 2006; 14 (3): 155-163.
11. Viricel W, Mbarek A, Leblond J. Switchable Lipids: Conformational Change for Fast pH-Triggered Cytoplasmic Delivery. *Angew Chem Int Ed Engl*. 2015; 54 (43): 12743-12747.
12. Leblond J, Petitjean A. Molecular Tweezers: Concepts and Applications. *ChemPhysChem*. 2011; 12 (6): 1043-1051.
13. Hardouin-Lerouge M, Hudhomme P, Sallé M. Molecular clips and tweezers hosting neutral guests. *Chem Soc Rev*. 2011; 40 (1): 30-43.

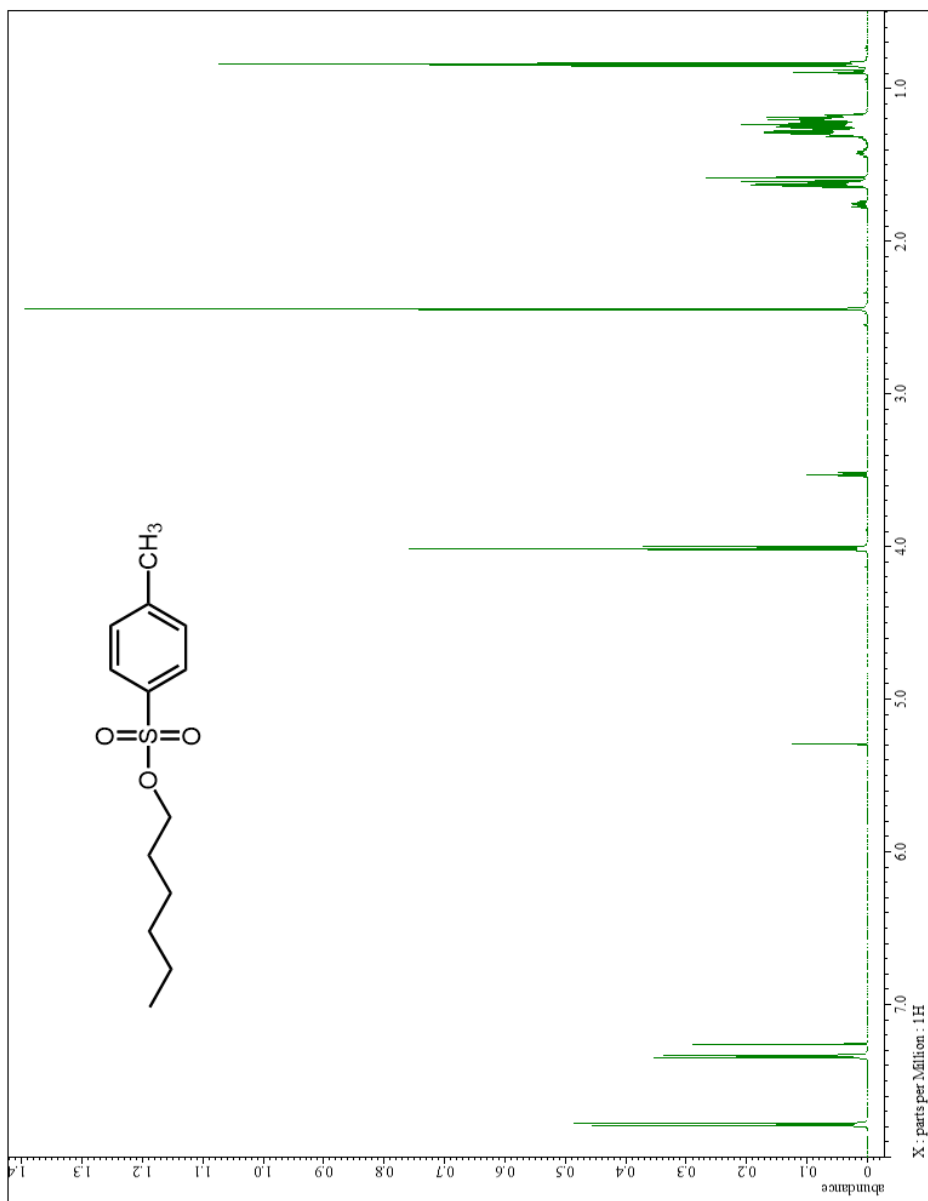
14. Feringa, BL. The Art of Building Small: From Molecular Switches to Molecular Motors. *J Org Chem.* 2007; 72 (18): 6635-6652.
15. Kay ER, Leigh DA, Zerbetto F. Synthetic Molecular Motors and Mechanical Machines. *Angew Chem Int Ed.* 2007; 46 (1-2): 72-191.
16. Feringa BL, ed. *Molecular Switches.* Wiley; 2001.
17. Gole B, Kauffmann B, Maurizot V, Huc I, Ferrand Y. Light-Controlled Conformational Switch of an Aromatic Oligoamide Foldamer. *Angew Chem.* 2019; 131 (24): 8147-8151.
18. Heydari Z, Rashidi-Ranjbar P. Synthesis and photophysical properties of a new carbazole-based acidochromic molecular switch. *J Photochem Photobiol A Chem.* 2019; 377: 8-13.
19. Griffiths JR. Are cancer cells acidic? *Br J Cancer.* 1991; 64 (3): 425-427.
20. Rajamäki K, Nordström T, Nurmi K, et al. Extracellular Acidosis Is a Novel Danger Signal Alerting Innate Immunity via the NLRP3 Inflammasome. *J Biol Chem.* 2013; 288 (19): 13410-13419.
21. Samoshin AV, Veselov IS, Chertkov VA, et al. Fliposomes: new amphiphiles based on trans-3,4-bis(acyloxy)-piperidine able to perform a pH-triggered conformational flip and cause an instant cargo release from liposomes. *Tetrahedron Lett.* 2013; 54 (41): 5600-5604.
22. Samoshin VV. Fliposomes: stimuli-triggered conformational flip of novel amphiphiles causes an instant cargo release from liposomes. *Biomol Concepts.* 2014; 5 (2): 131-141.
23. Samoshina NM, Liu X, Brazdova B, Franz AH, Samoshin VV, Guo X. Fliposomes: pH-Sensitive Liposomes Containing a trans-2-morpholinocyclohexanol-Based Lipid That Performs a Conformational Flip and Triggers an Instant Cargo Release in Acidic Medium. *Pharmaceutics.* 2011; 3 (3): 379-405.
24. Brazdova B, Zhang N, Samoshin VV, Guo X. trans-2-Aminocyclohexanol as a pH-sensitive conformational switch in lipid amphiphiles. *Chem Commun.* 2008; (39): 4774-4776.
25. Mathews CK, van Holde KE. *Biochemistry.* The Benjamin/Cummings Publishing Company; 1990.
26. Eyring H, Grant DM, Hecht H. The rotational barrier in ethane. *J Chem Educ.* 1962; 39 (9): 466-468.
27. Rablen PR. Computational Analysis of the Solvent Effect on the Barrier to Rotation about the Conjugated C–N Bond in Methyl N,N-Dimethylcarbamate. *J Org Chem.* 2000; 65

- (23): 7930-7937.
28. Barrows S, Eberlein T. Understanding Rotation about a C=C Double Bond. *J Chem Educ* 2005; 82 (9): 1329-1333.
 29. Yamasaki R, Tanatani A, Azumaya I, Saito S, Yamaguchi K, Kagechika H. Amide Conformational Switching Induced by Protonation of Aromatic Substituent. *Org Lett*. 2003; 5 (8): 1265-1267.
 30. Okamoto I, Terashima M, Masu H, et al. Acid-induced conformational alteration of cis-preferential aromatic amides bearing N-methyl-N-(2-pyridyl) moiety. *Tetrahedron*. 2011; 67 (44): 8536-8543.
 31. Szostak R, Meng G, Szostak M. Resonance Destabilization in N-Acylanilines (Anilides): Electronically-Activated Planar Amides of Relevance in N-C(O) Cross-Coupling. *J Org Chem*. 2017; 82 (12): 6373-6378.
 32. Anet FAL, Bourn AJR. Nuclear Magnetic Resonance Spectral Assignments from Nuclear Overhauser Effects. *J Am Chem Soc*. 1965; 87 (22): 5250-5251.
 33. Nouls JC, Van Binst G, Martin RH. VII. Physico-chemical study of models of indole alkaloids confirmation of the assignment of the geometry of the two isomeric 3-ethylidene-1-azabicyclo [2,2,2] octane by the study of the nuclear overhauser effect (NOE). *Tetrahedron Lett*. 1967; 8 (41): 4065-4068.
 34. Ito A, Ishii A, Amaki T, Fukuda K, Yamasaki R, Okamoto I. Synthesis and conformational analysis of N-aryl-N-(6-azulenyl)acetamides. *Tetrahedron Lett*. 2019; 60 (29): 1929-1933.
 35. Kubyshkin V, Budisa N. Amide rotation trajectories probed by symmetry. *Org Biomol Chem*. 2017; 15 (32): 6764-6772.
 36. Friebolin H. *Basic One- and Two-Dimensional NMR Spectroscopy*. Fifth. Wiley; 2011.
 37. LaPlanche LA, Rogers MT. *cis* and *trans* Configurations of the Peptide Bond in N-Monosubstituted Amides by Nuclear Magnetic Resonance. *J Am Chem Soc*. 2002; 86 (3): 337-341.
 38. Needham D, McIntosh TJ, Lasic DD. Repulsive interactions and mechanical stability of polymer-grafted lipid membranes. *Biochim Biophys Acta - Biomembr*. 1992; 1108 (1): 40-48.
 39. Ladokhin AS, Wimley WC, Hristova K, White SH. Mechanism of leakage of contents of membrane vesicles determined by fluorescence reuquenching. *Methods Enzymol*. 1997; 278 (23): 474-486.
 40. Chen H, Zhang H, McCallum CM, Szoka FC, Guo X. Unsaturated Cationic Ortho Esters

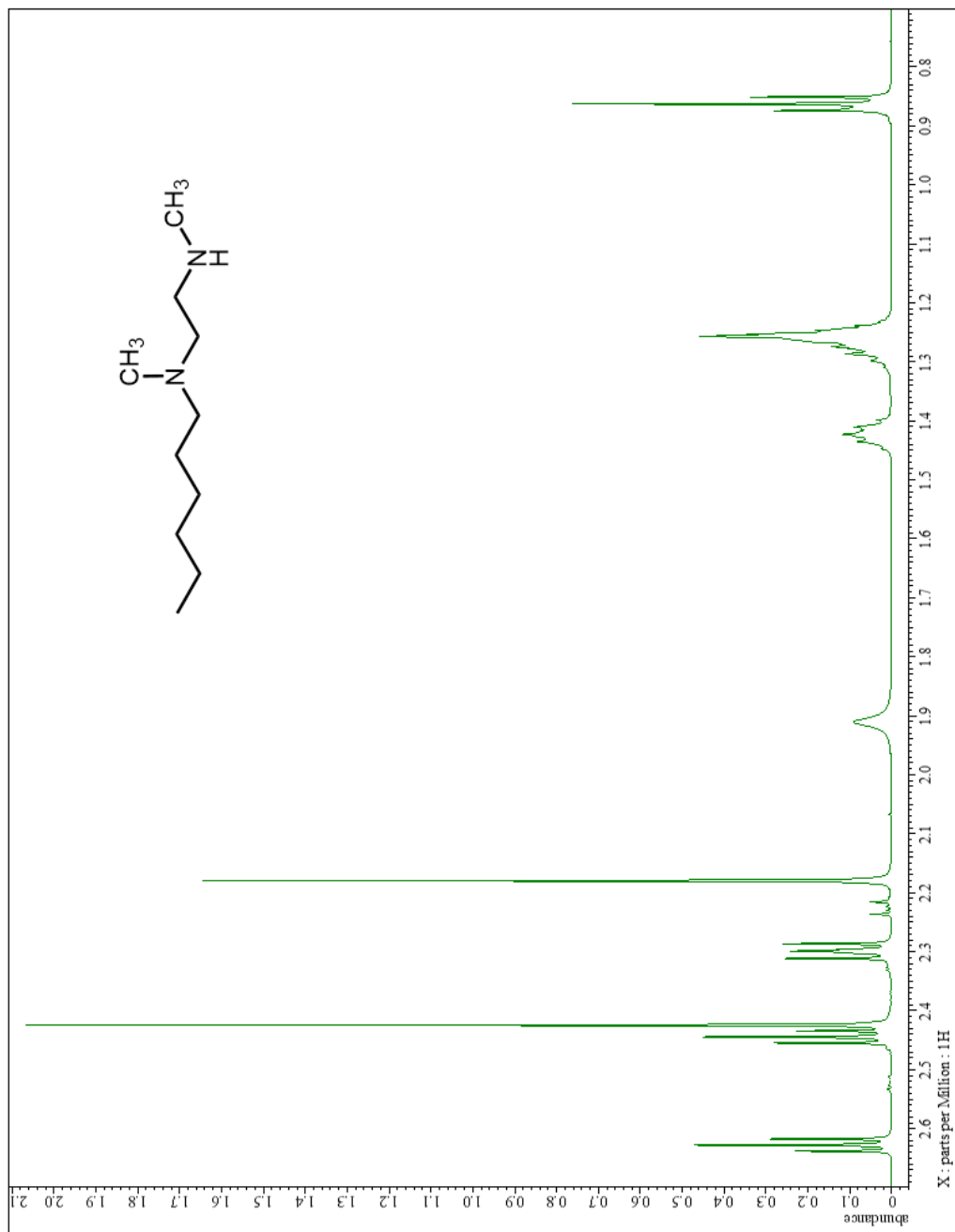
- for Endosome Permeation in Gene Delivery. *J Med Chem.* 2007; 50 (18): 4269-4278.
41. Zheng Y, Liu X, Samoshina NM, Samoshin VV., Franz AH, Guo X. trans-2-Aminocyclohexanol-based amphiphiles as highly efficient helper lipids for gene delivery by lipoplexes. *Biochim Biophys Acta - Biomembr.* 2015; 1848 (12): 3113-3125.
 42. Zheng Y, Liu X, Samoshina NM, Samoshin VV., Franz AH, Guo X. Fliposomes: trans-2-aminocyclohexanol-based amphiphiles as pH-sensitive conformational switches of liposome membrane – a structure-activity relationship study. *Chem Phys Lipids.* 2017; 210 (2018): 129-141.
 43. (ChemIDplus: Toxicology Data Network: U.S. National Library of Medicine). Dimethylethylenediamine. <https://chem.nlm.nih.gov/chemidplus/rn/110-70-3>. Published 2019. Accessed August 19, 2019.
 44. Jensen FR, Noyce DS, Sederholm CH, Berlin AJ. THE ENERGY BARRIER FOR THE CHAIR-CHAIR INTERCONVERSION OF CYCLOHEXANE. *J Am Chem Soc.* 2002; 82 (5): 1256-1257.
 45. Hirano T, Osaki T, Fujii S, et al. Fluorescent visualization of the conformational change of aromatic amide or urea induced by N-methylation. *Tetrahedron Lett.* 2009; 50 (4): 488-491.
 46. Abraham RJ, Aboitiz N, Filippi M, Genesisio E, Piaggio P, Sancassan F. Conformational analysis, part 43. A theoretical and LIS/NMR investigation of the conformations of substituted benzamides. *Magn Reson Chem.* 2015; 53 (7): 498-508.
 47. Galan JF, Tang CN, Chakrabarty S, Liu Z, Moyna G, Pophristic V. Conformational preferences of furan- and thiophene-based arylamides: a combined computational and experimental study. *Phys Chem Chem Phys.* 2013; 15 (28): 11883-11892.
 48. Muller P. Glossary of terms used in physical organic chemistry (IUPAC Recommendations 1994). *Pure Appl Chem.* 1994; 66 (5): 1077-1184.
 49. Po HN, Senozan NM. The Henderson-Hasselbalch Equation: Its History and Limitations. *J Chem Educ.* 2001; 78 (11): 1499-1503.
 50. Hannu R, Lajunen LHJ, Popov K. Guidelines for NMR measurements for determination of high and low pKa values (IUPAC Technical Report). *Pure Appl Chem.* 2006; 78 (3): 663-675.
 51. Hall HK. Correlation of the Base Strengths of Amines1. *J Am Chem Soc.* 2002; 79 (20): 5441-5444.
 52. Ouellette RJ, Rawn JD. *Organic Chemistry Study Guide: Key Concepts, Problems, and Solutions.* Elsevier; 2015.

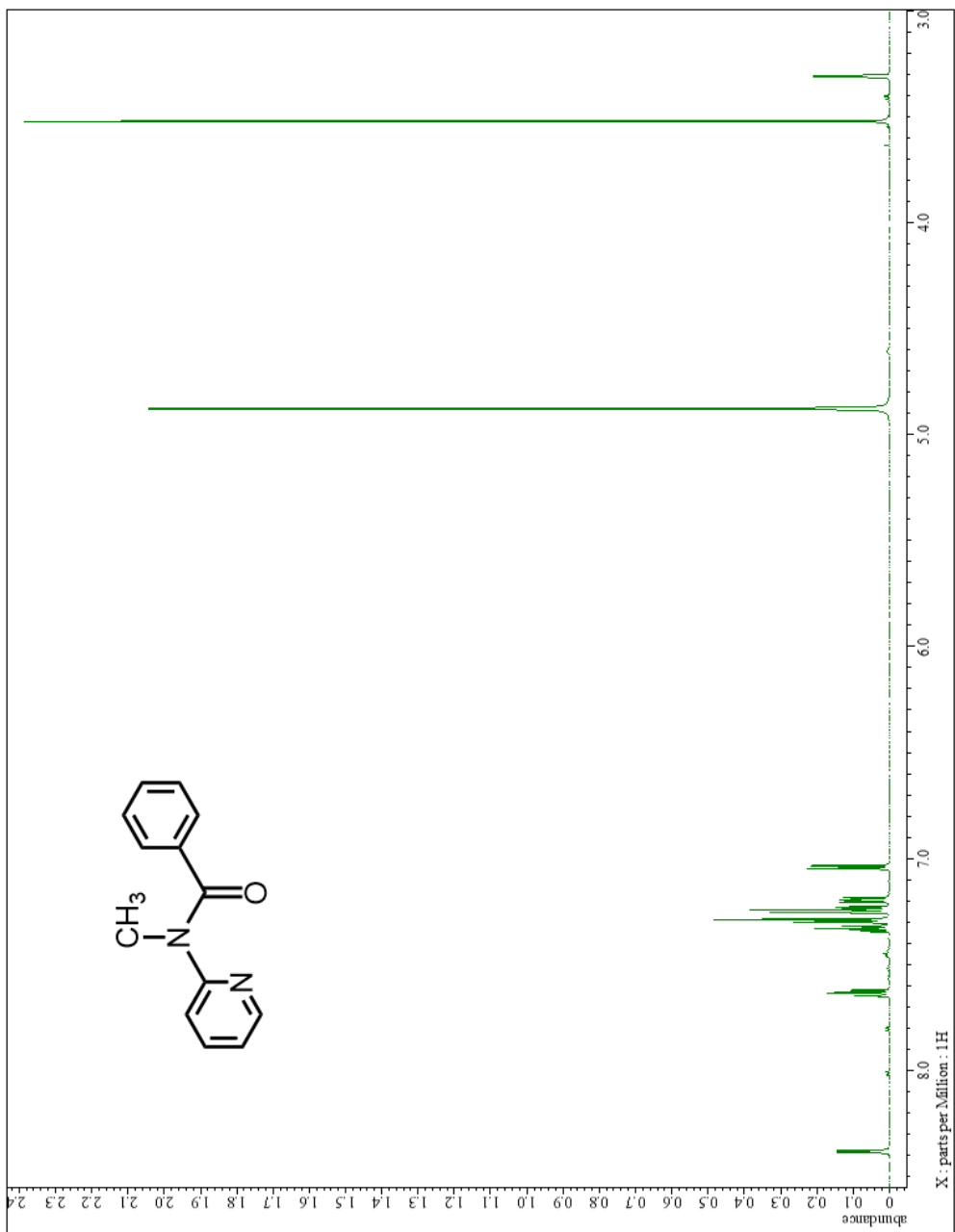
53. Khalili F, Henni A, East ALL. pKa Values of Some Piperazines at (298, 303, 313, and 323) K. *J Chem & Eng Data*. 2009; 54 (10): 2914-2917.

APPENDIX A: SELECTED $^1\text{H-NMR}$ SPECTRACompound I: $^1\text{H-NMR}$, CDCl_3

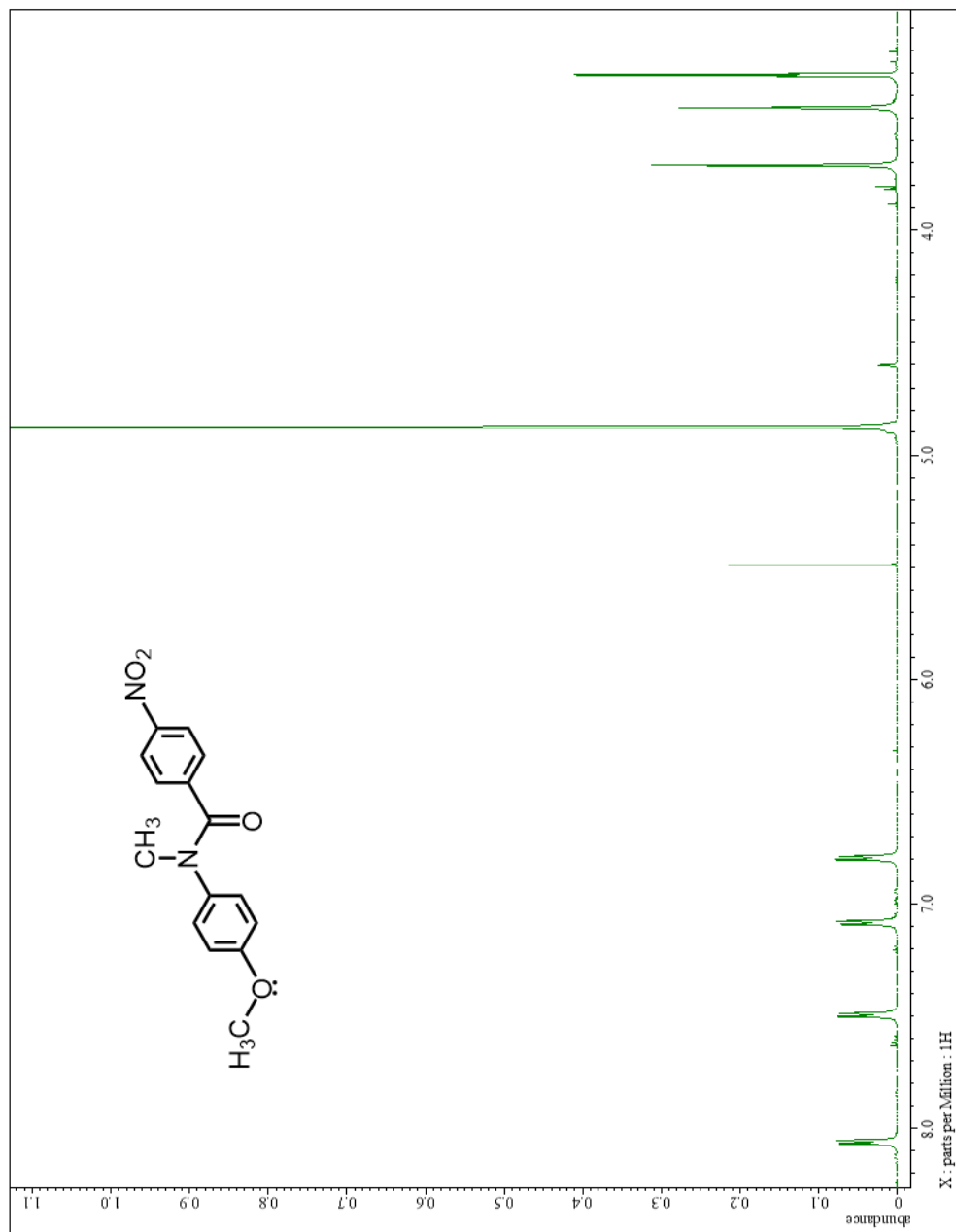


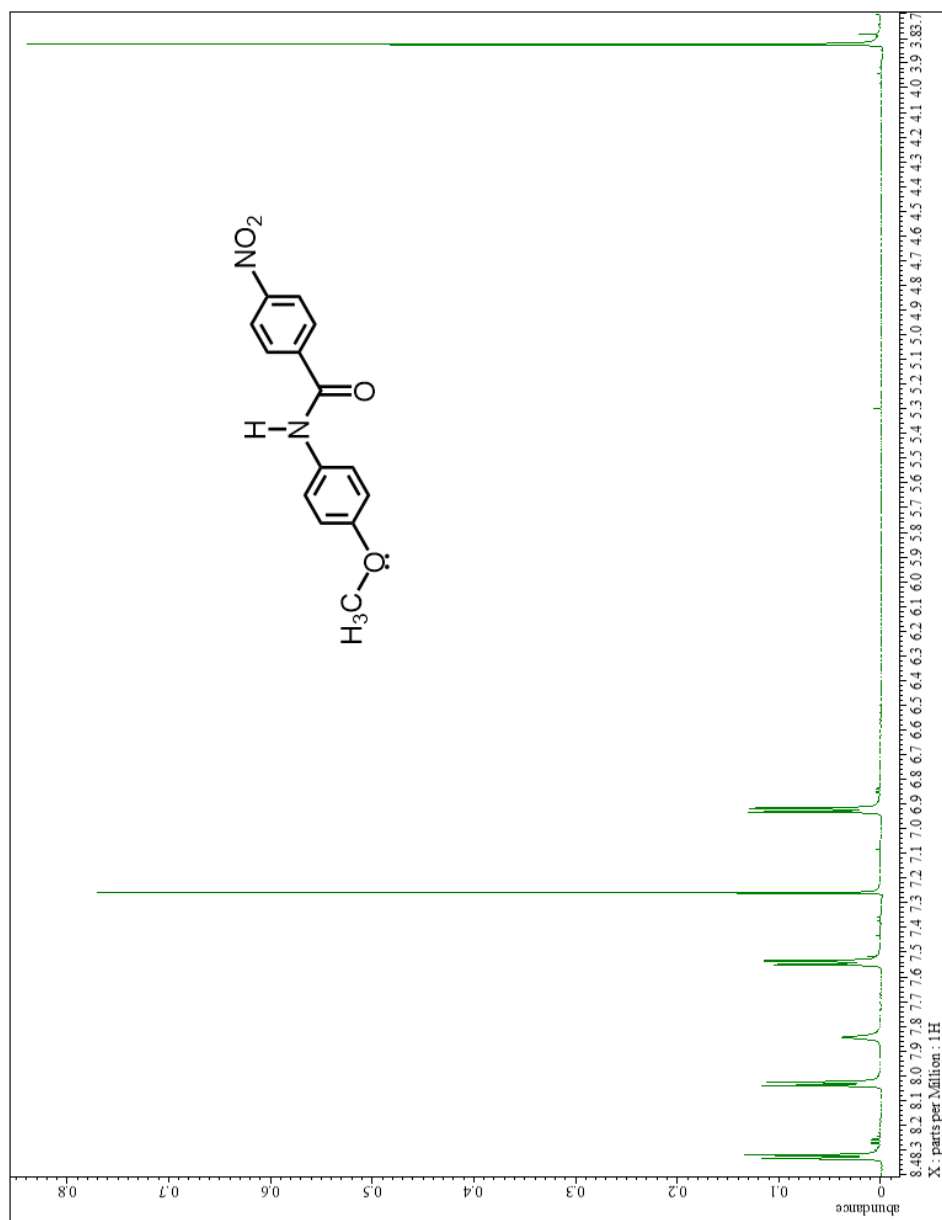
Compound II: ¹H-NMR, CDCl₃

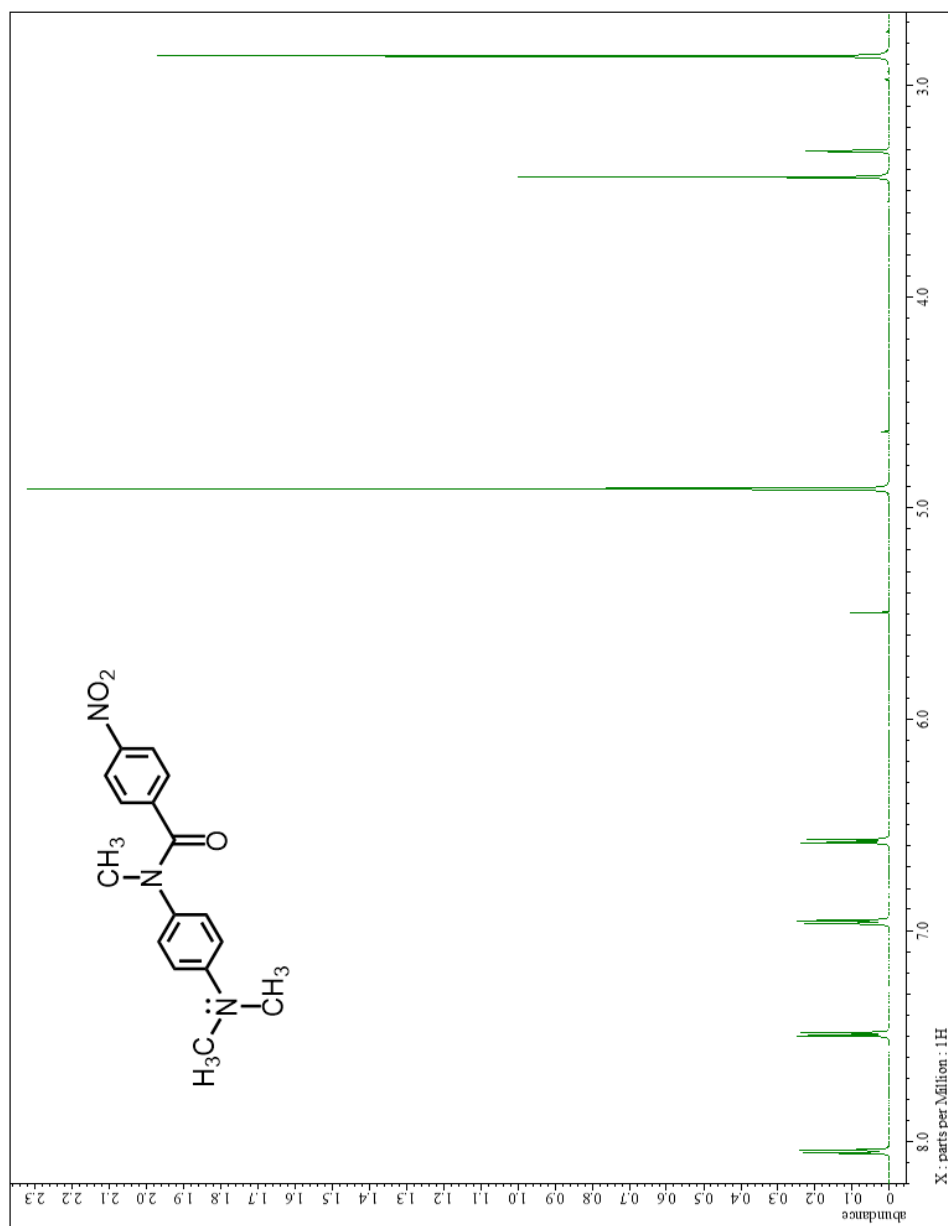
Compound III: $^1\text{H-NMR}$, CDCl_3

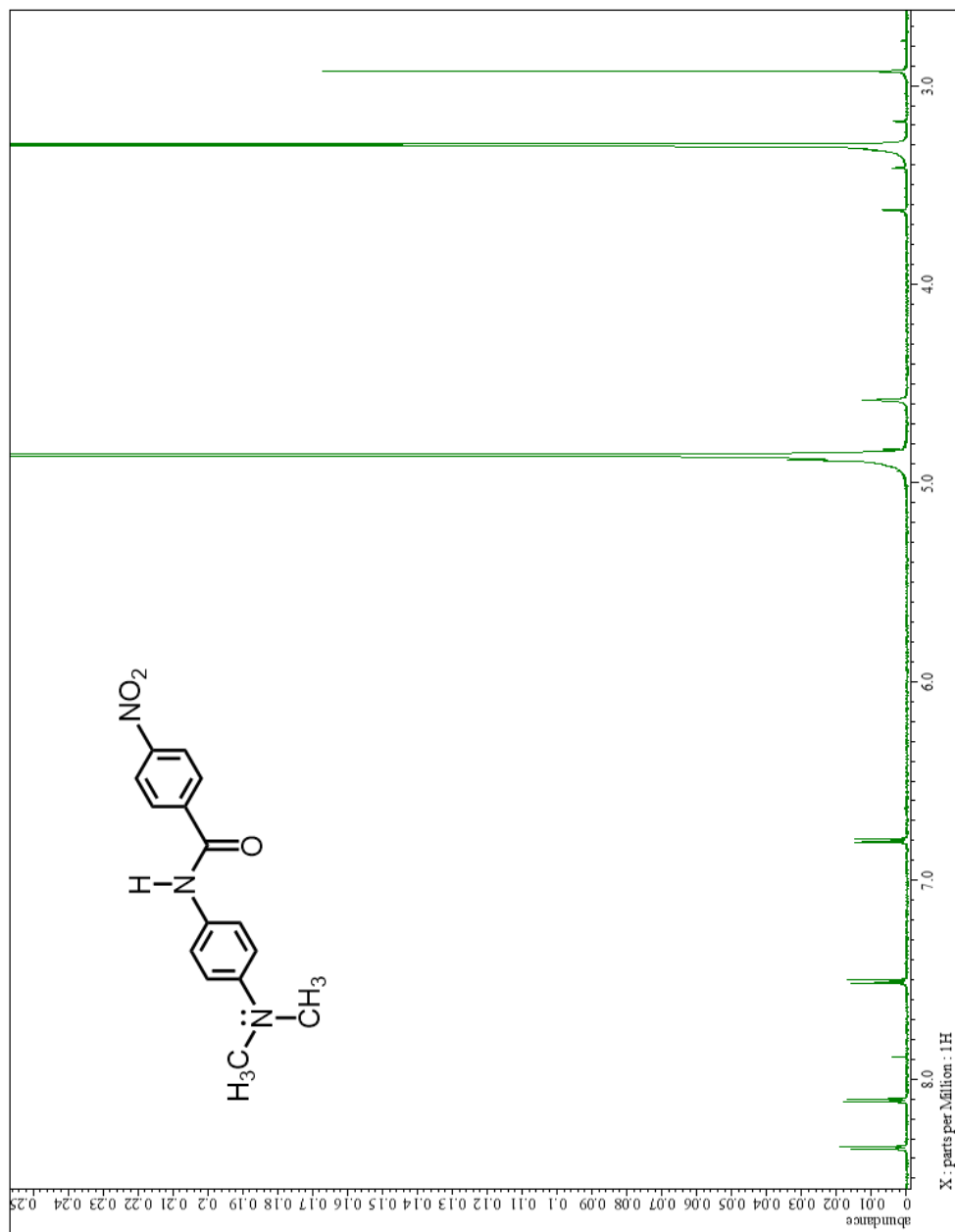


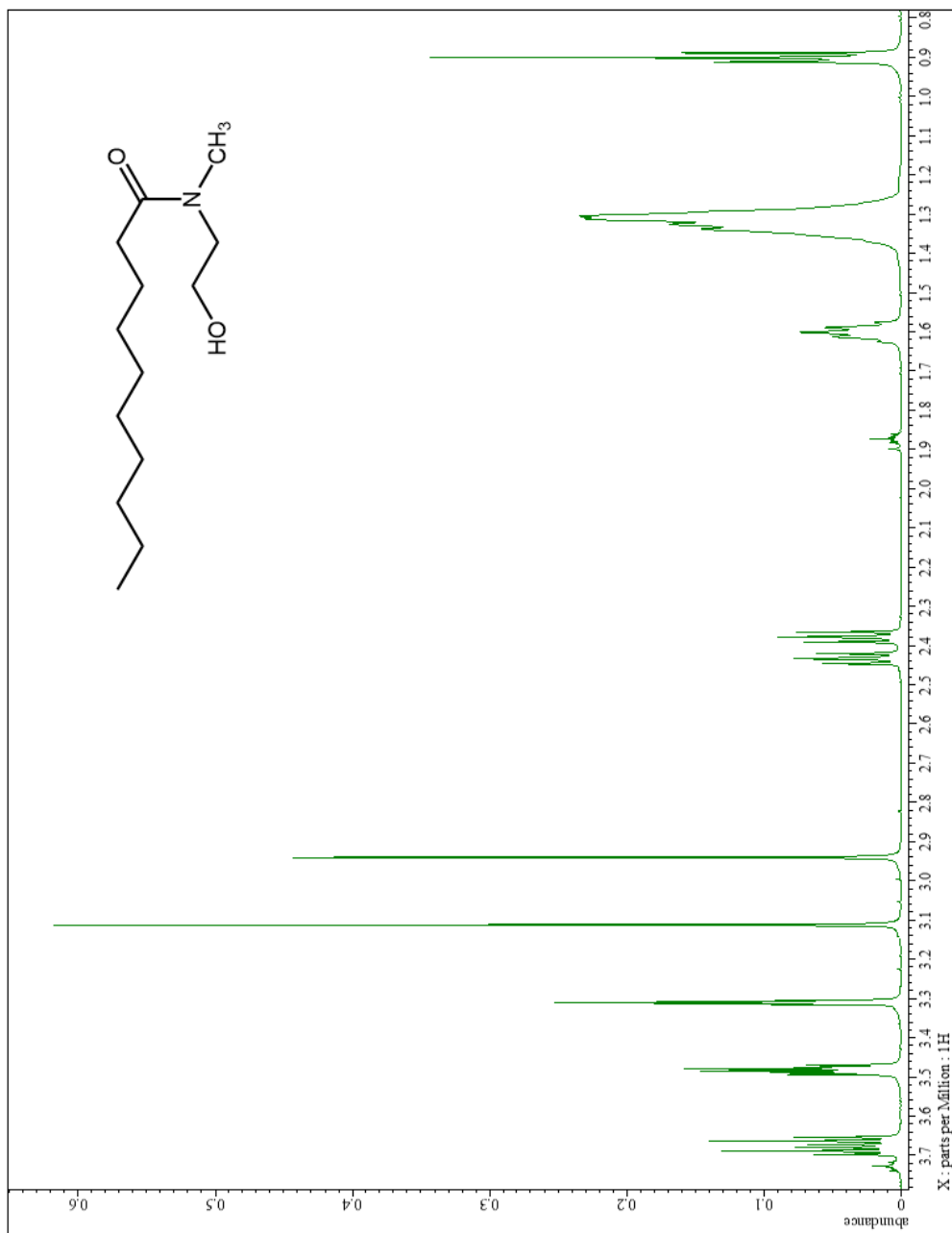
Compound **IV**: ¹H-NMR, CD₃OD

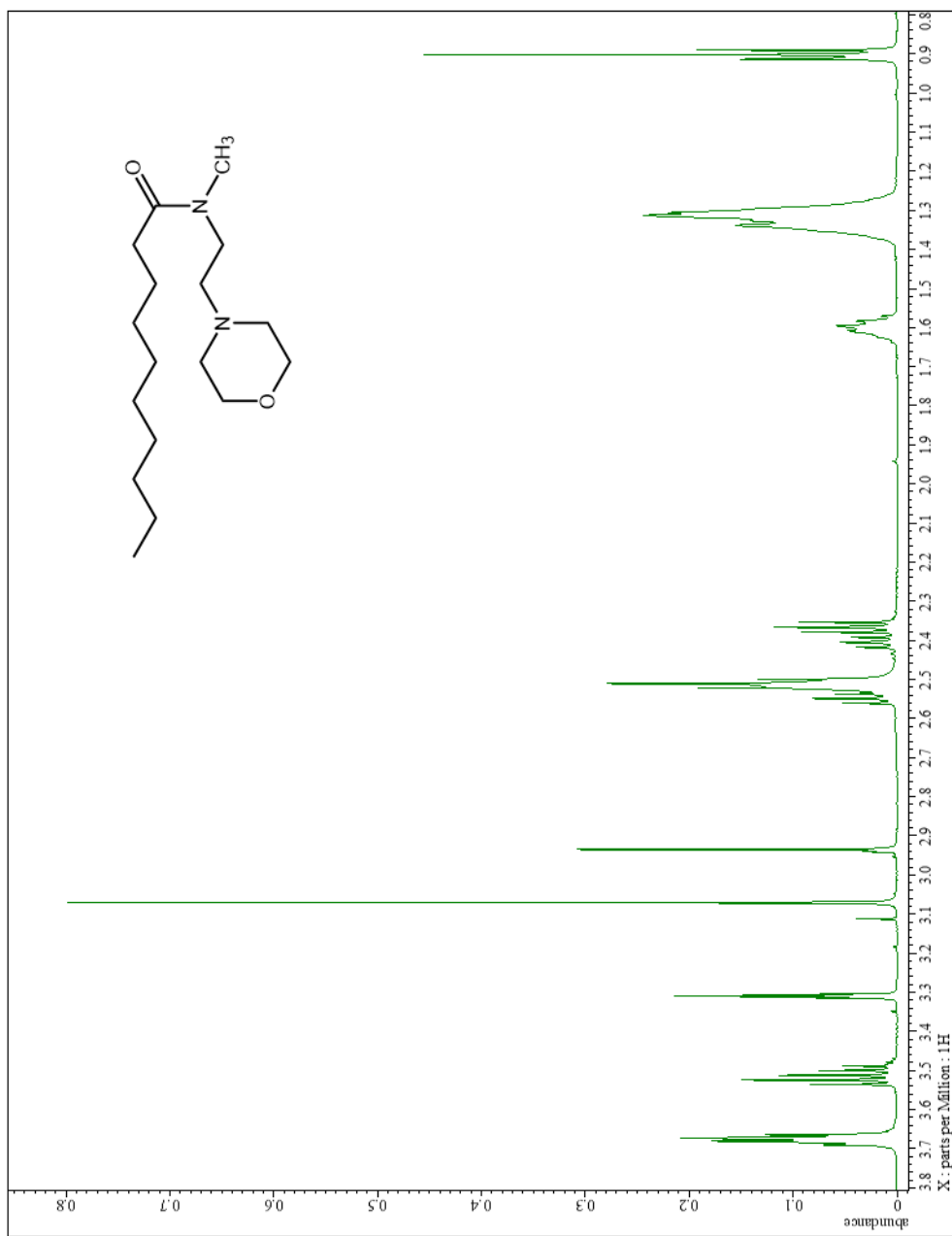
Compound V: $^1\text{H-NMR}$, CD_3OD

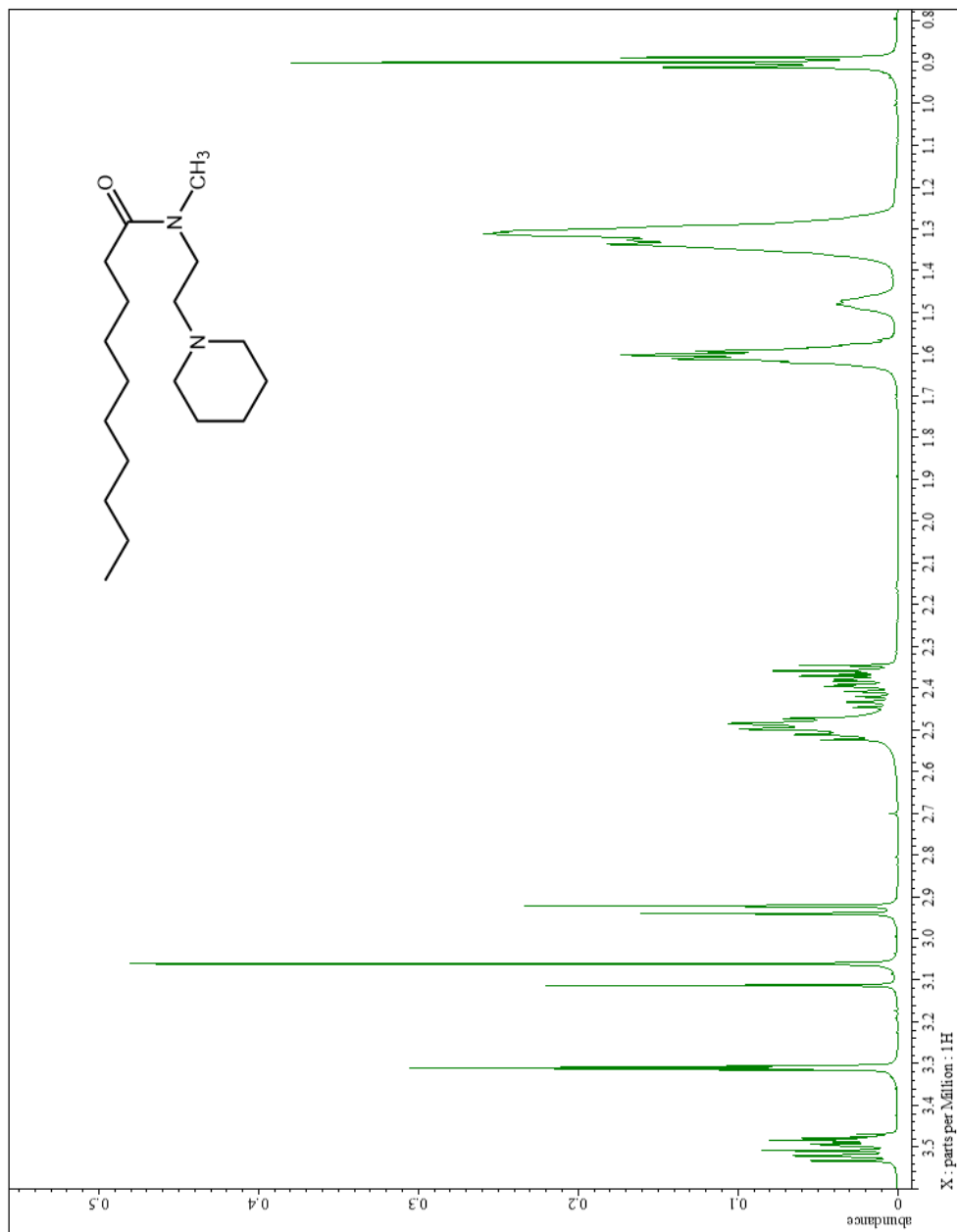
Compound VI: $^1\text{H-NMR}$, CDCl₃

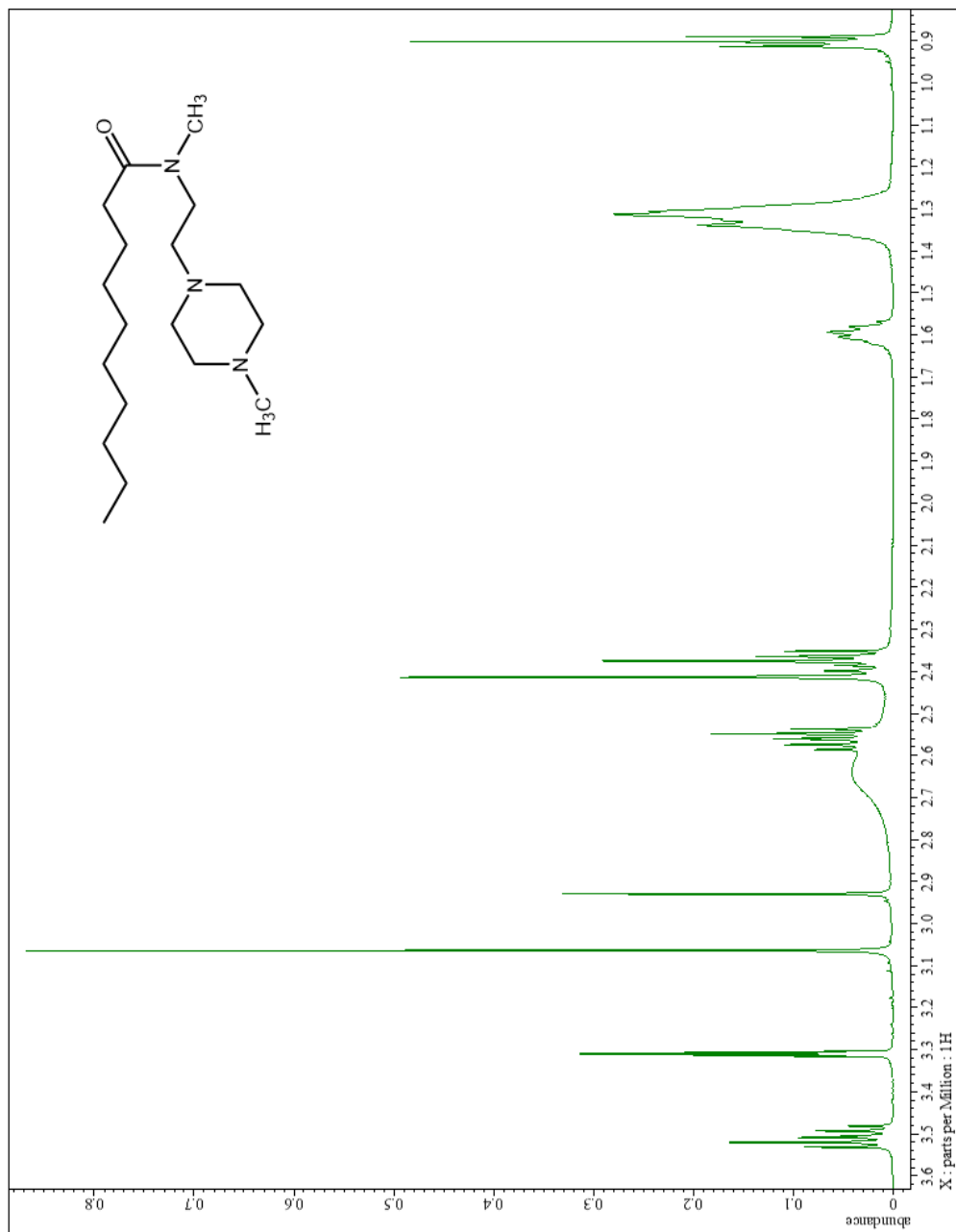
Compound VII: $^1\text{H-NMR}$, CD_3OD

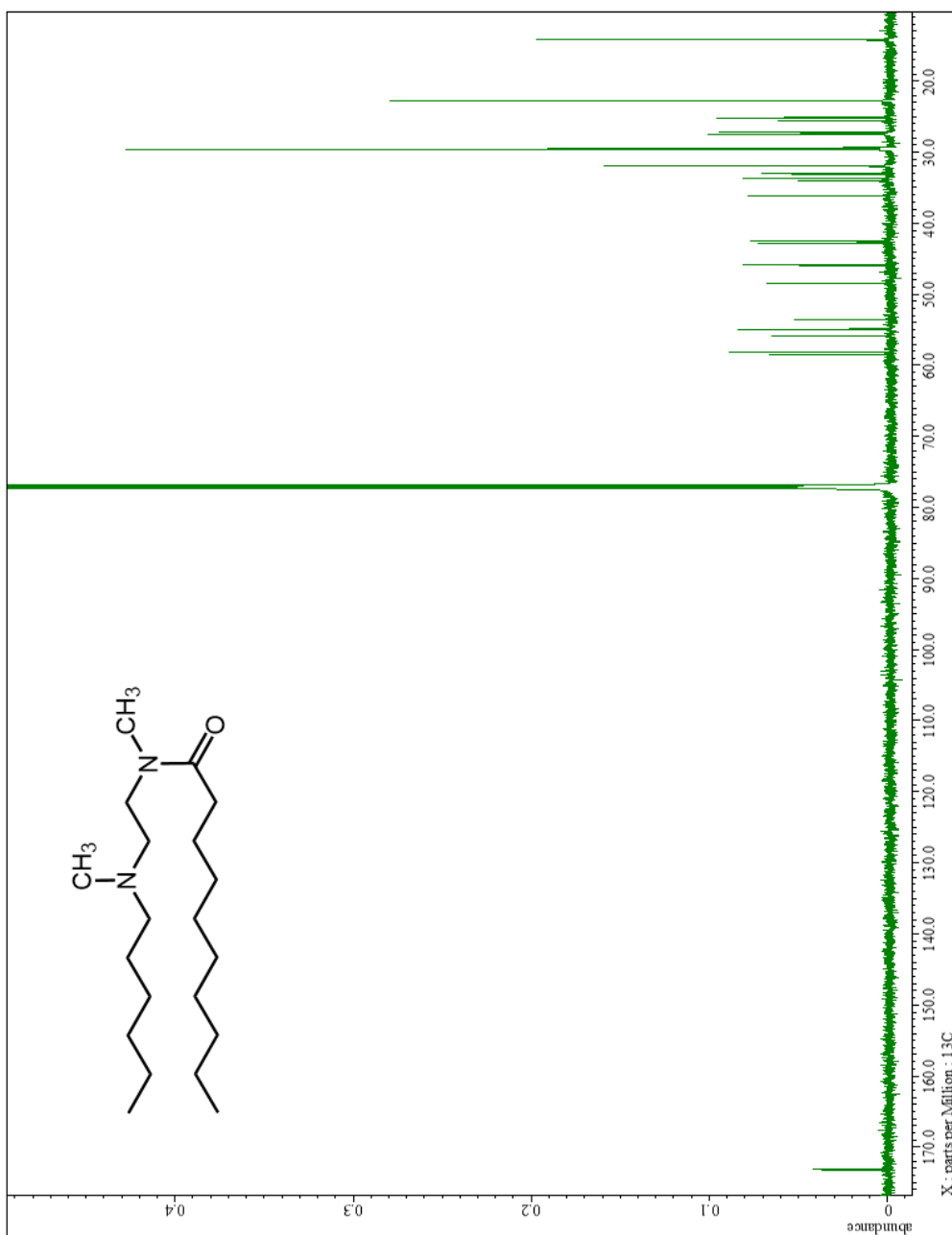
Compound VIII: ¹H-NMR, CD₃OD

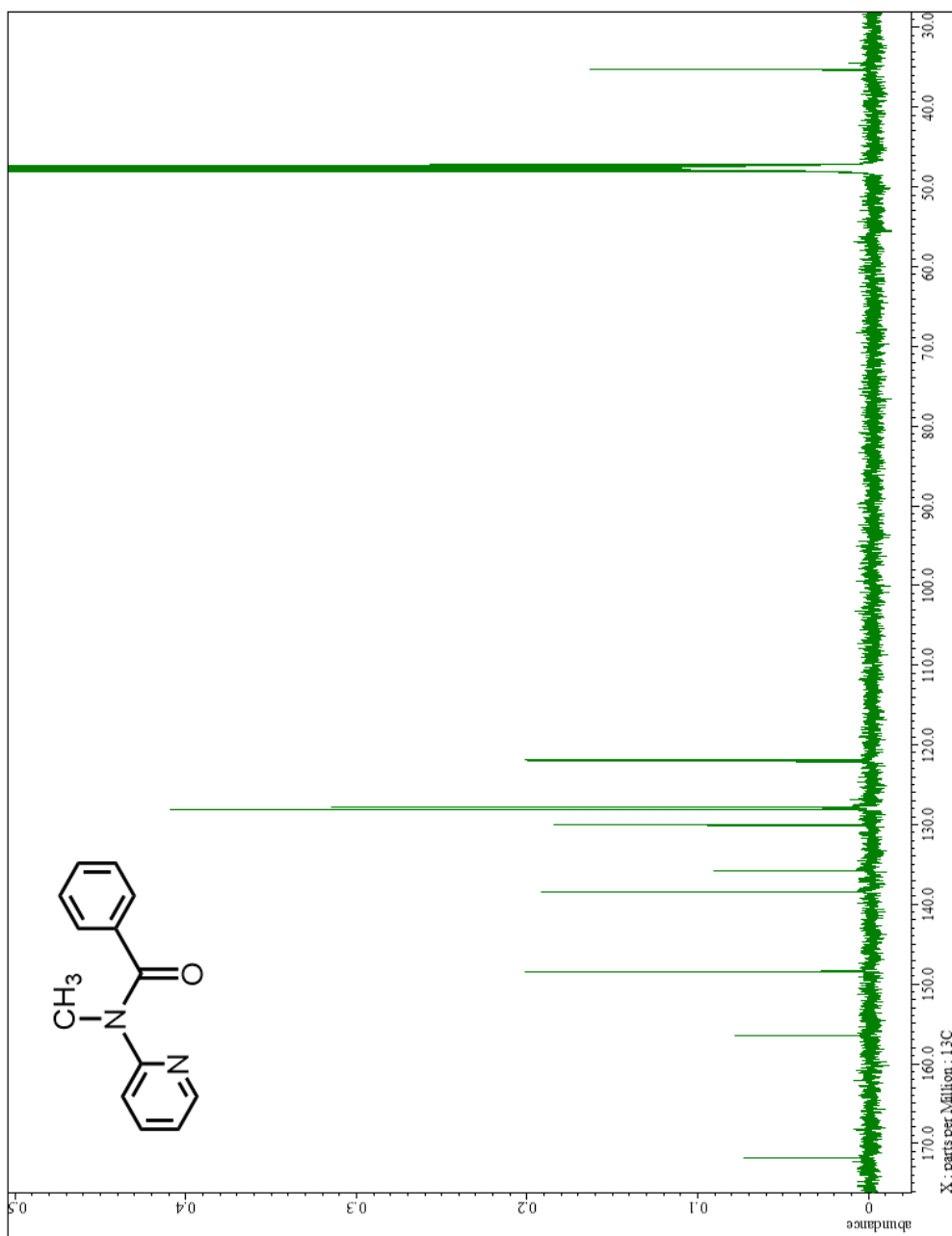
Compound X: $^1\text{H-NMR}$, CD_3OD

Compound XII: ¹H-NMR, CD₃OD

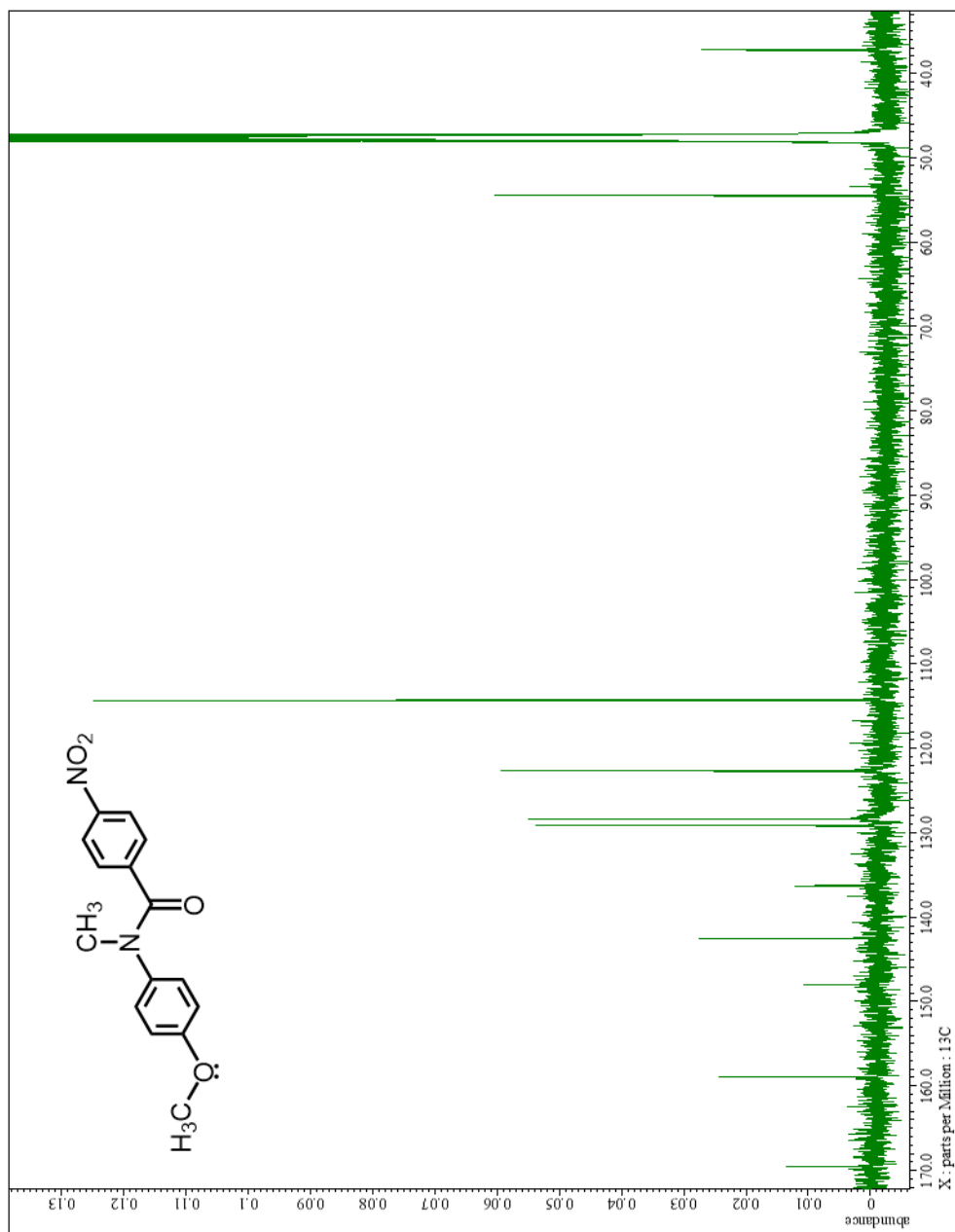
Compound XIII: $^1\text{H-NMR}$, CD_3OD

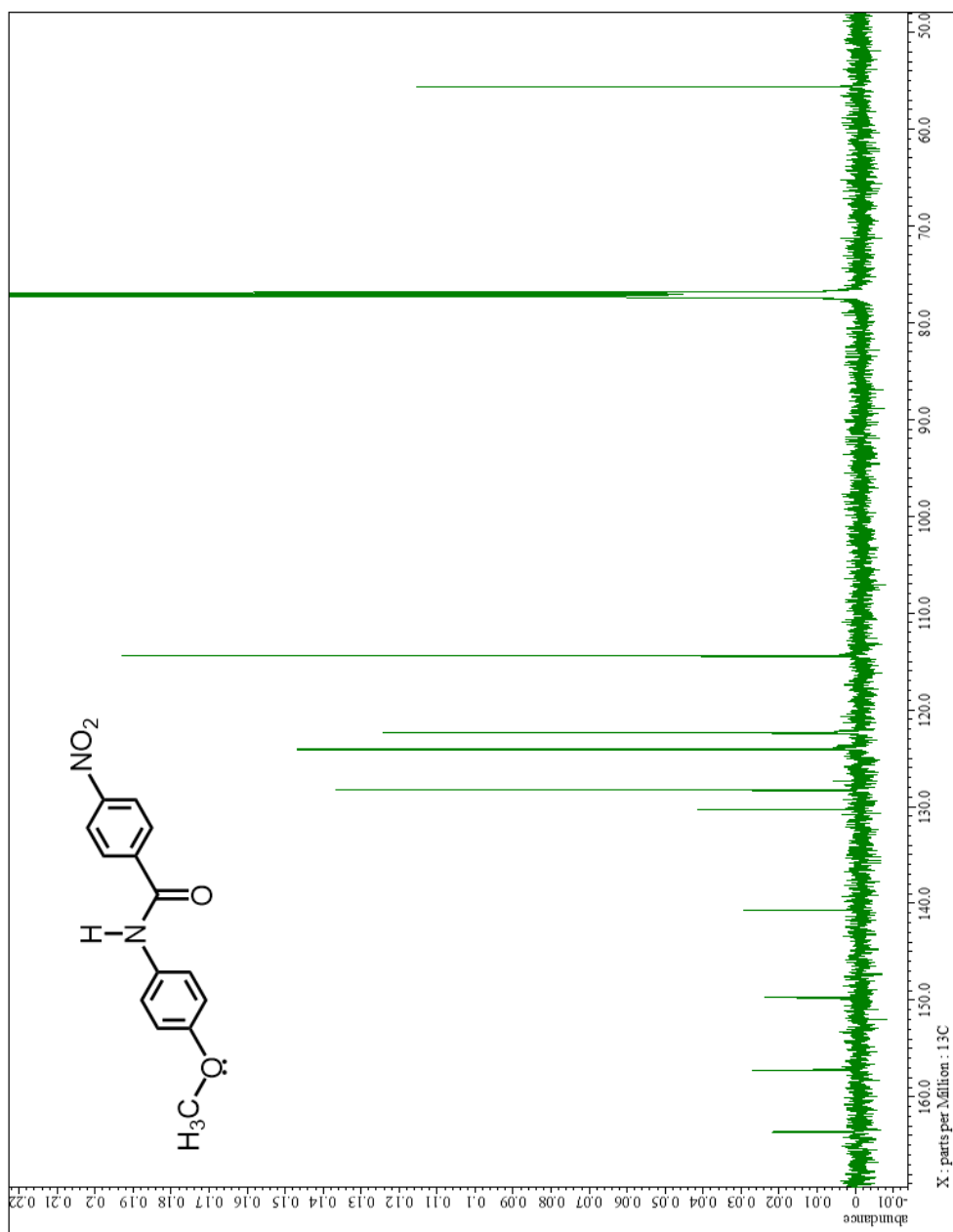
Compound XIV: $^1\text{H-NMR}$, CD_3OD

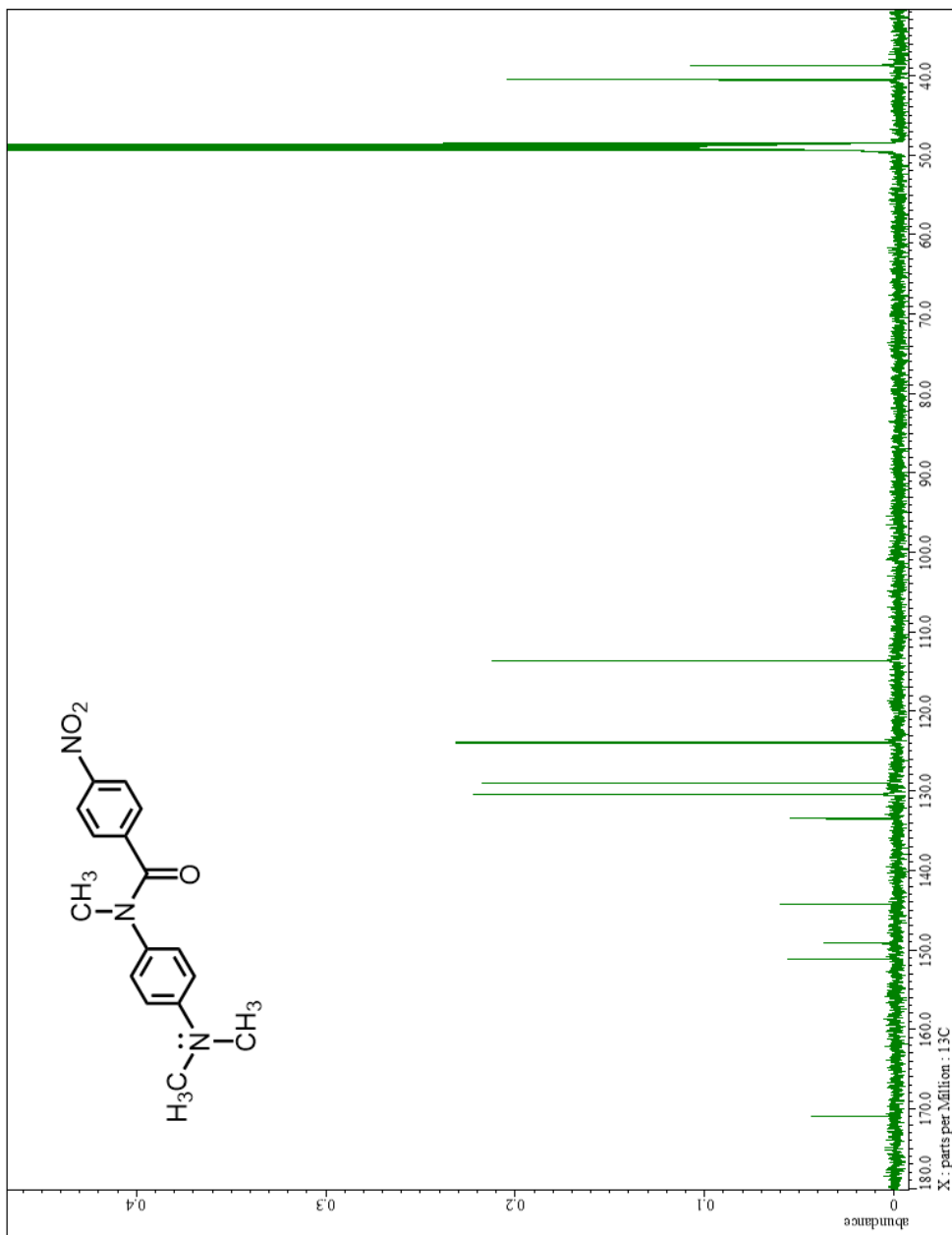
APPENDIX B: SELECTED ^{13}C -NMR SPECTRACompound I: ^{13}C -NMR, CDCl_3

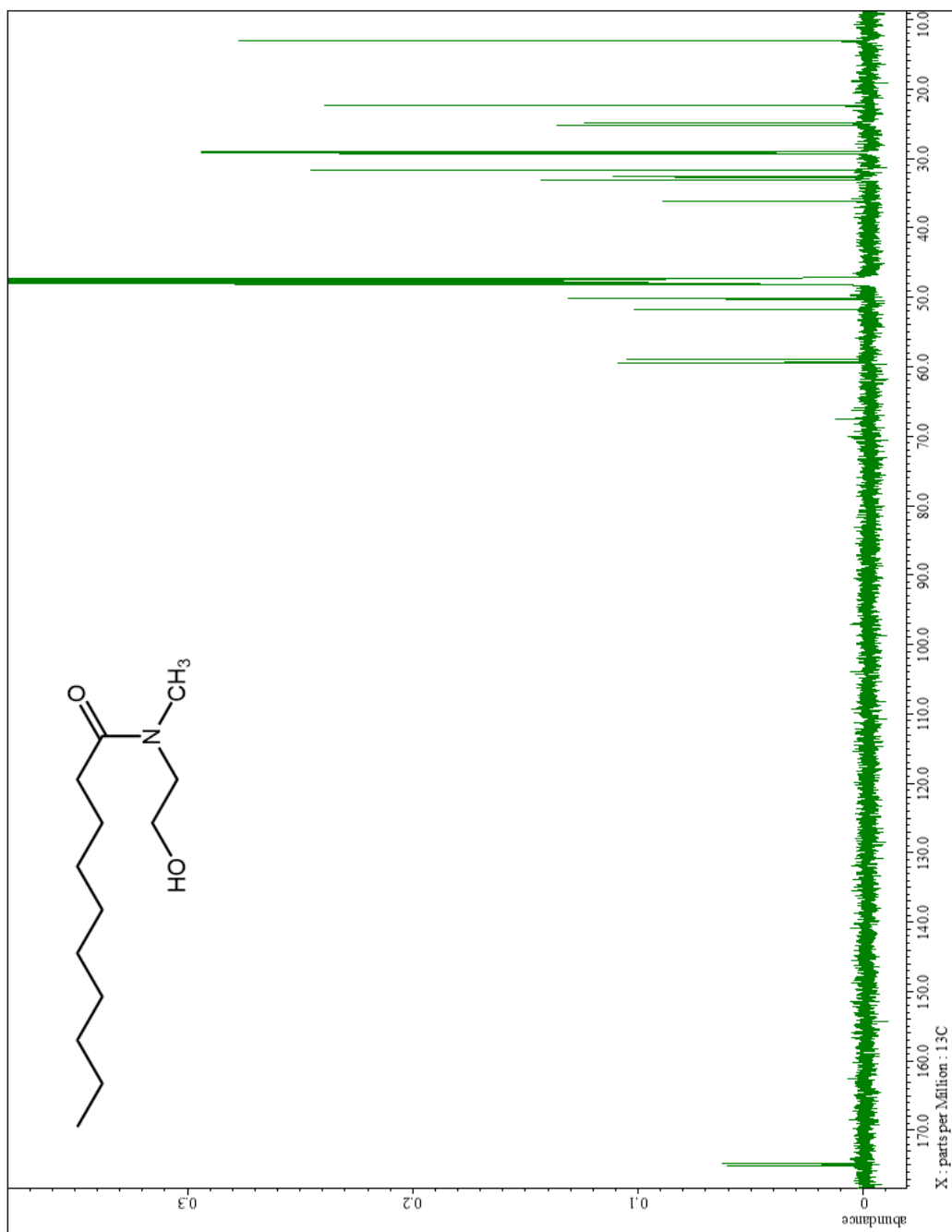


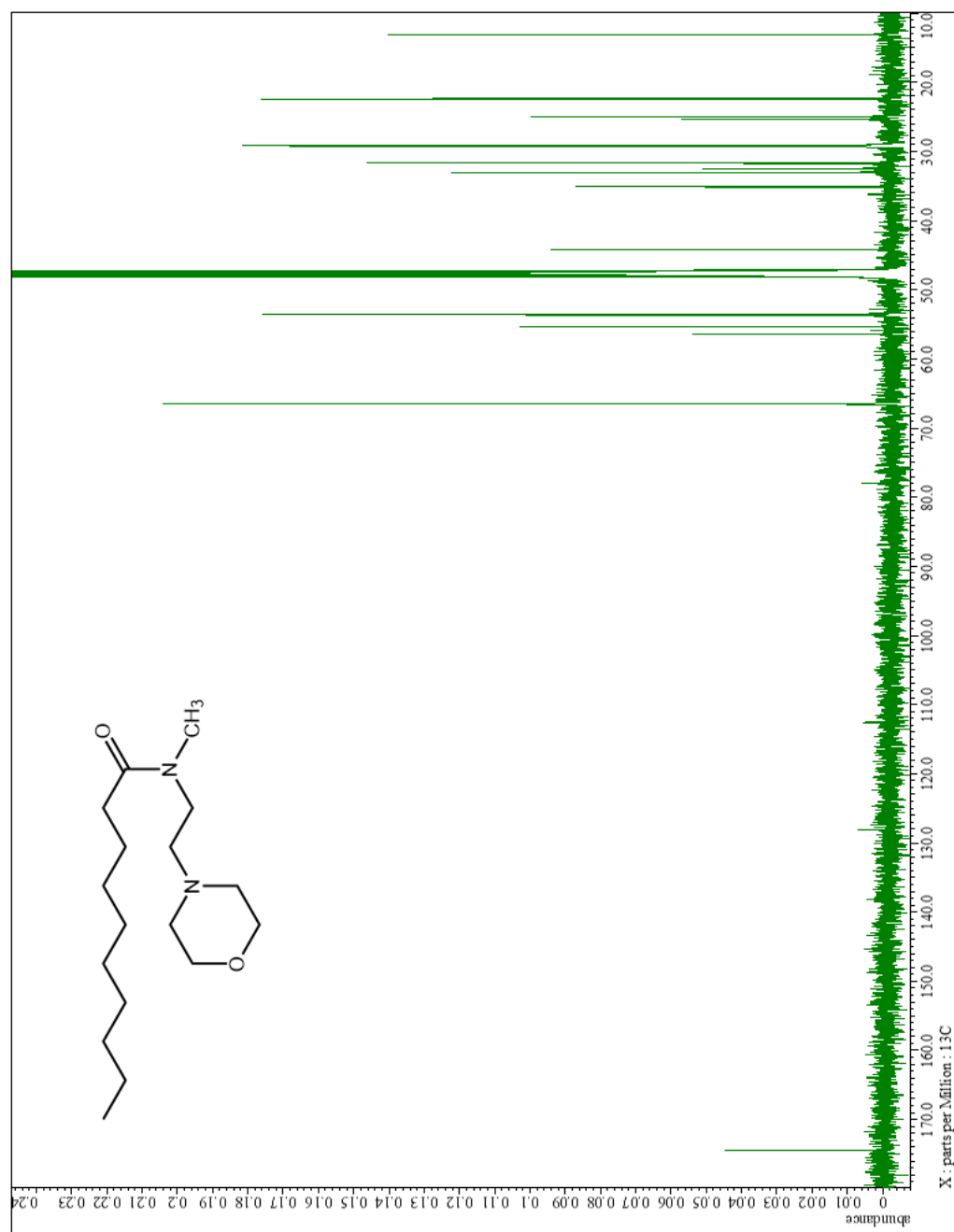
Compound IV: ¹³C-NMR, CD₃OD

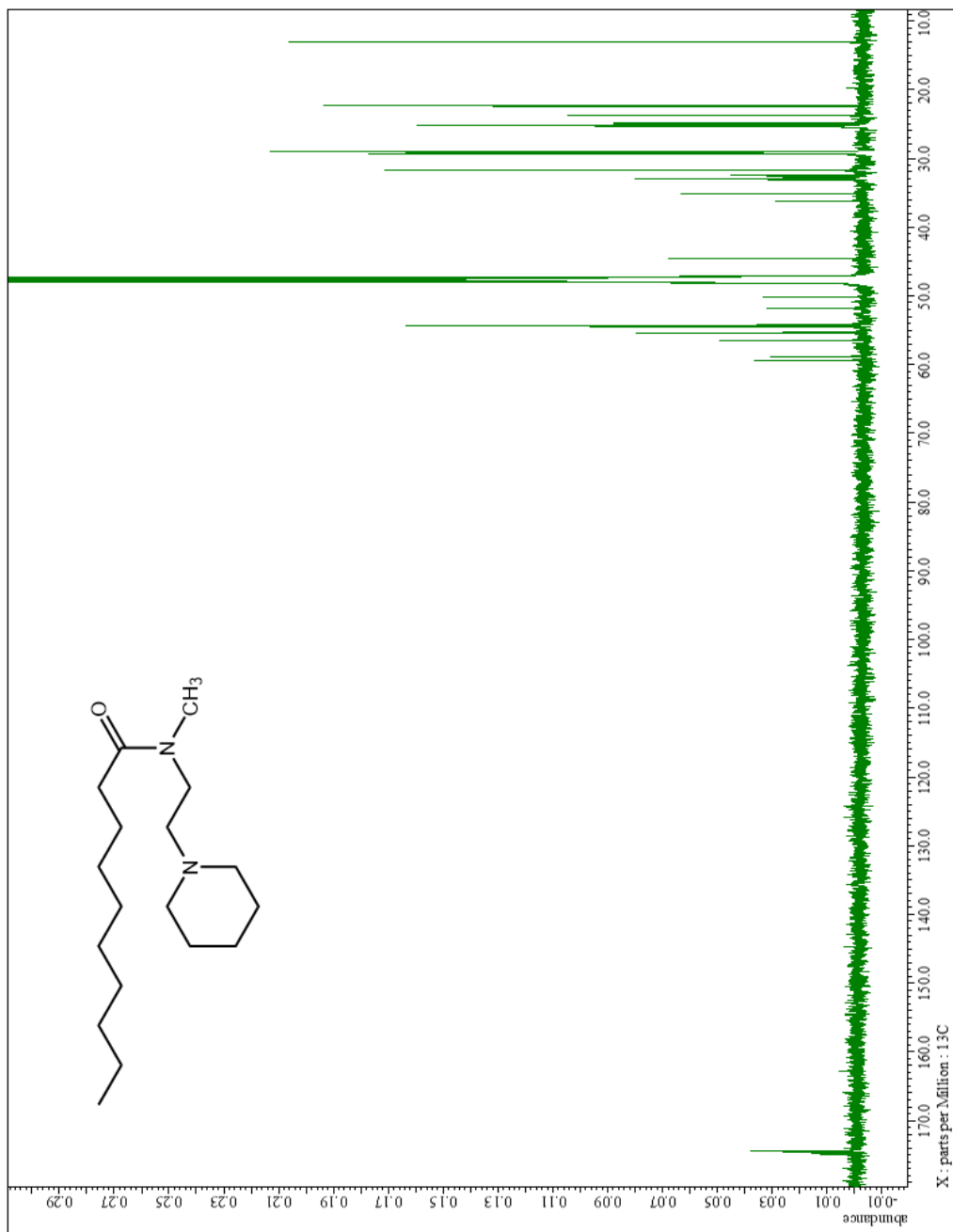
Compound V: ^{13}C -NMR, CD_3OD

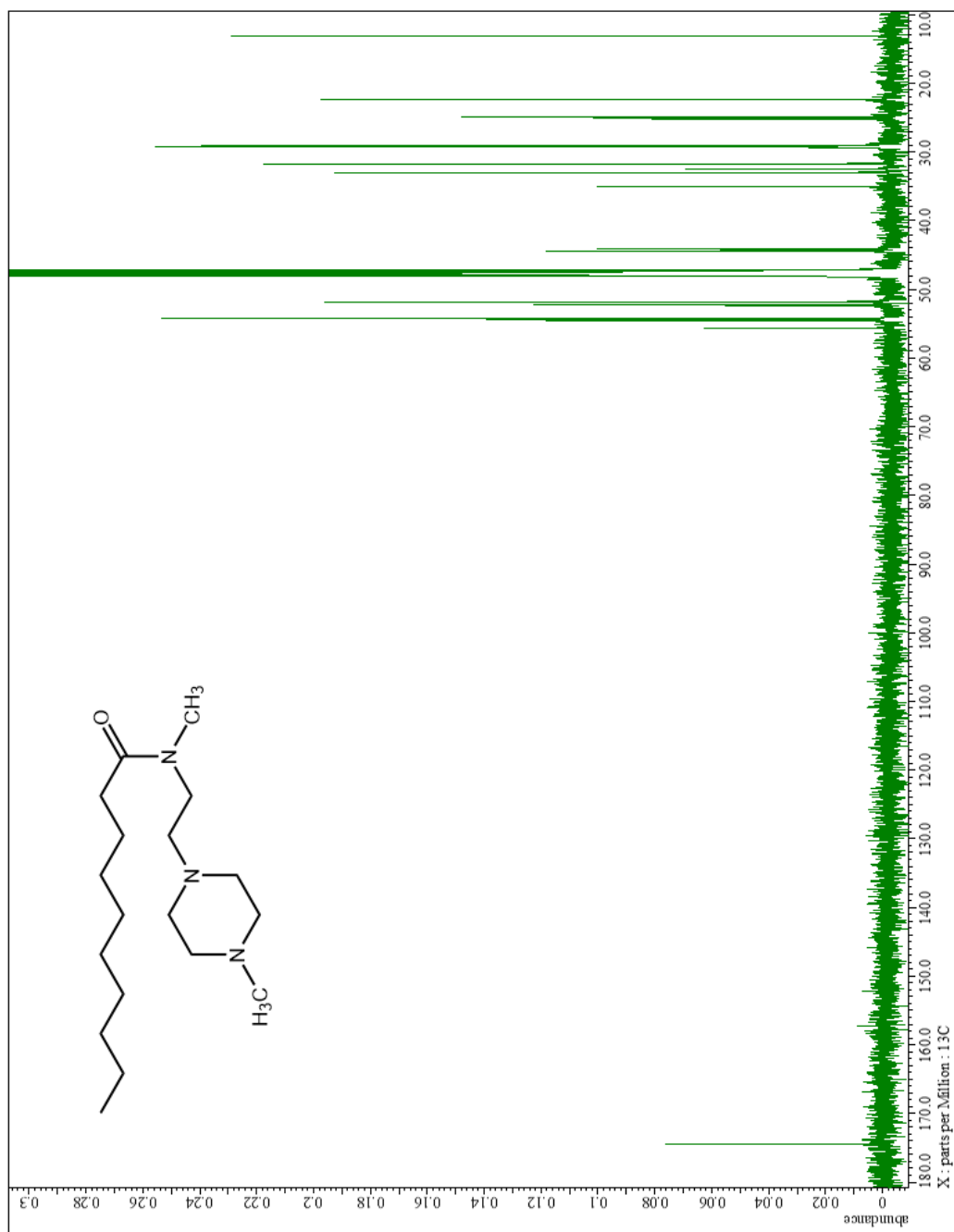
Compound VI: ^{13}C -NMR, CDCl_3

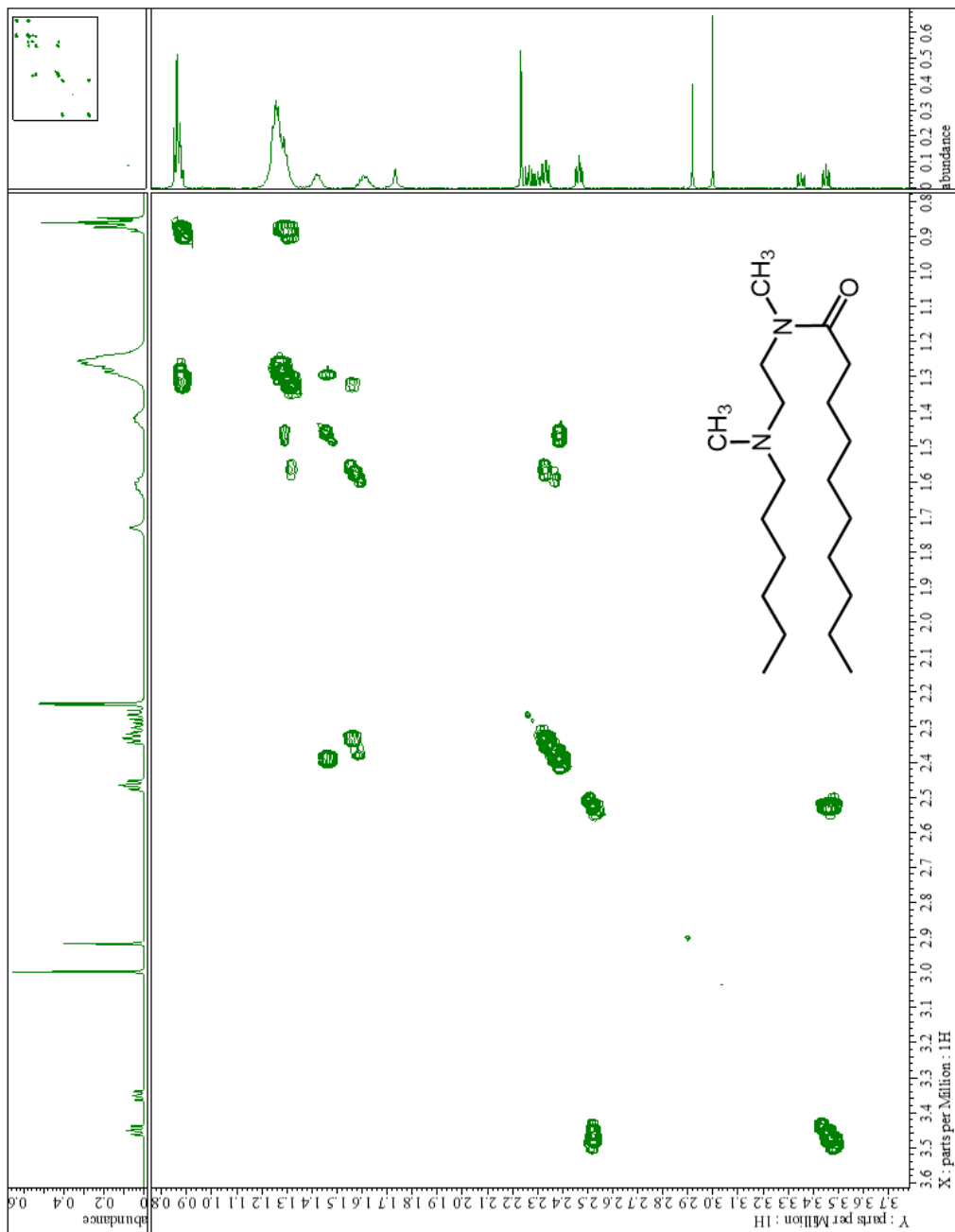
Compound VII: ^{13}C -NMR, CD_3OD

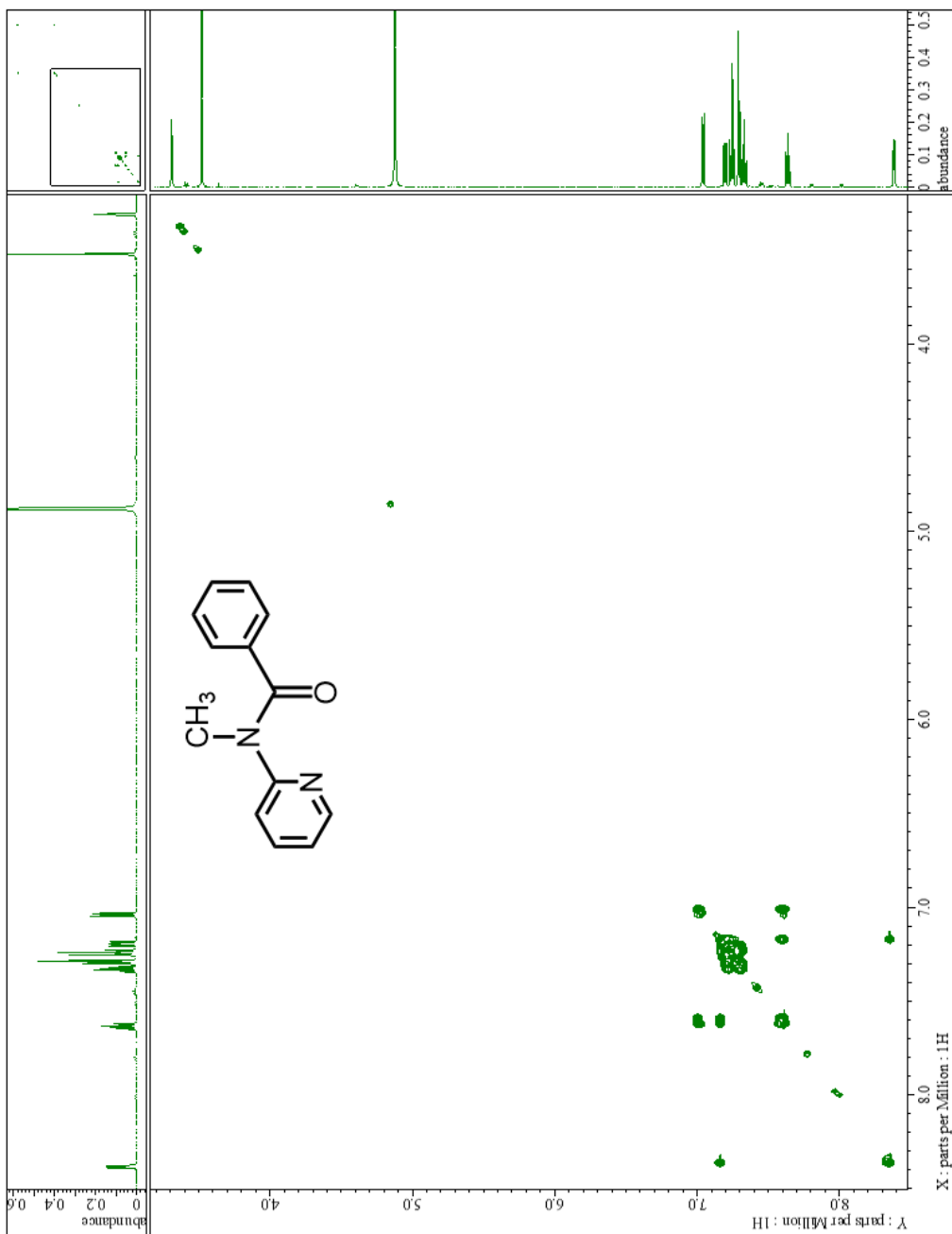
Compound X: $^{13}\text{C-NMR}$, CD₃OD

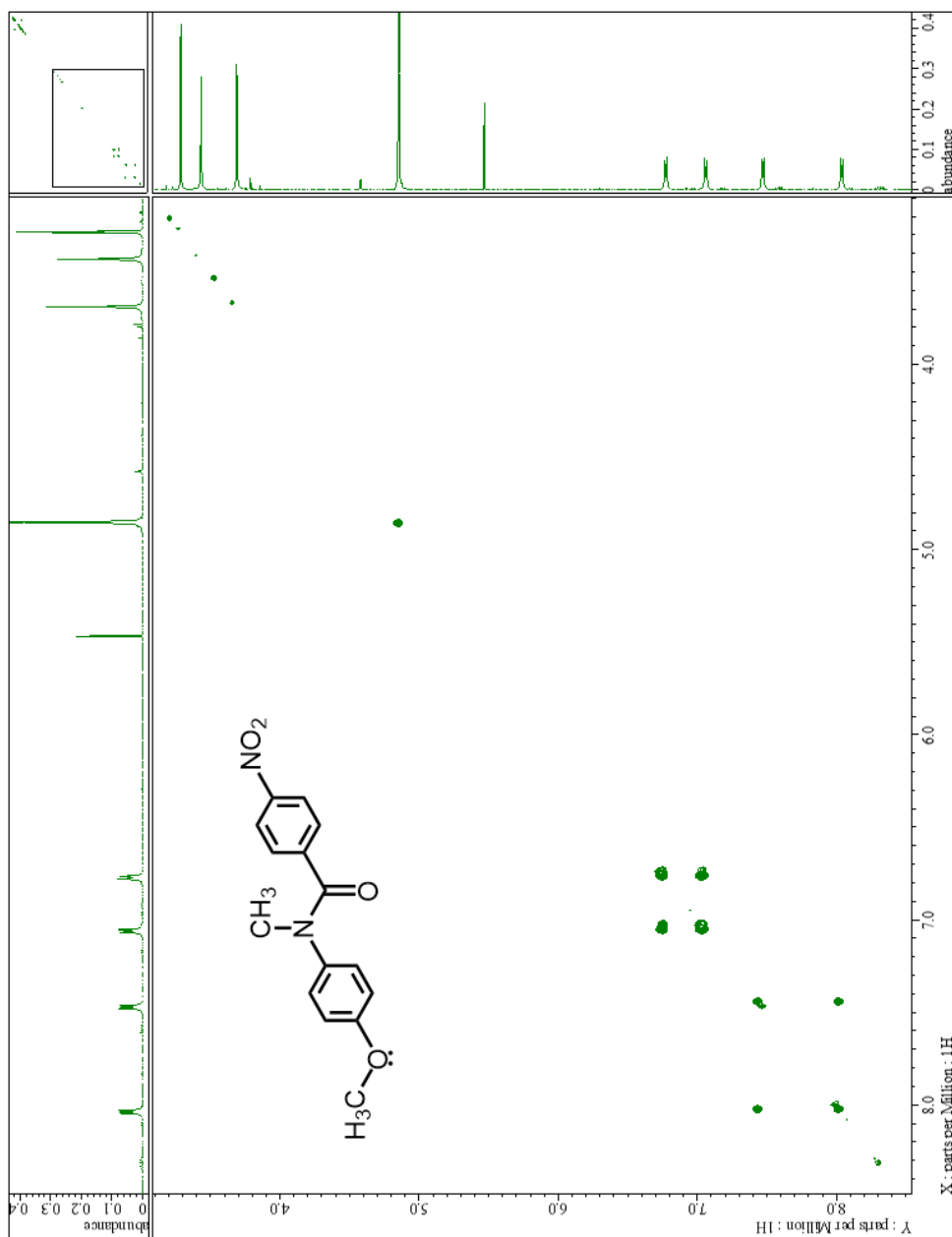
Compound XII: ^{13}C -NMR, CD_3OD

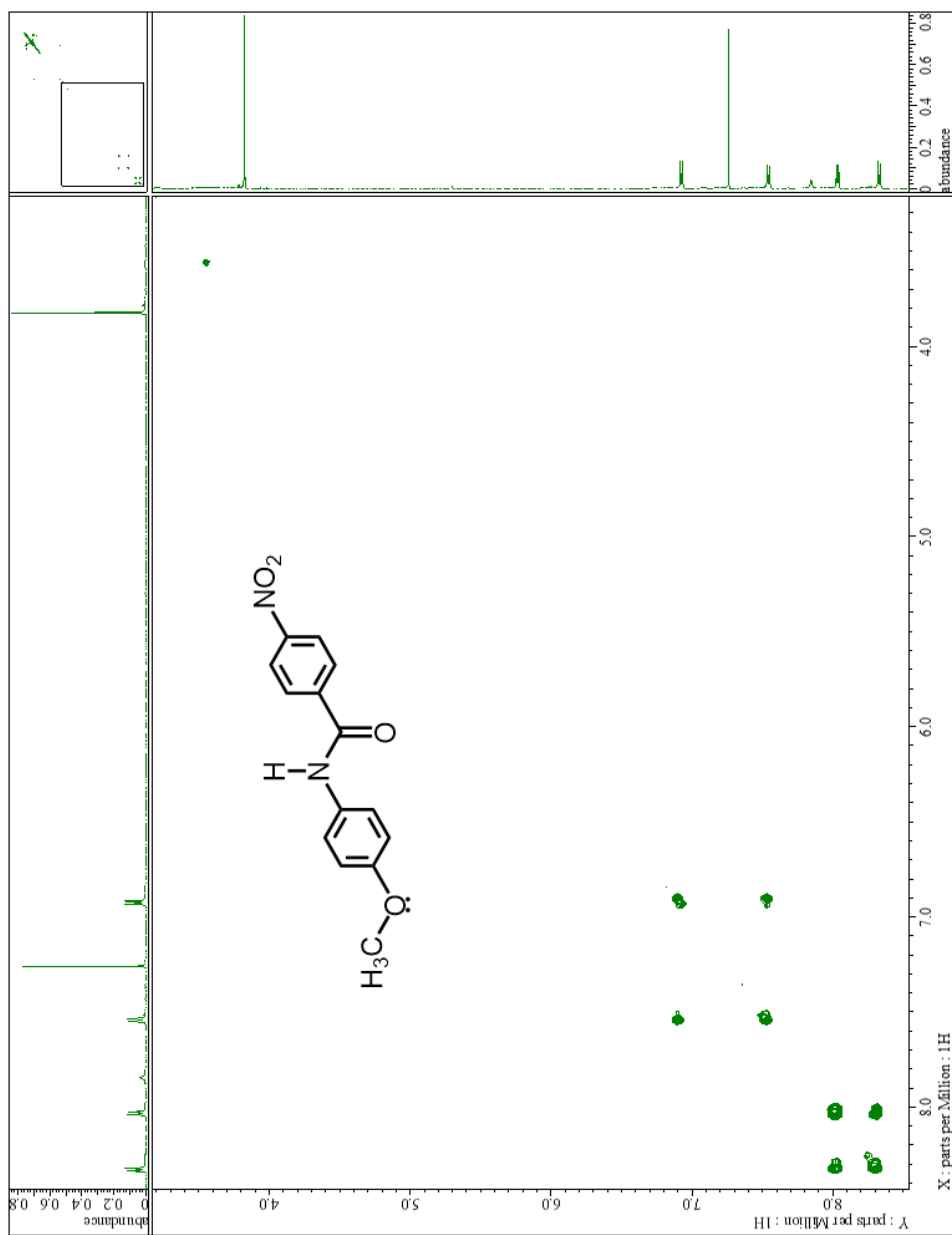
Compound XIII: ^{13}C -NMR, CD_3OD

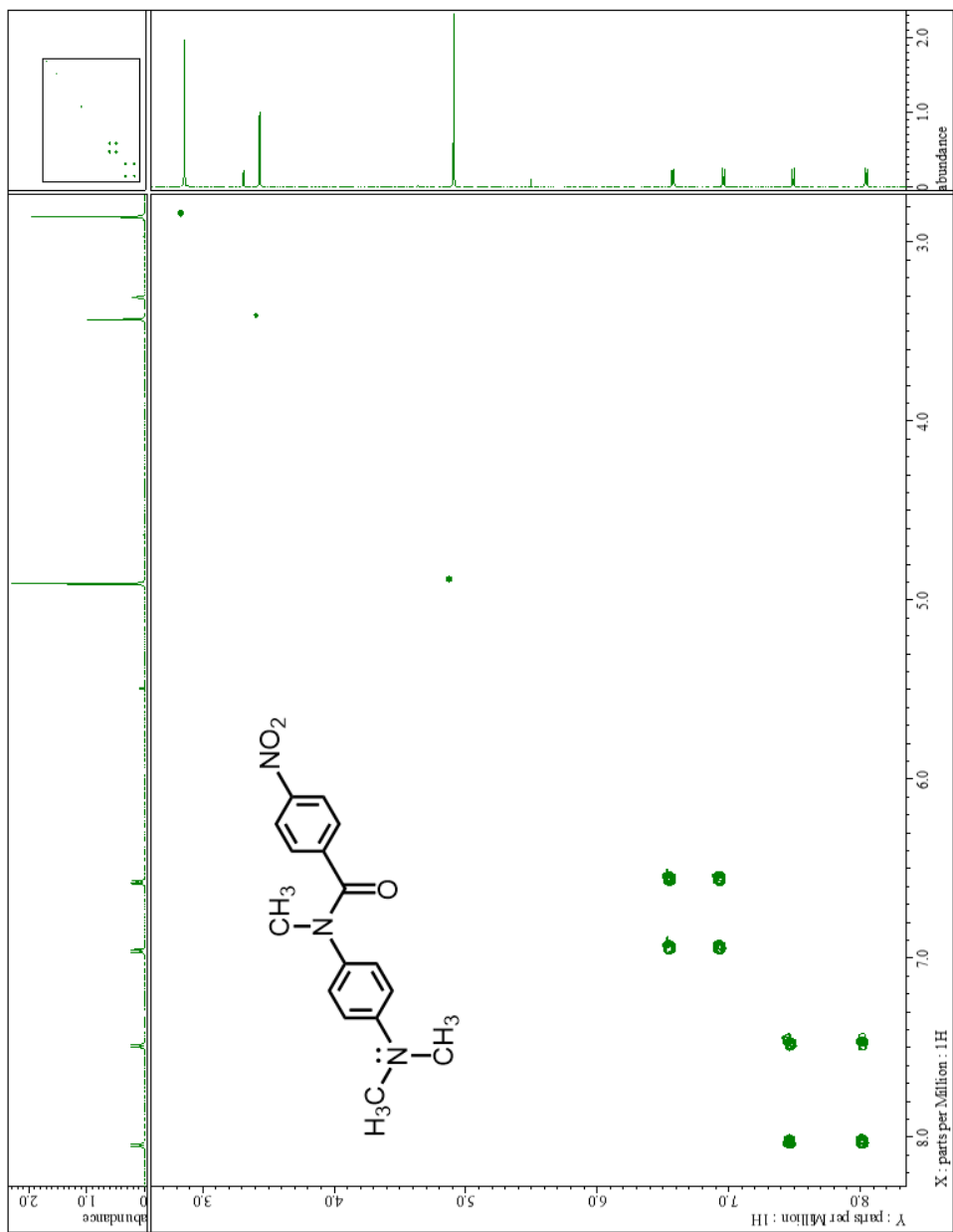
Compound XIV: ^{13}C -NMR, CD_3OD

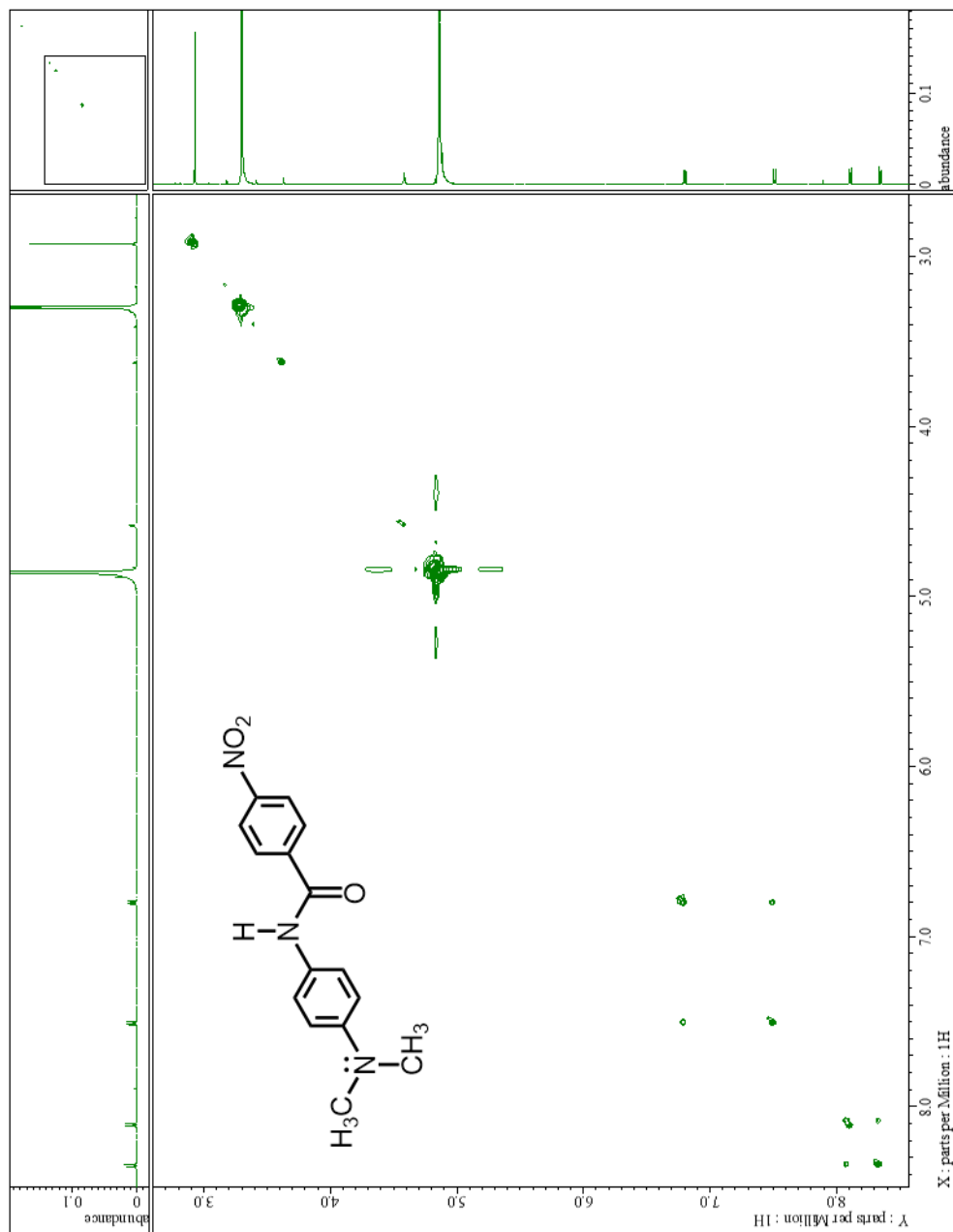
APPENDIX C: SELECTED ^1H - ^1H COSY SPECTRACompound I: ^1H - ^1H NMR, CDCl_3

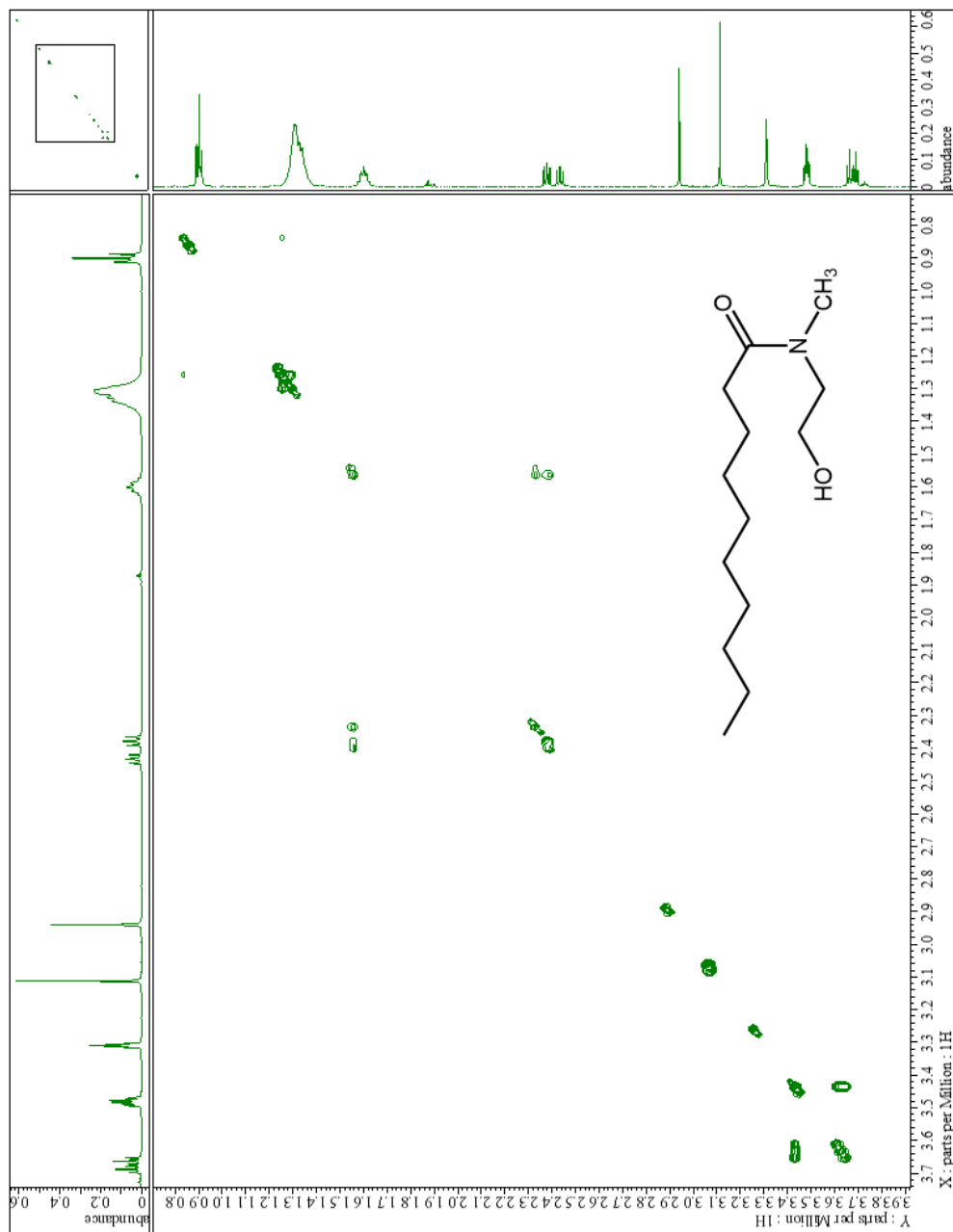
Compound IV: ^1H - ^1H NMR, CD_3OD

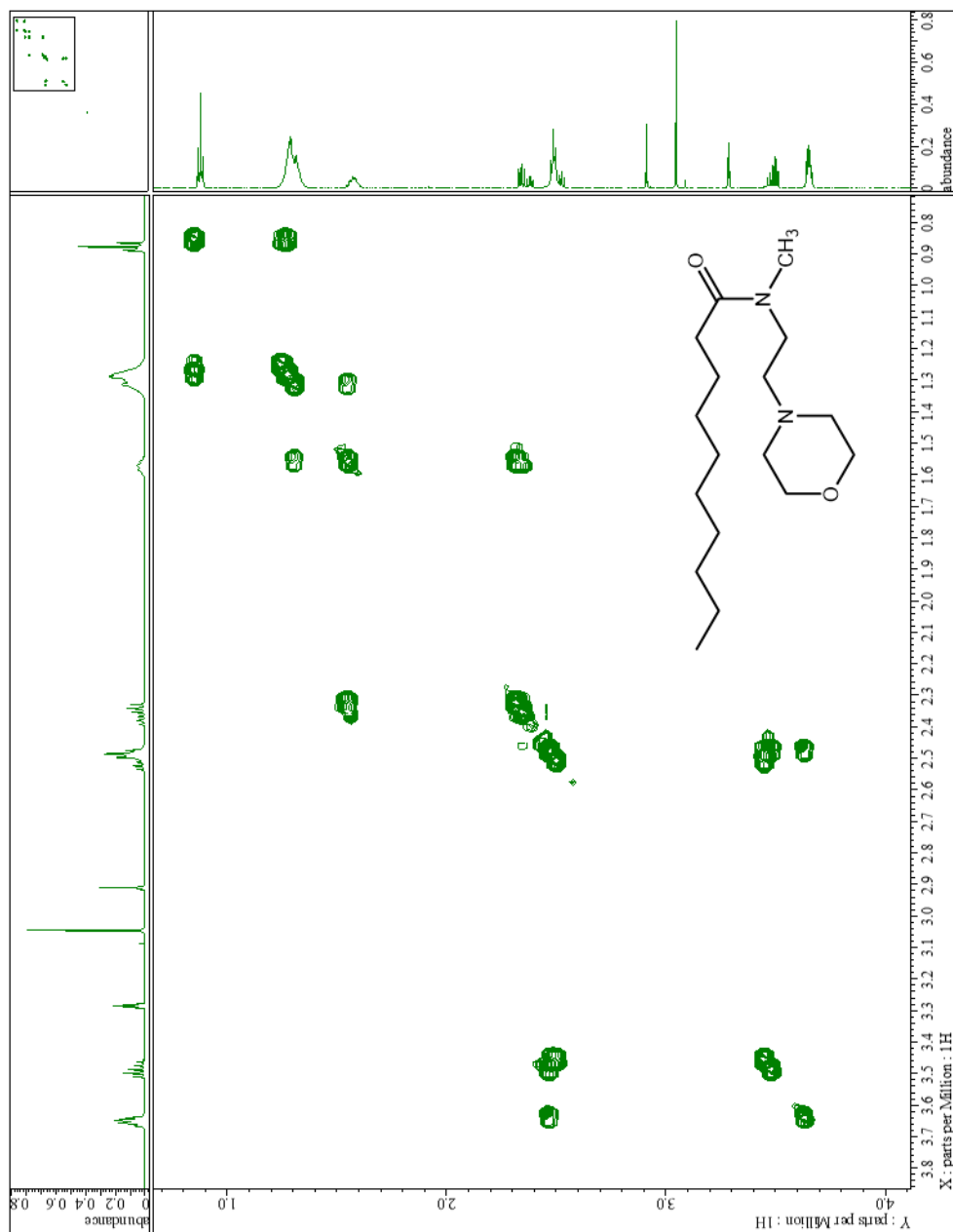
Compound V: ^1H - ^1H NMR, CD₃OD

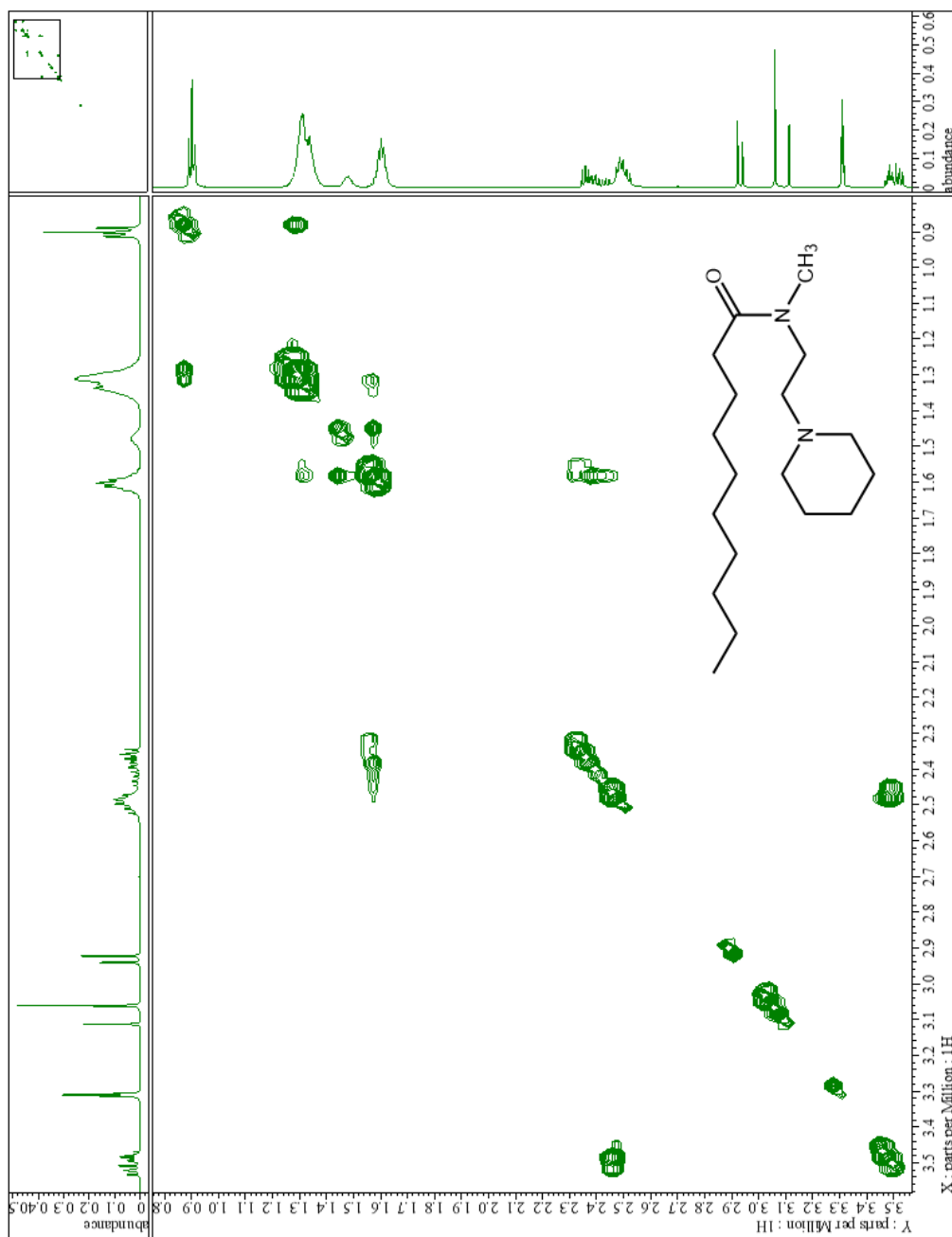
Compound VI: $^1\text{H-NMR}$, CDCl₃

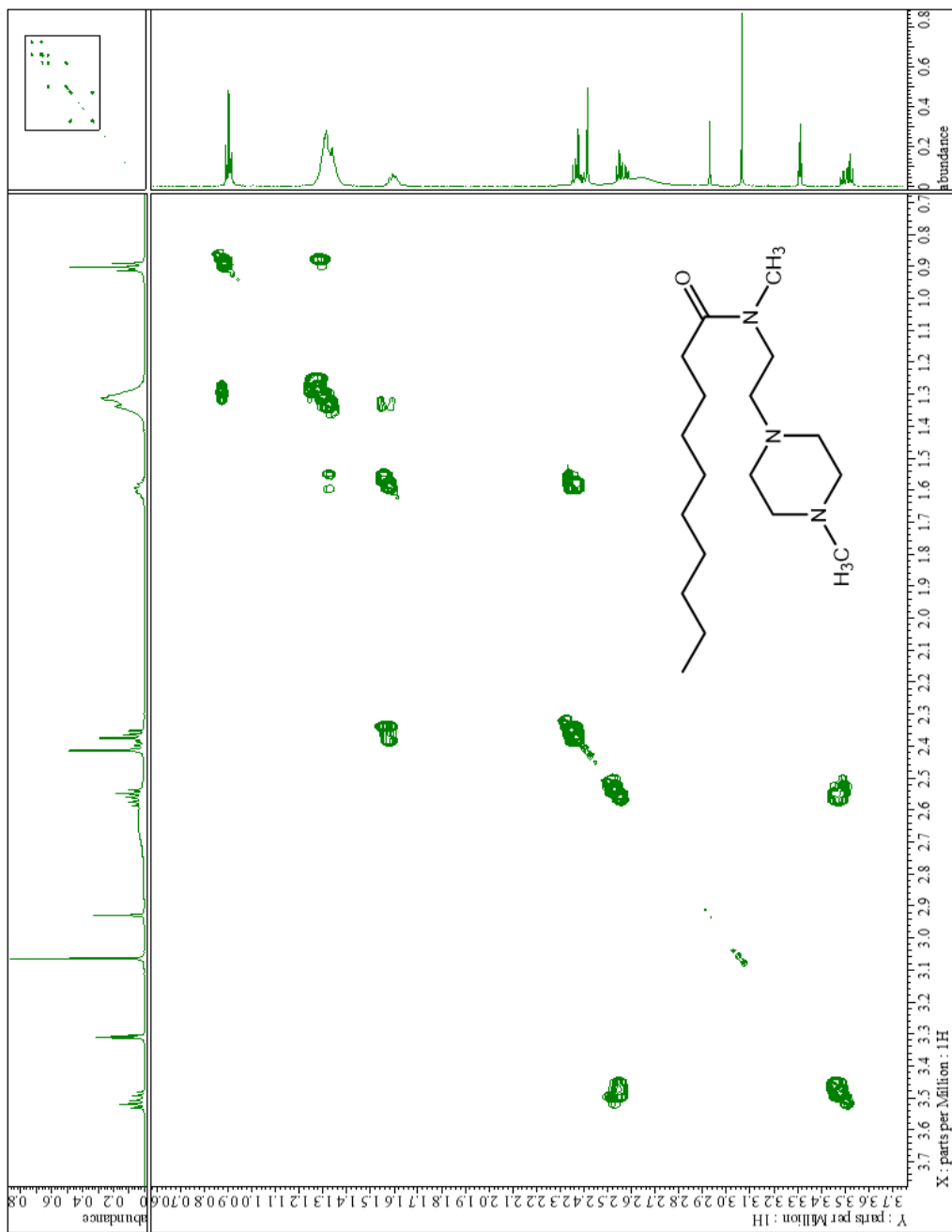
Compound VII: ^1H - ^1H NMR, CD₃OD

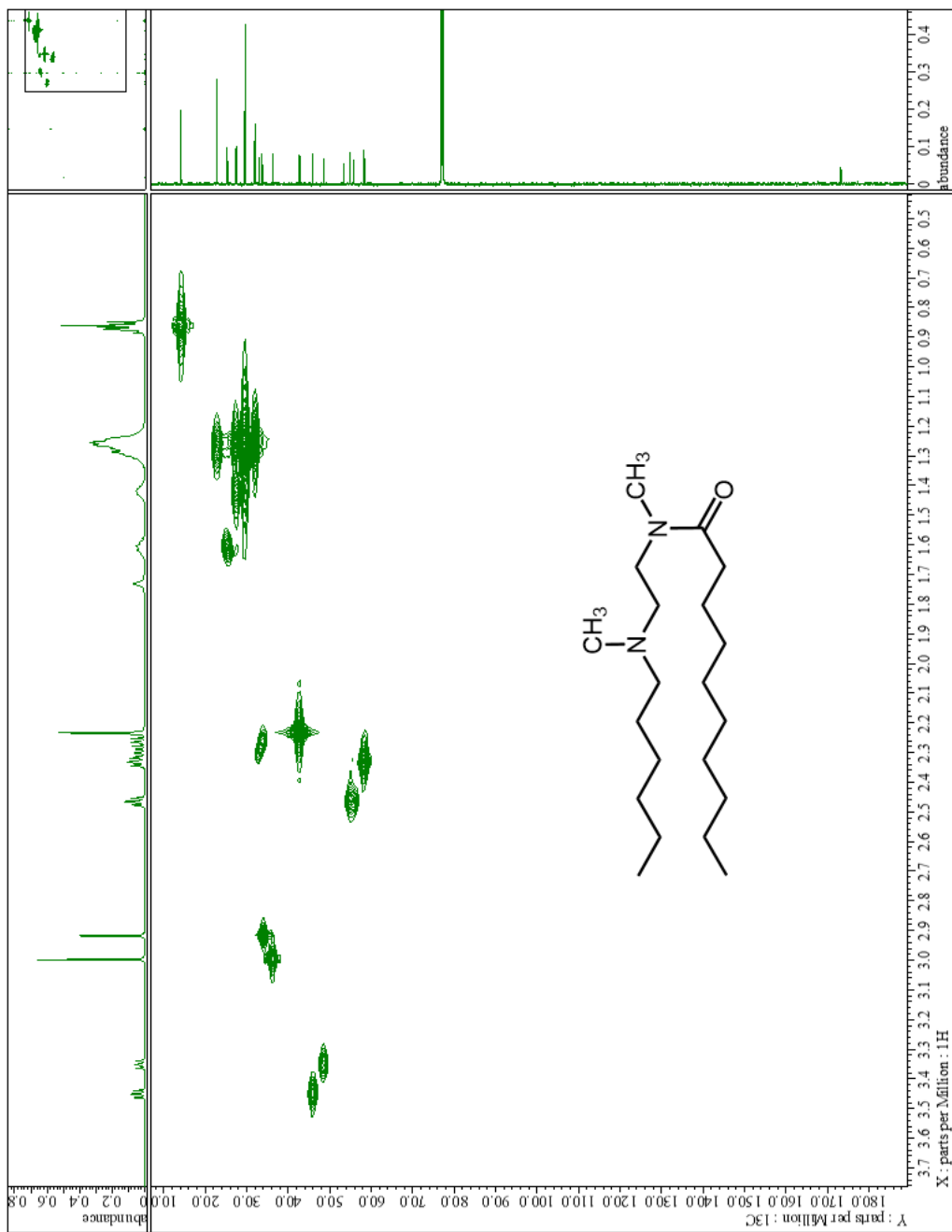
Compound VIII: ^1H - ^1H NMR, CD_3OD

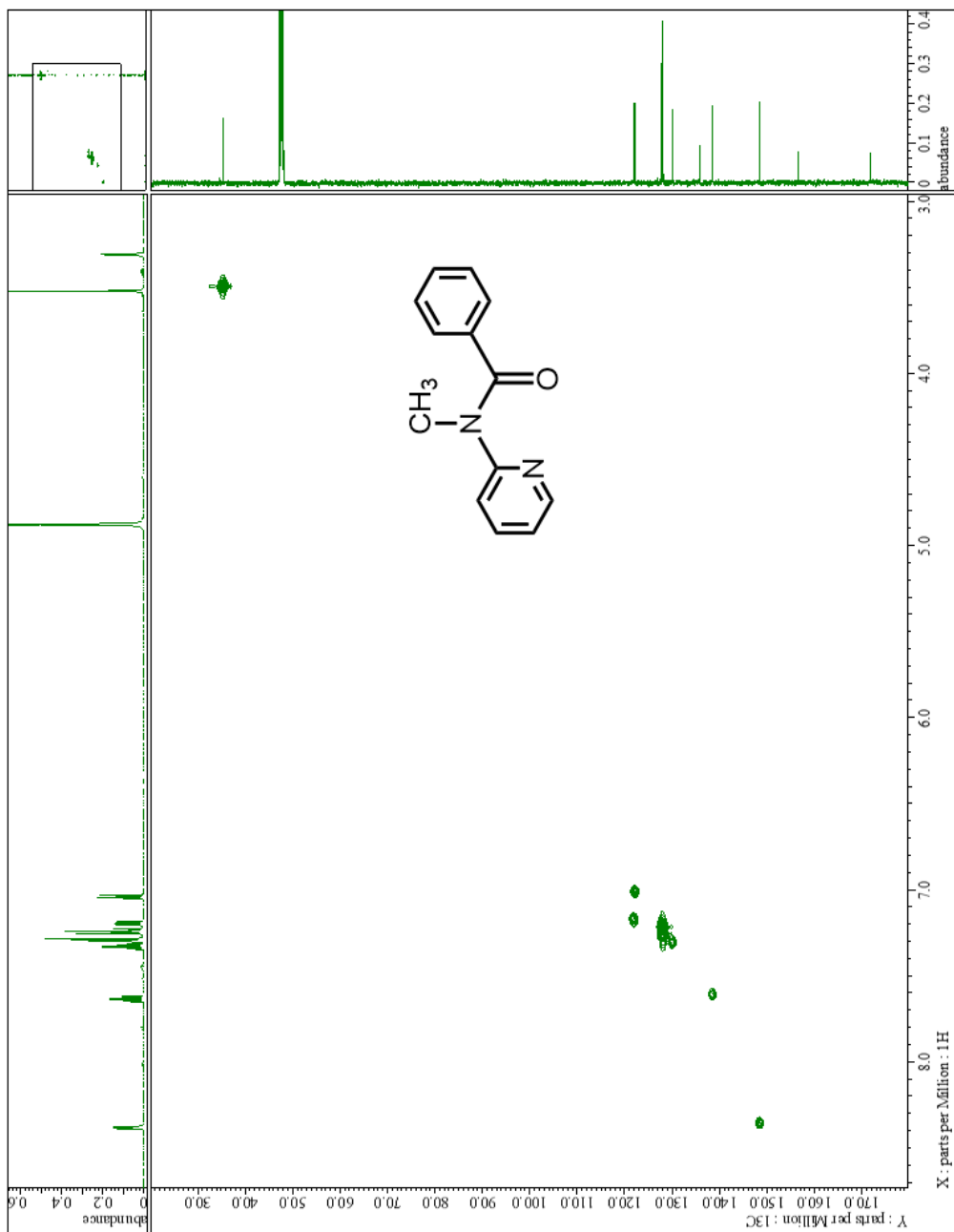
Compound X: ^1H - ^1H NMR, CD_3OD

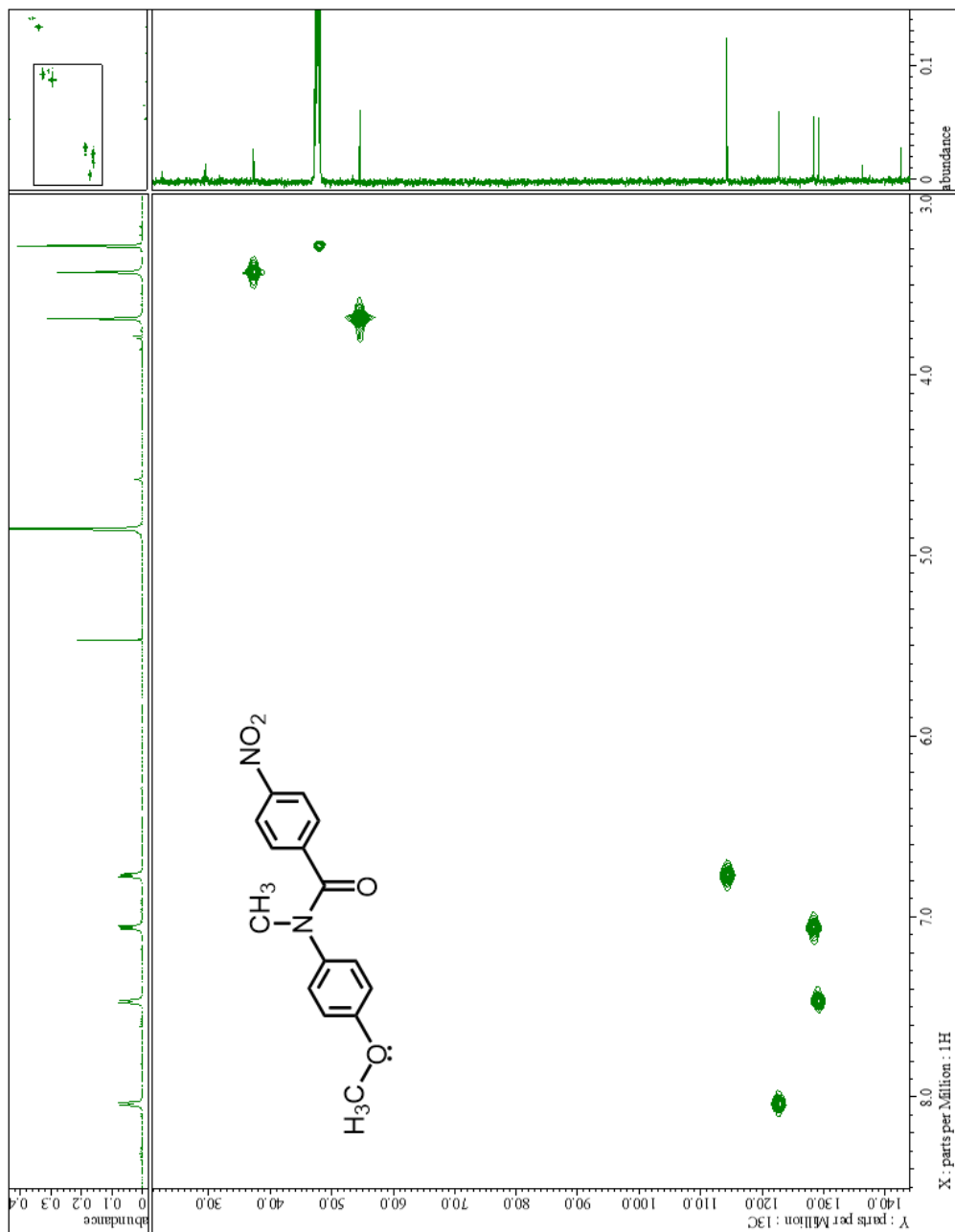
Compound XII: $^1\text{H-NMR}$, CD₃OD

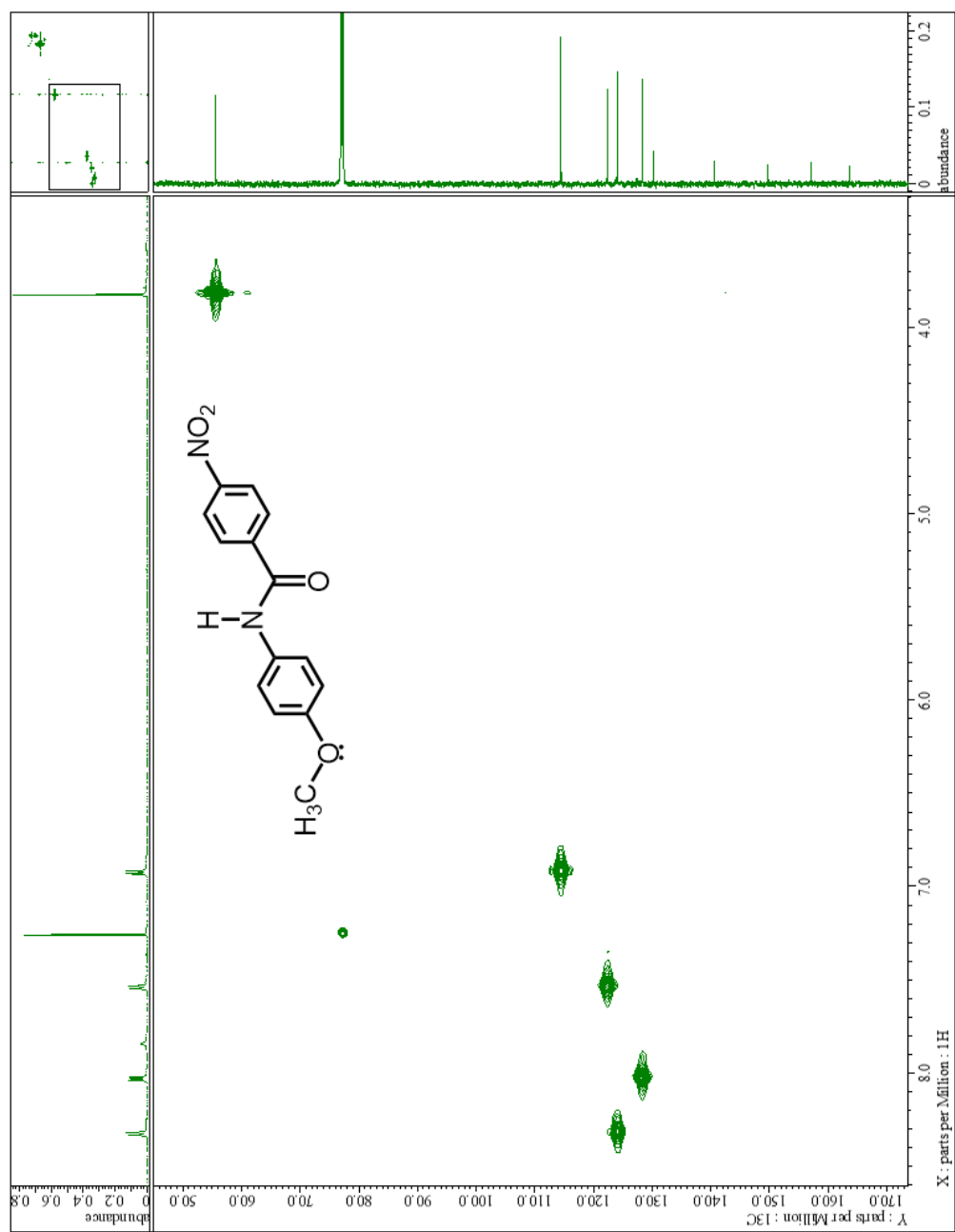


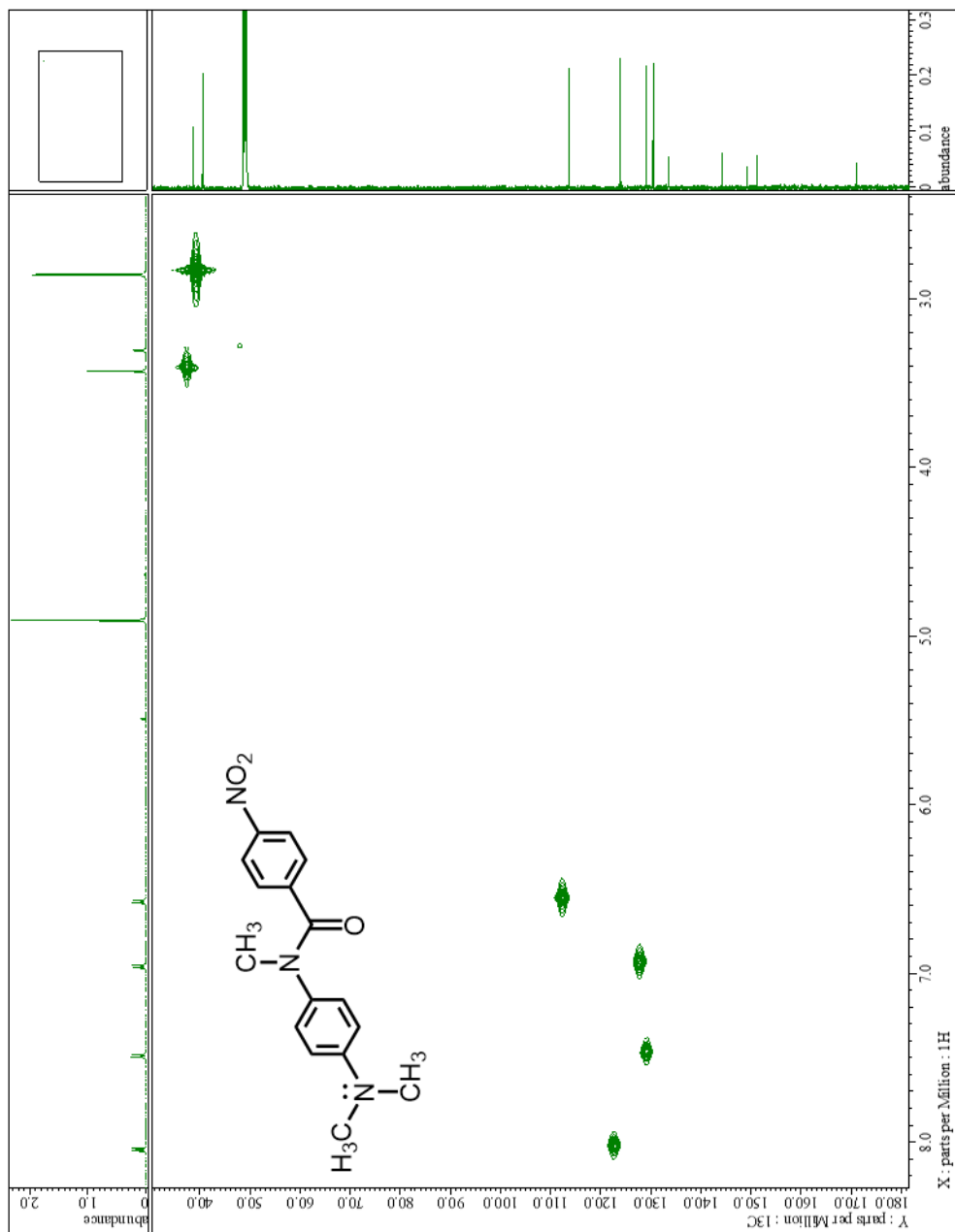
Compound XIV: ^1H - ^1H NMR, CD_3OD

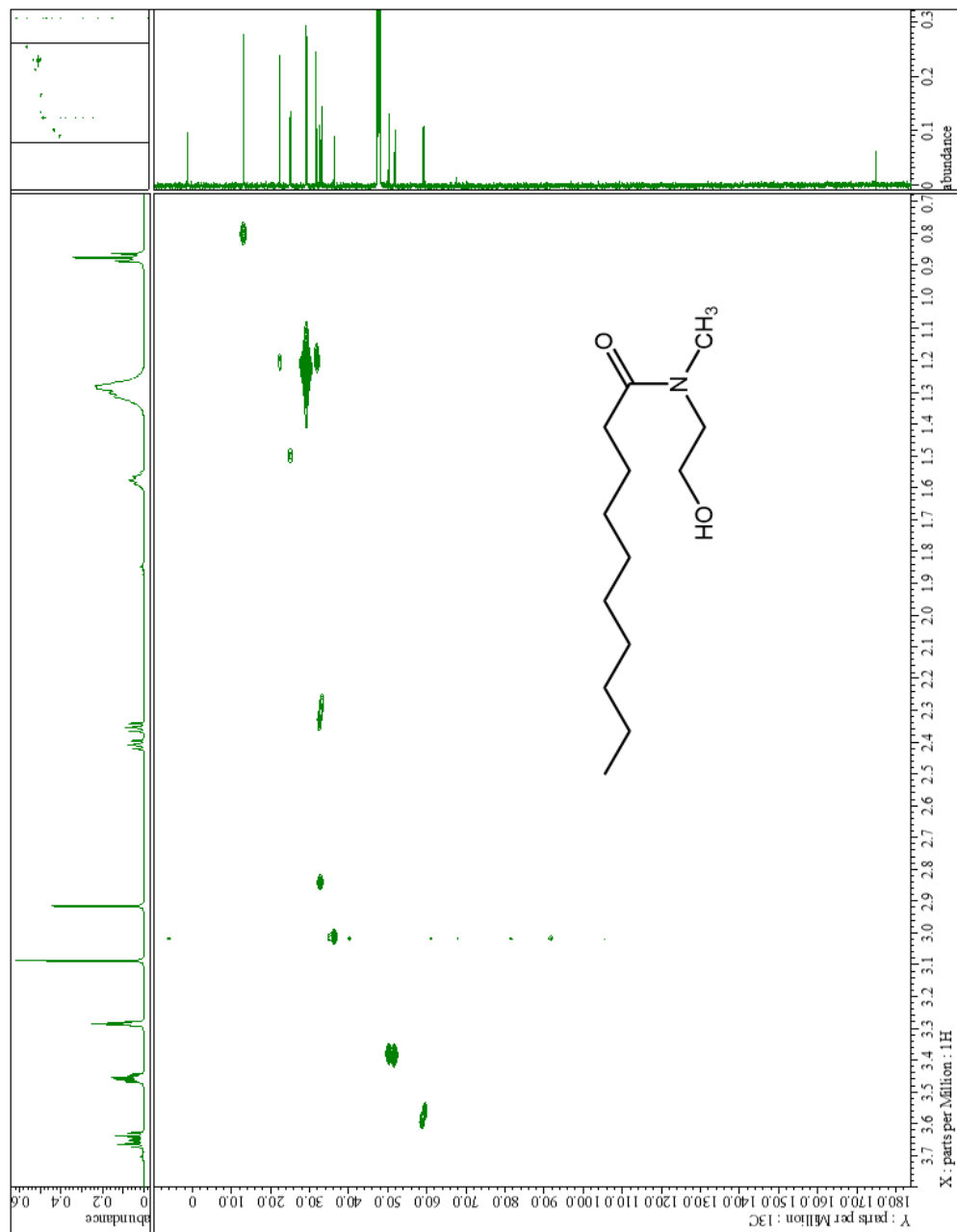
APPENDIX D: SELECTED ^1H - ^{13}C HMQC SPECTRACompound I: ^1H - ^{13}C NMR, CDCl_3

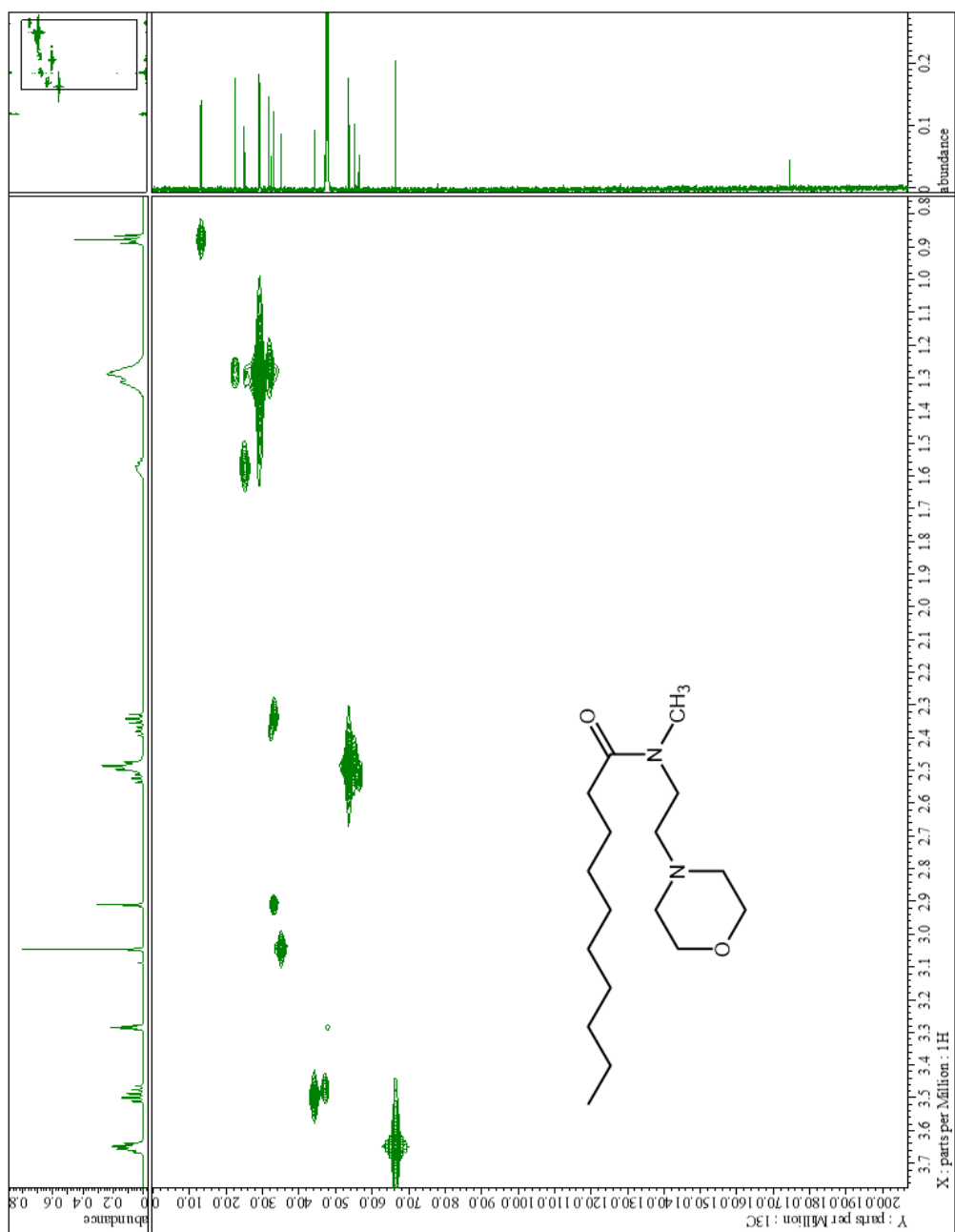
Compound IV: ^1H - ^{13}C NMR, CD_3OD

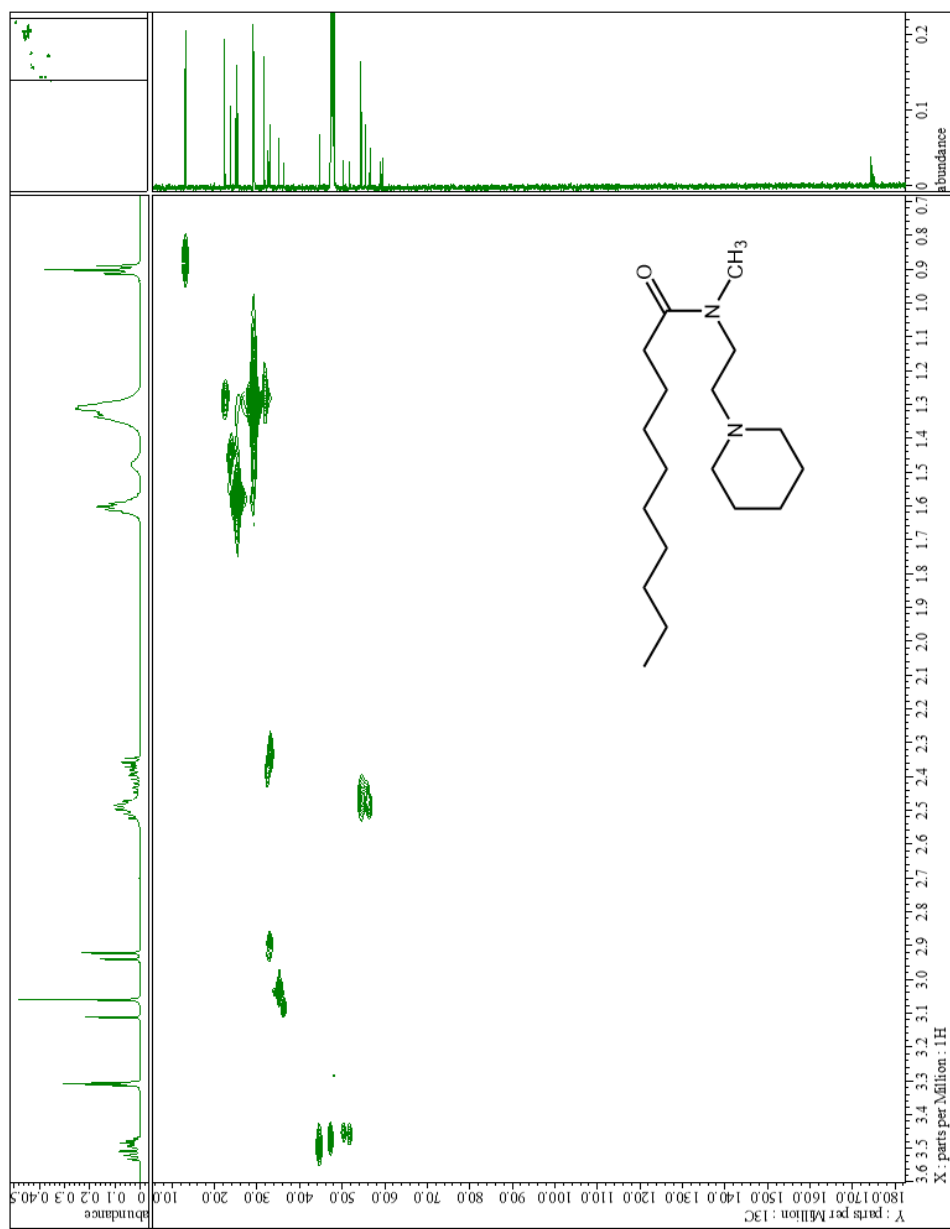
Compound V: ^1H - ^{13}C NMR, CD₃OD

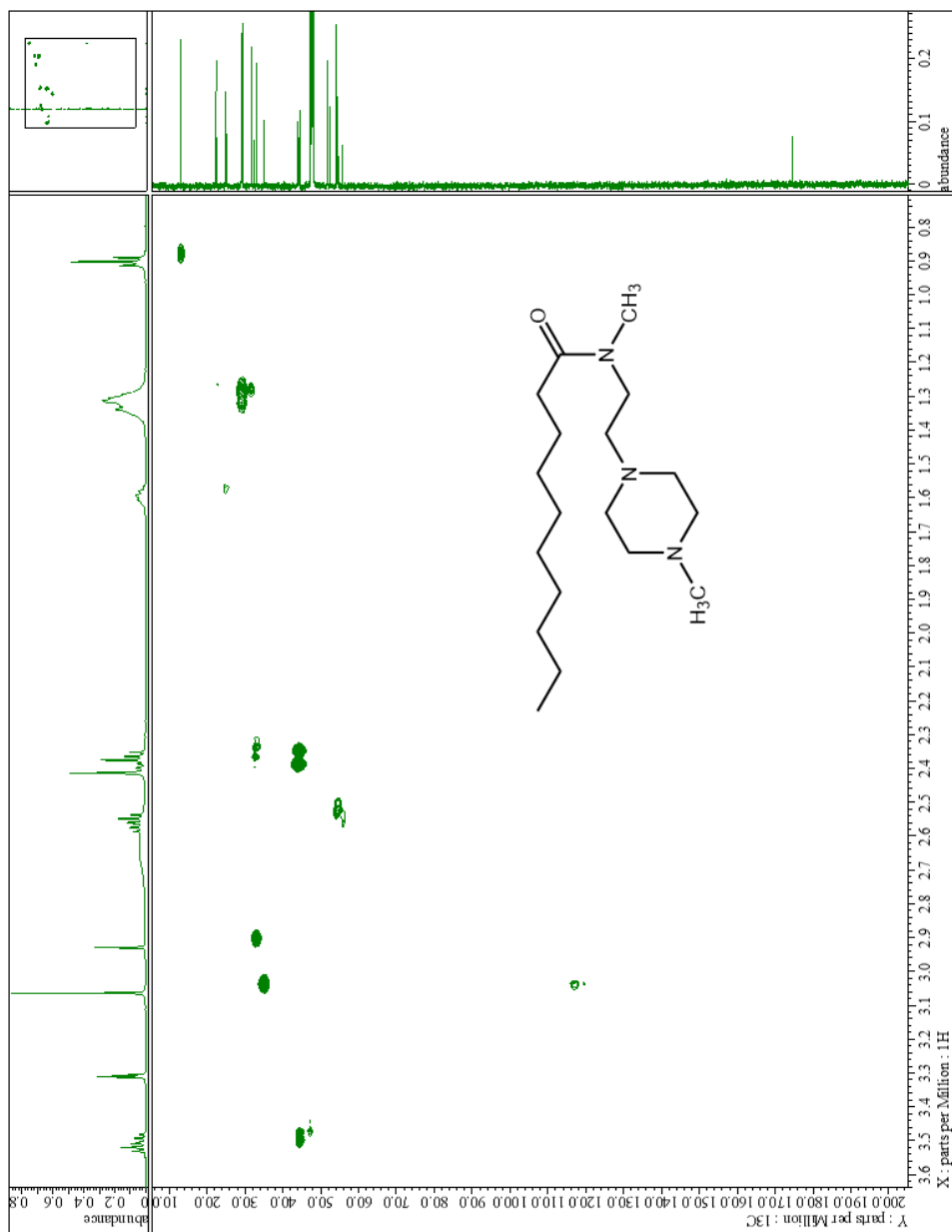
Compound VI: ^1H - ^{13}C NMR, CDCl_3

Compound VII: ^1H - ^{13}C NMR, CD_3OD

Compound X: ^1H - ^{13}C NMR, CD_3OD

Compound XII: ^1H - ^{13}C NMR, CD_3OD

Compound XIII: ^1H - ^{13}C NMR, CD_3OD

Compound XIV: ^1H - ^{13}C NMR, CD_3OD

APPENDIX E: SELECTED ¹H-NMR TITRATION DATA

Table 1

Titration Data for Compound I

TFA* Added (μL)	Total TFA (μL)	TFA:Flipid Molar Ratio	Average pH	T (3.062 ppm)	C (2.925 ppm)	% anti
0.00	0.00	0.0 : 1.0	8.22	1.95	0.99	66.3%
7.00	7.00	0.2 : 1.0	8.07	1.92	0.97	66.4%
10.00	17.00	0.5 : 1.0	7.89	2.01	0.90	69.1%
7.00	24.00	0.7 : 1.0	7.74	2.04	0.88	69.9%
7.00	31.00	0.9 : 1.0	7.65	2.07	0.87	70.4%
10.00	41.00	1.2 : 1.0	7.60	2.12	0.81	72.4%
14.00	55.00	1.6 : 1.0	7.42	2.20	0.73	75.1%
14.00	69.00	2.0 : 1.0	7.14	2.31	0.62	78.8%
14.00	83.00	2.5 : 1.0	6.73	2.57	0.36	87.7%
14.00	97.00	2.9 : 1.0	5.82	2.80	0.13	95.6%
14.00	111.00	3.3 : 1.0	2.80	2.83	0.10	96.6%

*TFA refers to a 1.0 mM solution of deuterated TFA in *d*-MeOH

Table 6

Titration Data for Compound XII

<i>d</i>-TFA* Added (μL)	Total <i>d</i>-TFA* (μL)	TFA:Flipid Molar Ratio	Average pH	T (3.072 ppm)	C (2.935 ppm)	% <i>anti</i>
0.00	0.00	0.0 : 1.0	6.79	1.88	0.99	65.5%
0.00	0.00	0.0 : 1.0	6.75	1.85	0.98	65.4%
9.00	9.00	0.2 : 1.0	6.17	1.90	0.94	66.9%
18.00	18.00	0.5 : 1.0	5.95	1.92	0.89	68.3%
18.00	27.00	0.7 : 1.0	5.76	1.97	0.82	70.6%
18.00	36.00	1.0 : 1.0	5.66	2.04	0.81	71.6%
18.00	45.00	1.2 : 1.0	5.61	2.06	0.79	72.3%
18.00	54.00	1.5 : 1.0	5.47	2.12	0.73	74.4%
18.00	63.00	1.7 : 1.0	5.34	2.31	0.54	81.1%
18.00	72.00	2.0 : 1.0	5.26	2.33	0.52	81.8%
18.00	81.00	2.2 : 1.0	5.07	2.41	0.44	84.6%
18.00	90.00	2.4 : 1.0	4.87	2.45	0.40	86.0%
18.00	99.00	2.7 : 1.0	3.64	2.64	0.21	92.6%
18.00	108.00	2.9 : 1.0	3.16	2.64	0.21	92.6%
18.00	117.00	3.2 : 1.0	2.60	2.64	0.21	92.6%
20.00	128.00	3.5 : 1.0	2.49	2.64	0.21	92.6%
20.00	137.00	3.7 : 1.0	2.22	2.64	0.21	92.6%
20.00	148.00	4.0 : 1.0	2.21	2.64	0.21	92.6%

*TFA refers to a 1.0 mM solution of deuterated TFA in *d*-MeOH

Two NMR samples were used simultaneously for this titration in order to increase efficiency. As one sample (gray rows in Table 6) was being analyzed by NMR, the second sample (white rows in Table 6) was being prepared by adding the appropriate amount of *d*-TFA.

Table 7

Titration Data for Compound XIII

<i>d</i>-TFA* Added (μL)	Total <i>d</i>-TFA* (μL)	TFA:Flipid Molar Ratio	Average pH	T (3.061 ppm)	C (2.922 ppm)	% <i>anti</i>
0.00	0.00	0.0 : 1.0	9.40	1.74	1.08	61.7%
0.00	0.00	0.0 : 1.0	9.50	1.78	1.12	61.4%
7.00	7.00	0.2 : 1.0	8.60	1.81	1.09	62.4%
13.50	13.50	0.4 : 1.0	8.15	1.89	0.93	67.0%
13.50	20.50	0.6 : 1.0	8.08	1.93	0.93	67.5%
13.50	27.00	0.8 : 1.0	7.86	Overlap	Overlap	N/A
13.50	34.00	1.0 : 1.0	7.72	2.06	0.79	72.3%
13.50	40.50	1.2 : 1.0	7.58	2.11	0.78	73.0%
13.50	47.50	1.4 : 1.0	7.45	Overlap	Overlap	N/A
13.50	54.00	1.6 : 1.0	7.36	2.37	0.52	82.0%
13.50	61.00	1.8 : 1.0	7.15	2.47	0.42	85.5%
13.50	67.50	2.0 : 1.0	7.07	2.48	0.41	85.8%
13.50	74.50	2.2 : 1.0	6.62	Overlap	Overlap	N/A
13.50	81.00	2.4 : 1.0	6.43	2.64	0.25	91.3%
10.50	85.00	2.5 : 1.0	5.82	2.61	0.25	91.3%
7.00	88.00	2.6 : 1.0	3.40	2.57	0.32	88.9%

*TFA refers to a 1.0 mM solution of deuterated TFA in *d*-MeOH

Two NMR samples were used simultaneously for this titration in order to increase efficiency. As one sample (gray rows in Table 7) was being analyzed by NMR, the second sample (white rows in Table 7) was being prepared by adding the appropriate amount of *d*-TFA.

Table 8

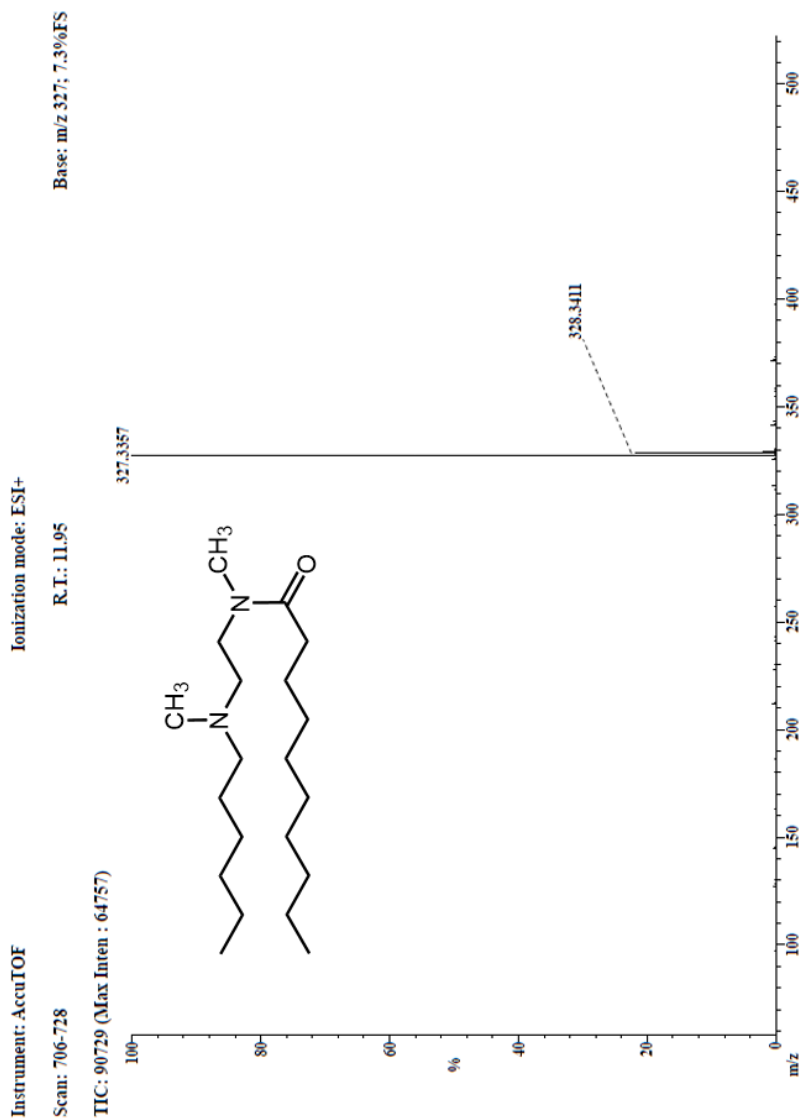
Titration Data for Compound XIV

<i>d</i>-TFA* Added (μL)	Final <i>d</i>- TFA* (μL)	TFA:Flipid Molar Ratio	Average pH	T (3.062 ppm)	C (2.928 ppm)	% <i>anti</i>
0.00	0.00	1 : 0.00	8.24	1.79	0.99	64.4%
0.00	0.00	1 : 0.00	7.89	1.81	0.98	64.9%
8.00	8.00	1 : 0.25	7.73	1.79	0.96	65.1%
16.00	16.00	1 : 0.50	7.46	1.83	0.96	65.6%
16.00	24.00	1 : 0.75	7.30	1.90	0.94	66.9%
16.00	32.00	1 : 1.00	7.21	1.91	0.92	67.5%
16.00	40.00	1 : 1.25	7.05	1.94	0.89	68.6%
16.00	48.00	1 : 1.50	6.77	1.99	0.81	71.1%
16.00	56.00	1 : 1.75	6.76	2.05	0.75	73.2%
16.00	64.00	1 : 2.00	6.47	Overlap	Overlap	N/A
16.00	72.00	1 : 2.25	6.33	2.08	0.72	74.3%
16.00	80.00	1 : 2.50	5.94	2.10	0.70	75.0%
16.00	88.00	1 : 2.75	4.88	2.12	0.68	75.7%
16.00	96.00	1 : 3.00	3.51	2.21	0.59	78.9%
16.00	104.00	1 : 3.25	3.21	2.28	0.52	81.4%
16.00	112.00	1 : 3.50	3.03	2.35	0.45	83.9%
16.00	120.00	1 : 3.75	2.89	2.39	0.41	85.4%
16.00	128.00	1 : 4.00	2.70	2.41	0.39	86.1%
16.00	136.00	1 : 4.25	2.57	2.47	0.33	88.2%
16.00	144.00	1 : 4.50	2.46	2.49	0.31	88.9%
16.00	152.00	1 : 4.75	2.37	2.51	0.29	89.6%
16.00	160.00	1 : 5.00	2.31	2.52	0.28	90.0%
16.00	168.00	1 : 5.25	2.25	2.54	0.26	90.7%
16.00	176.00	1 : 5.50	2.24	2.55	0.25	91.1%
16.00	184.00	1 : 5.75	2.19	2.57	0.23	91.8%
16.00	192.00	1 : 6.00	2.15	2.58	0.22	92.1%
100.00	284.00	1 : 8.85	1.69	2.62	0.18	93.6%

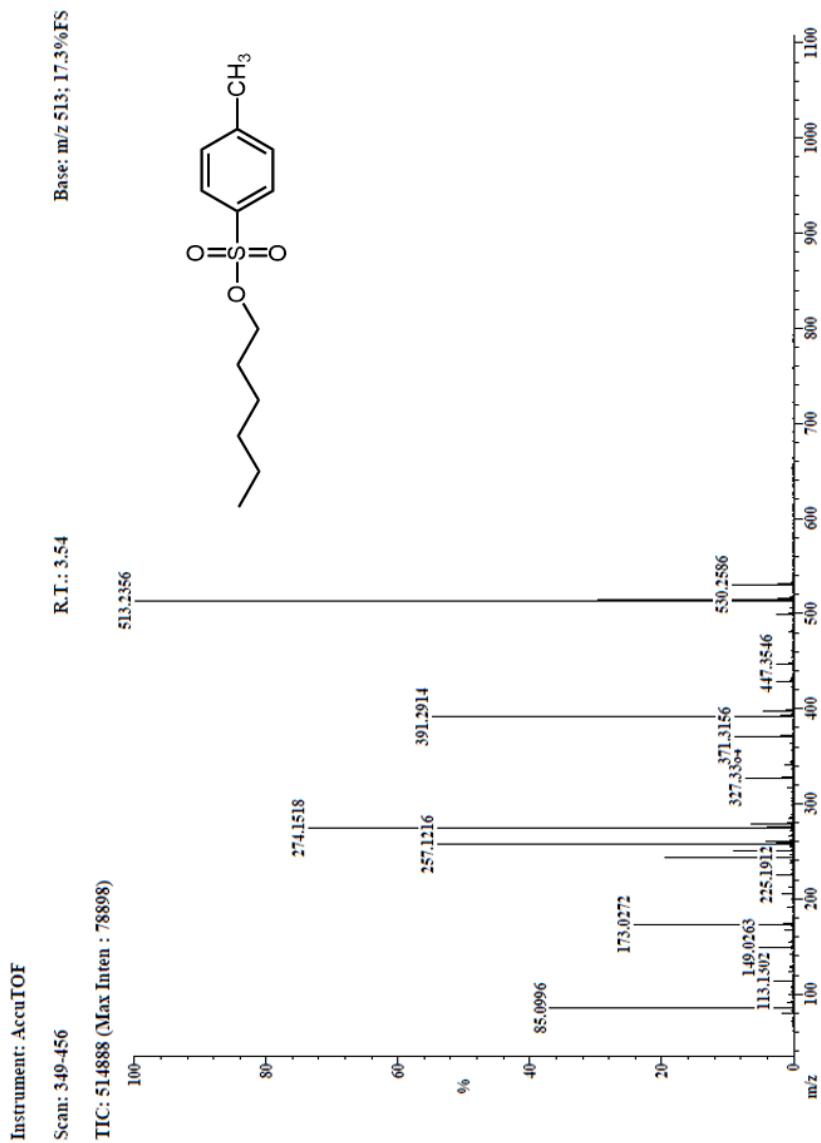
*TFA refers to a 1.0 mM solution of deuterated TFA in *d*-MeOH

Two NMR samples were used simultaneously for this titration in order to increase efficiency. As one sample (gray rows in Table 8) was being analyzed by NMR, the second sample (white rows in Table 8) was being prepared by adding the appropriate amount of *d*-TFA.

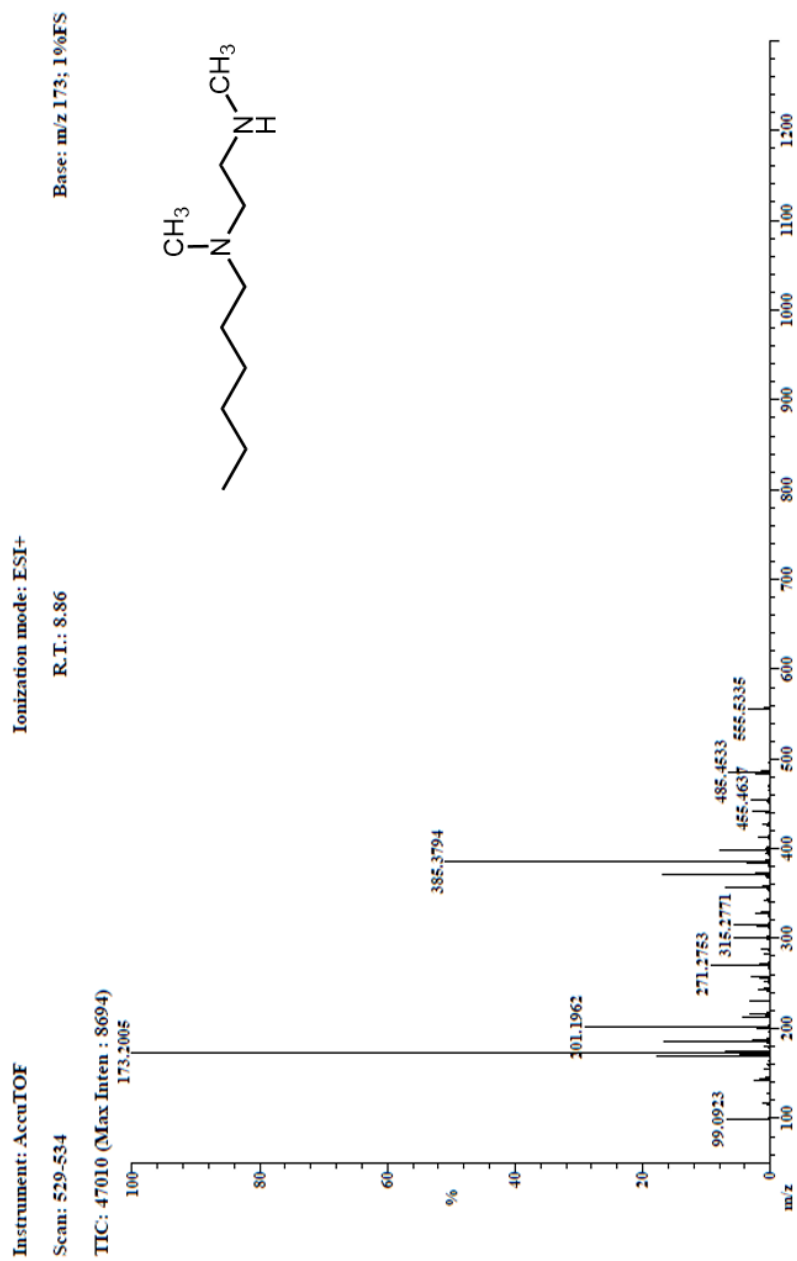
APPENDIX F: SELECTED MASS SPECTRA



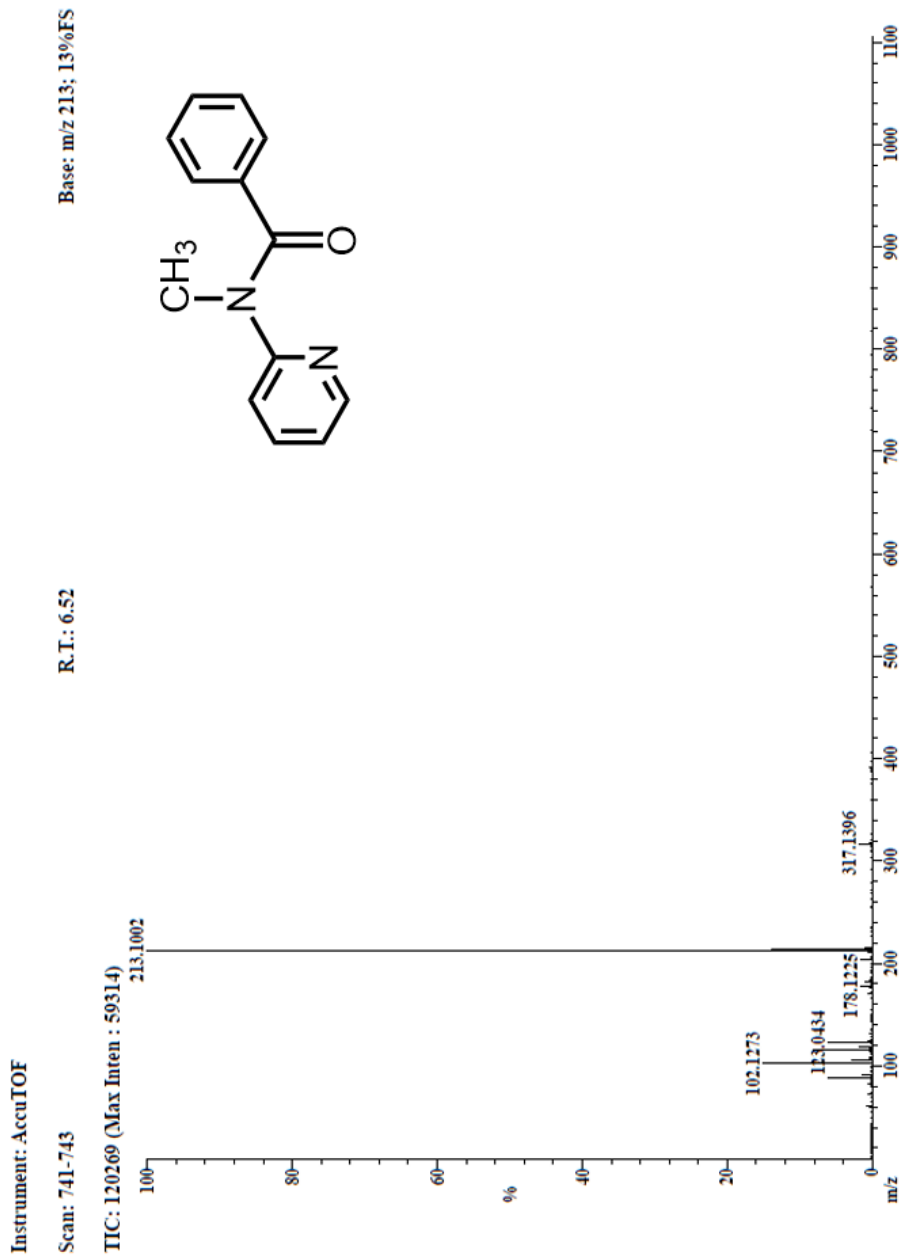
Compound I: DART Ion Source



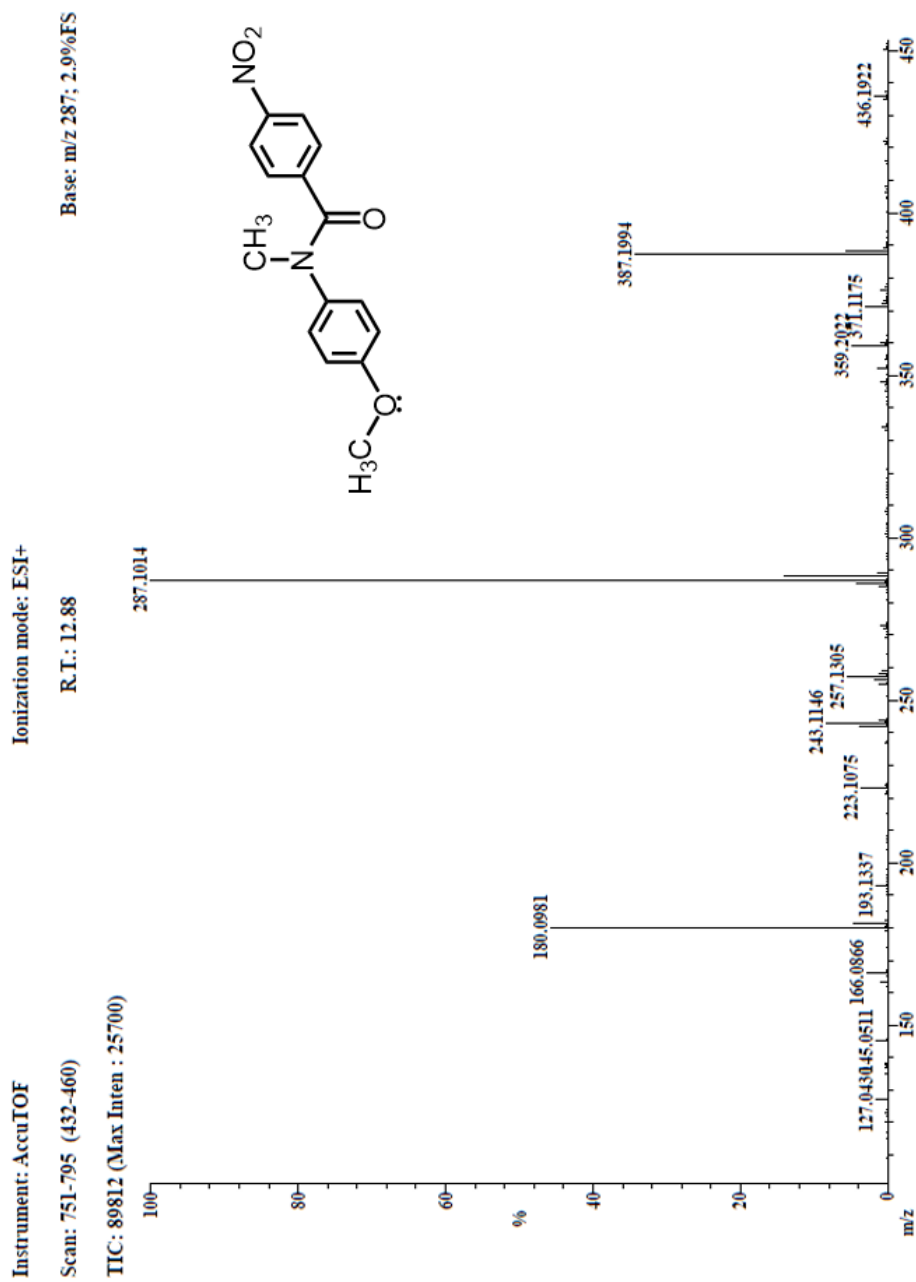
Compound II: DART Ion Source



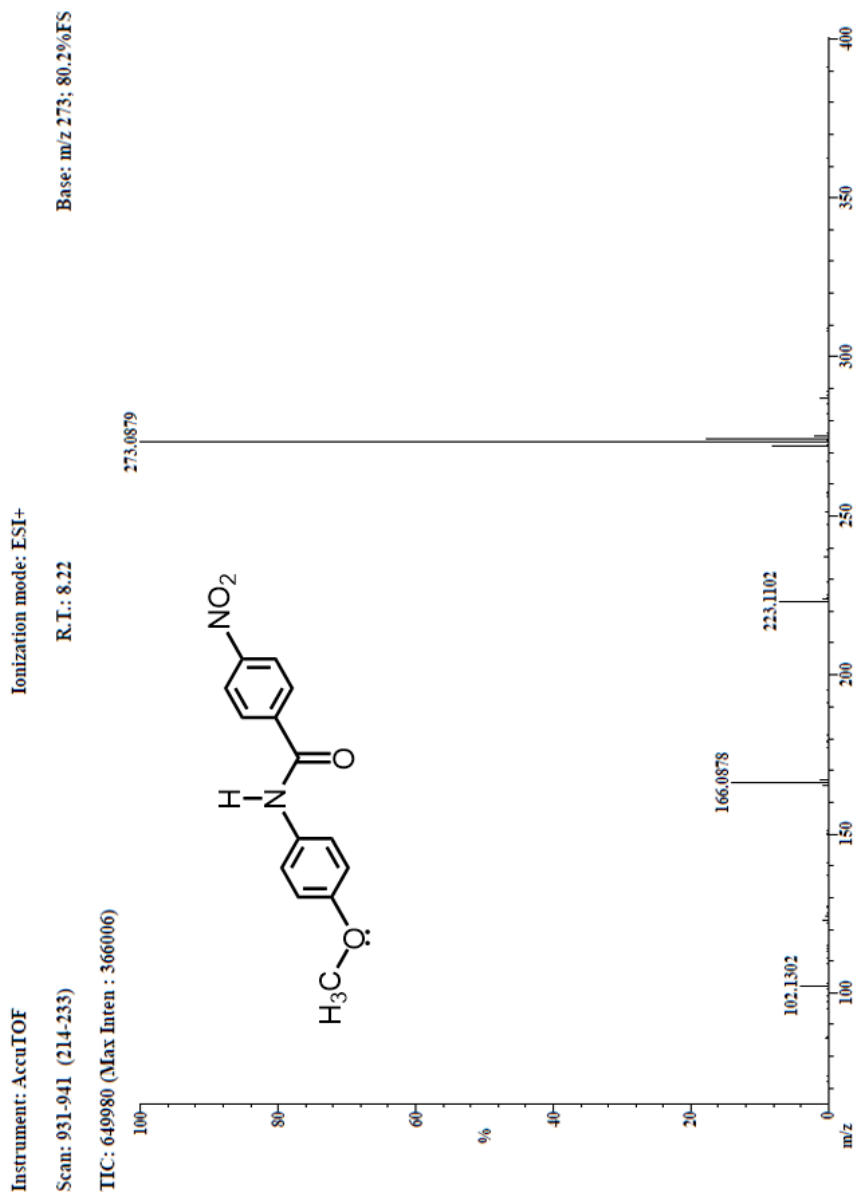
Compound III: DART Ion Source



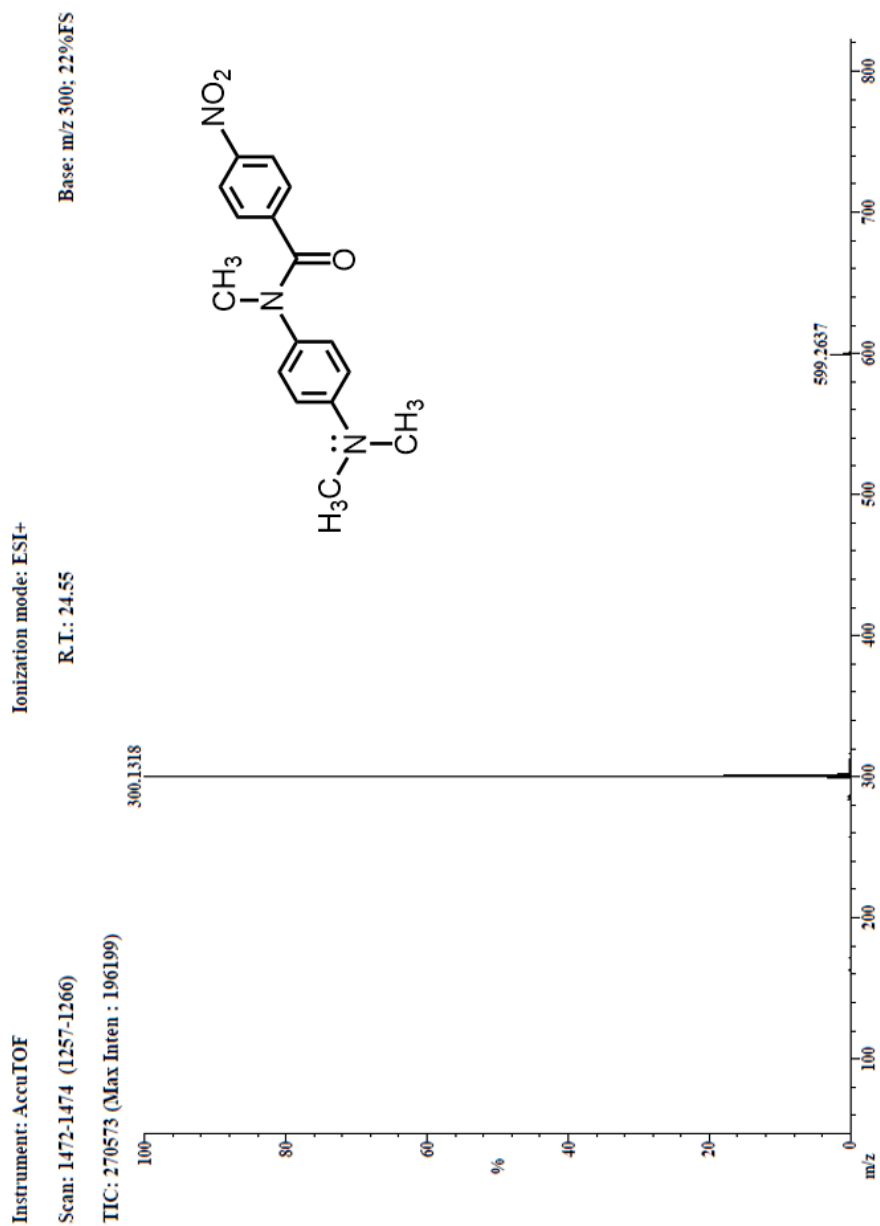
Compound IV: DART Ion Source



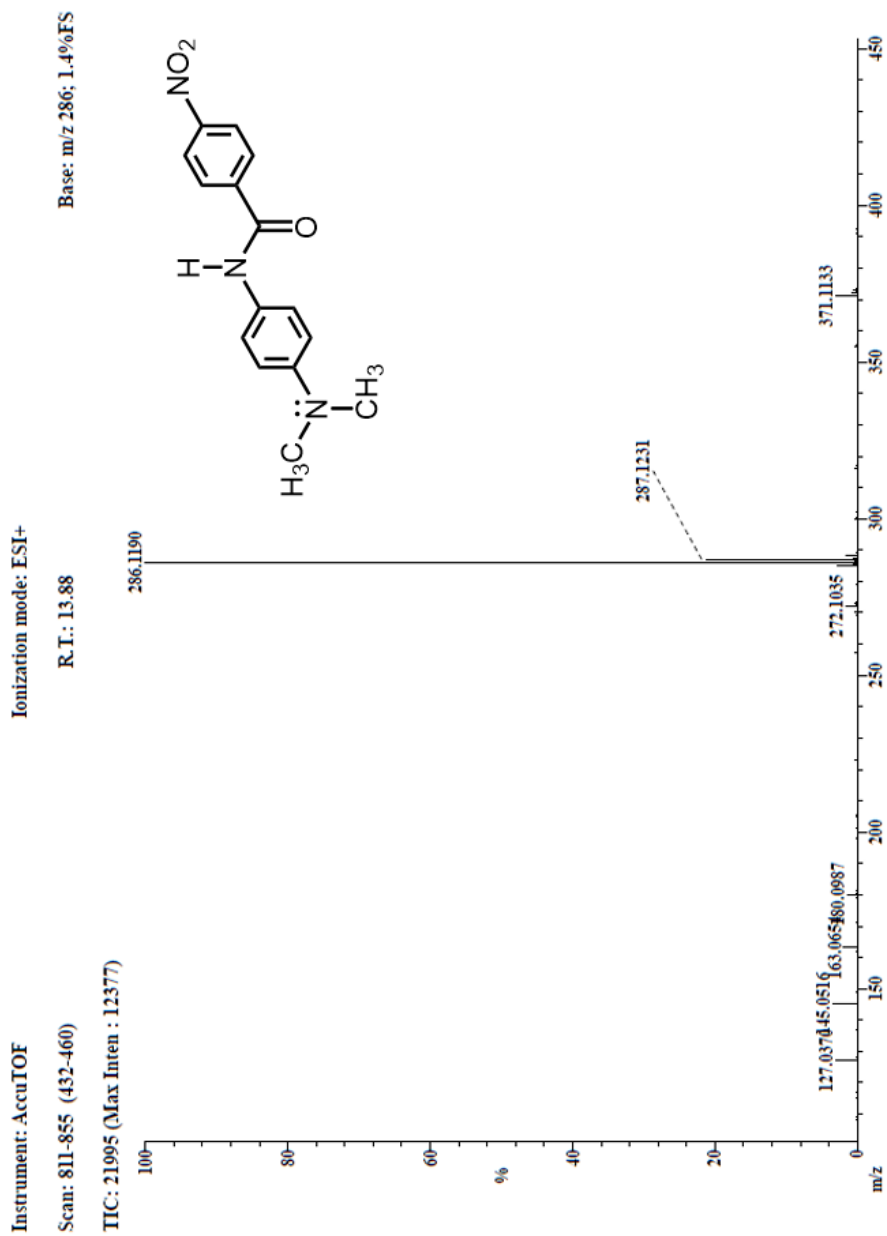
Compound V: DART Ion Source



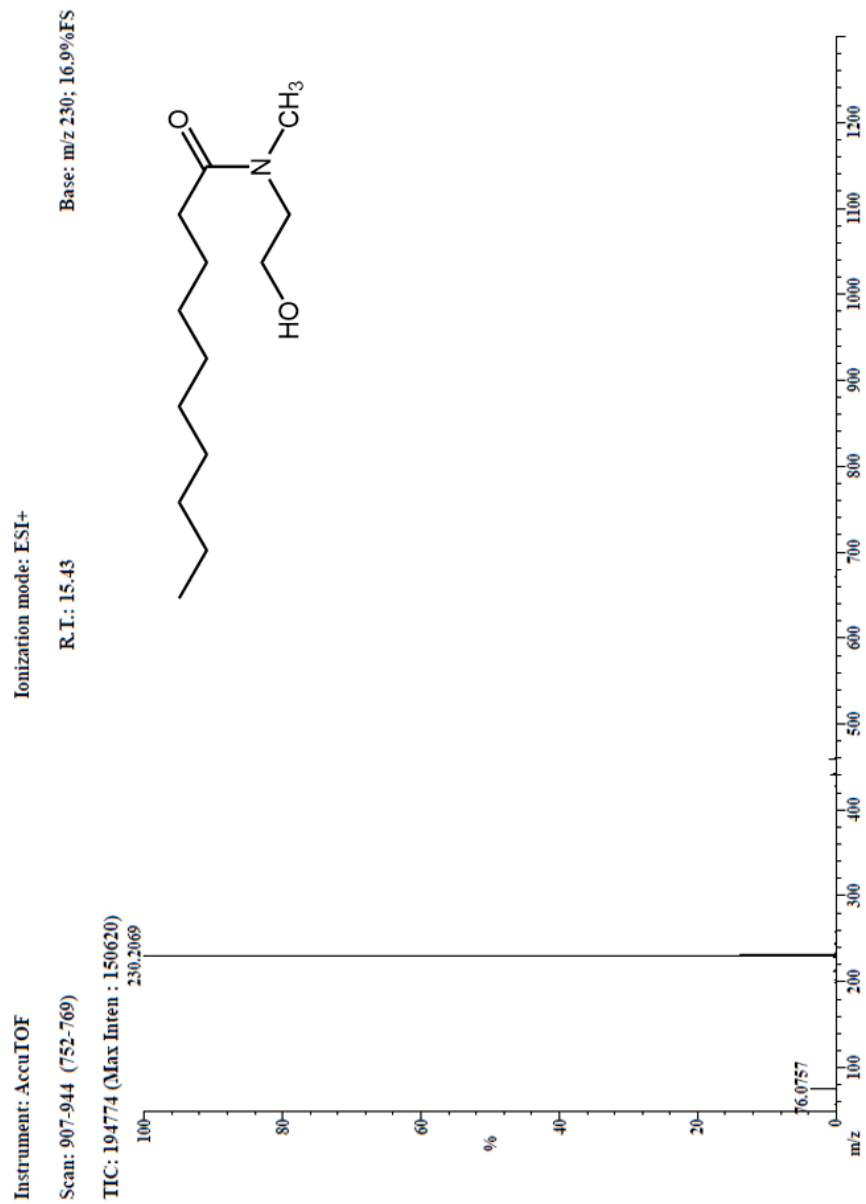
Compound VI: DART Ion Source



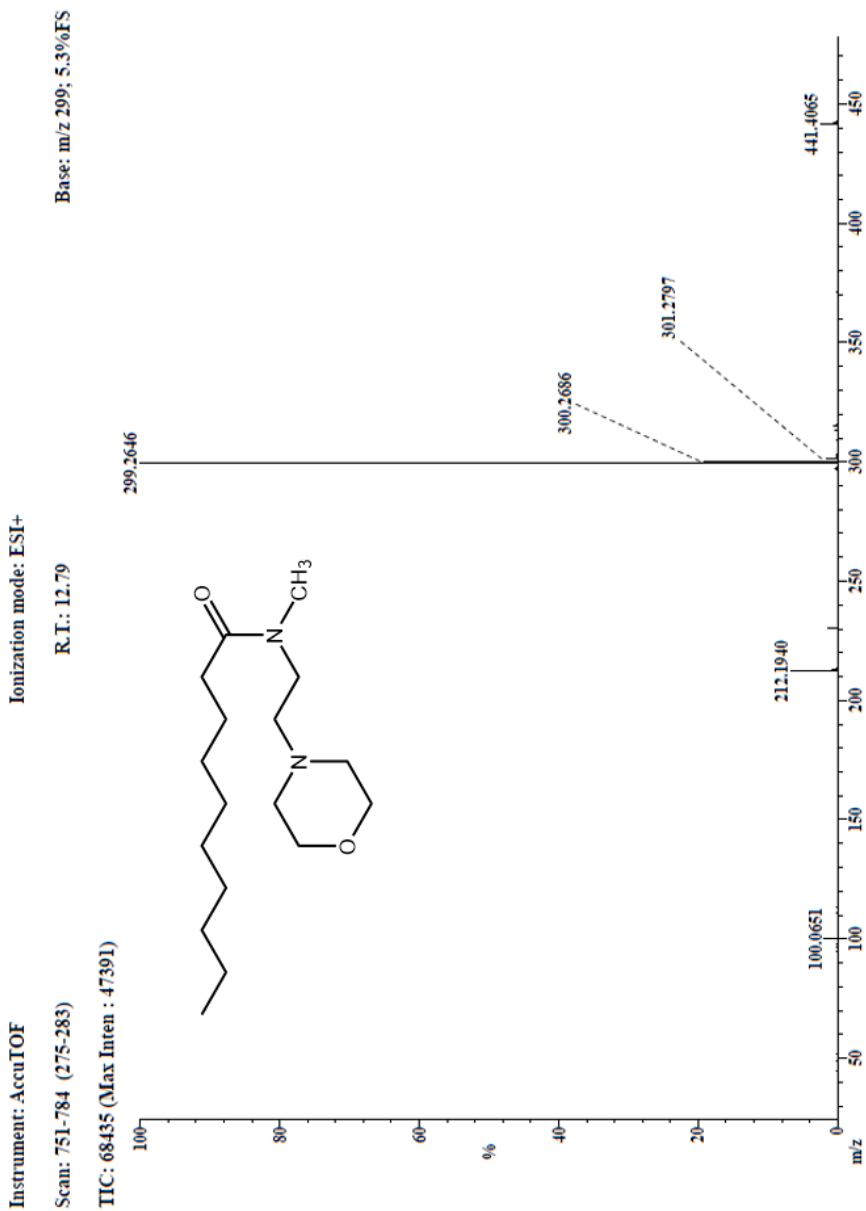
Compound VII: DART Ion Source

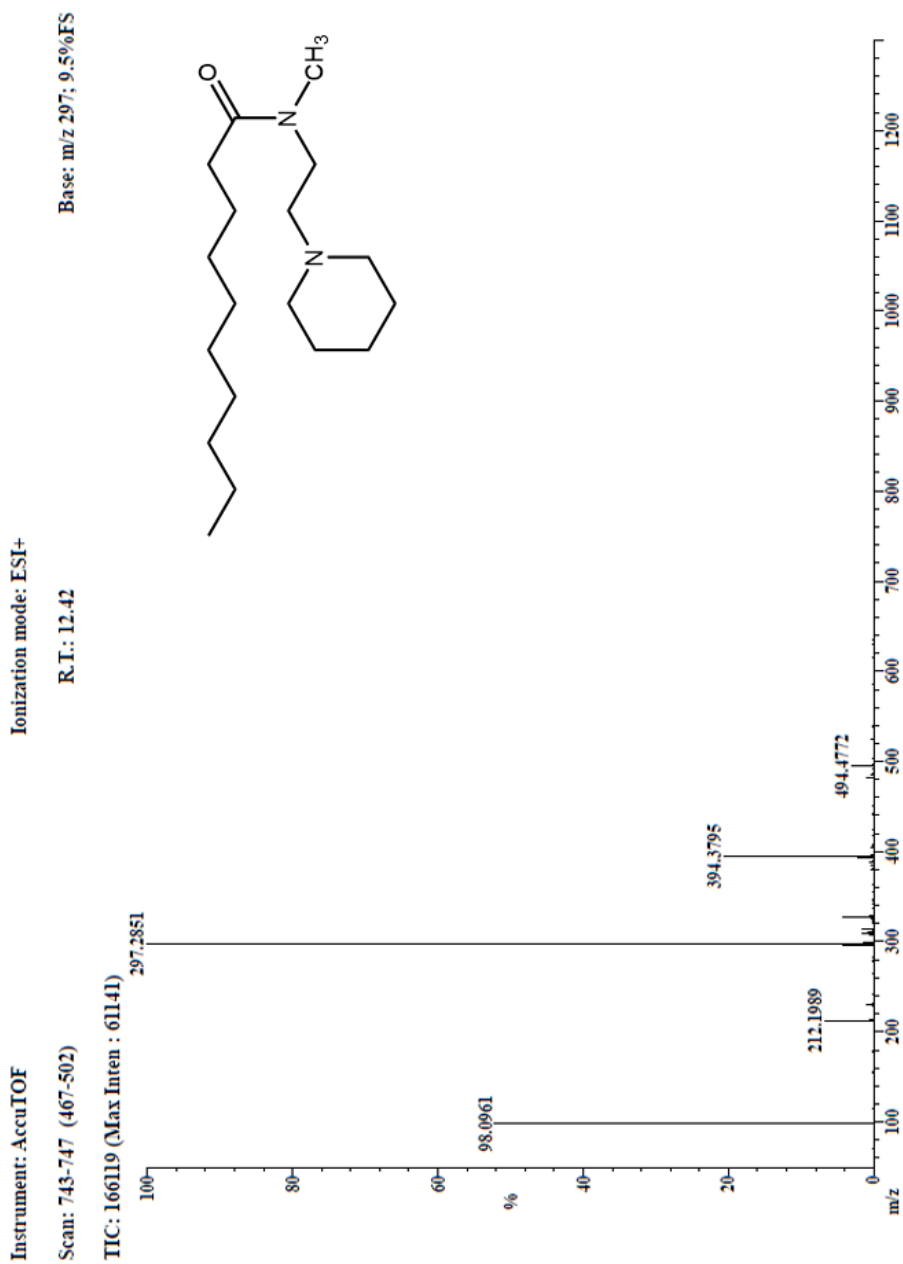


Compound VIII: DART Ion Source

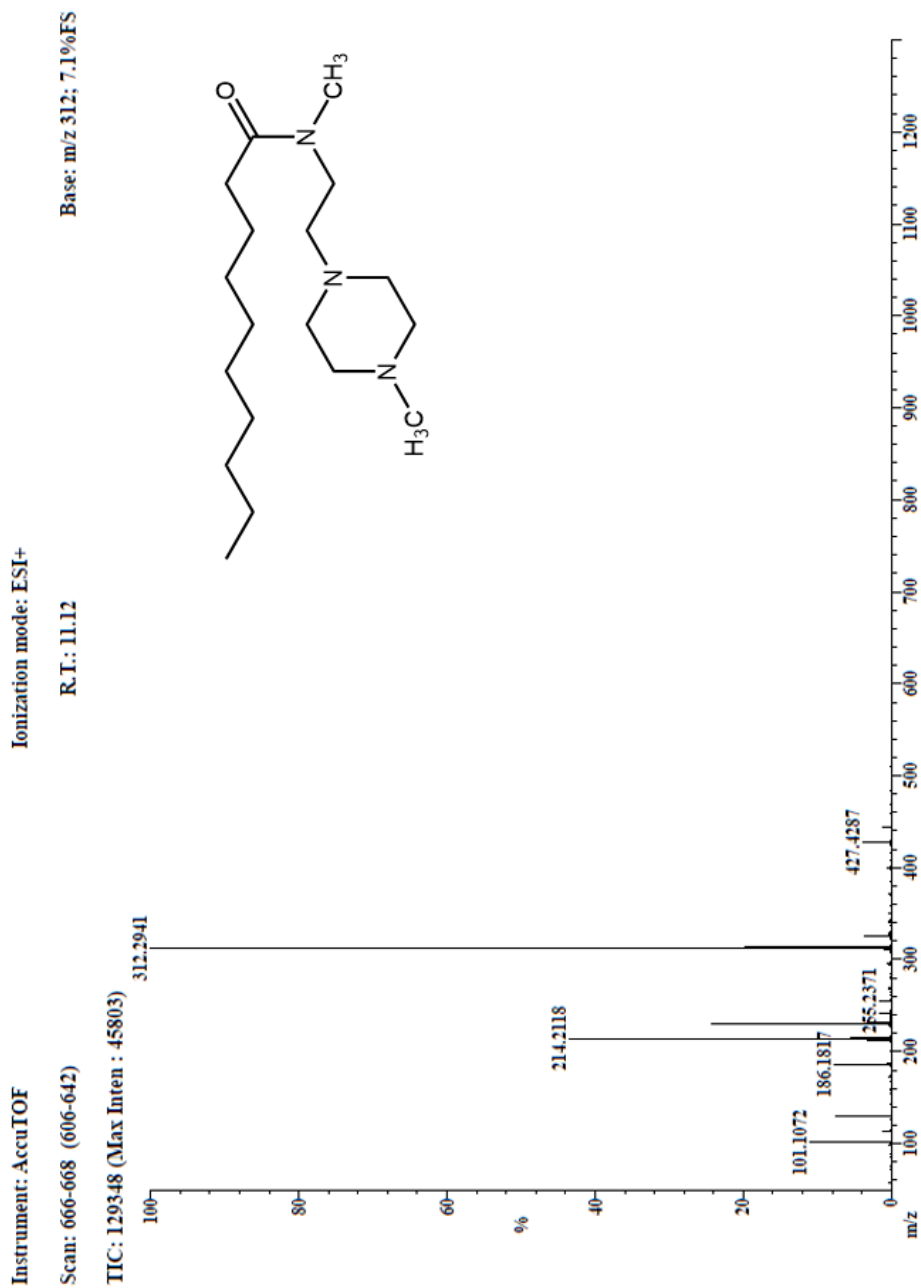


Compound X: DART Ion Source

Compound **XII**: DART Ion Source



Compound XIII: DART Ion Source



Compound XIV: DART Ion Source